10-4-2013 12:00 AM

Numerical and Experimental Analysis of Retrofit System for Light-Framed Wood Structures Under Wind Loading

Ryan B. Jacklin
The University of Western Ontario

Supervisor
Dr. Ashraf El Damatty
The University of Western Ontario

Graduate Program in Civil and Environmental Engineering
A thesis submitted in partial fulfillment of the requirements for the degree in Master of Engineering Science

NUMERICAL AND EXPERIMENTAL ANALYSIS OF RETROFIT SYSTEM FOR LIGHT-FRAMED WOOD STRUCTURES UNDER WIND LOADING

(Thesis format: Integrated Article)

by

Ryan B. Jacklin

Graduate Program in Engineering Science
Department of Civil and Environmental Engineering

A thesis submitted in partial fulfillment
of the requirements for the degree of
Master of Engineering Science

The School of Graduate and Postdoctoral Studies
The University of Western Ontario
London, Ontario, Canada

Abstract

Past high speed wind events have exposed the vulnerability of the roof systems of existing light-framed wood structures to the uplift forces resulting from high speed winds, contributing greatly to economic and human loss. This research focuses on developing a retrofit system to increase the uplift capacity of the roofs of these structures using numerical and experimental techniques. The proposed system provides the uplift forces an alternate load path to the ground, reducing the demand placed on the weak, nailed connections within the structure. A three-dimensional finite-element model of a roof system of full-scale wood structure has been developed. The model is compared to the results of a full-scale experiment in both the linear and nonlinear ranges, proving the ability of the model to predict the deflected shape of the structure. The numerical results identify the importance of considering the nonlinear plastic damage that occurs to the roof-to-wall connection under realistic wind loading. The validated numerical model is then extended to include the proposed retrofit idea. A rigorous analysis of the behaviour of the structure after application is then carried out. The model predicts that application of the retrofit system can increase the critical mean hourly wind velocity from 38m/s to 50m/s. An experiment has been conducted, proving the retrofit system is effective at increasing the uplift capacity of light-framed wood structures. The results of the experiment have been used to validate the assumptions of the numerical model, proving that the model captures the structural interaction between the retrofit and truss systems.

Keywords: Light-Framed Wood Structures, Finite-Element Modeling, Hurricane Damage Mitigation, Roof to Wall Connection, Retrofit

Co-Authorship Statement

This thesis has been prepared in accordance with the regulations for an Integrated-Article format thesis stipulated by the School of Graduate and Postdoctoral Studies at the University of Western Ontario and has been co-authored as:

Chapter Two: Finite-Element Modeling of a Light-Framed Wood Roof System

The initial numerical model was developed by A. Dessouki. Modifications to the numerical model and the numerical analysis were completed by R. Jacklin under the supervision of Dr. A. A. El Damatty. Drafts of the work were prepared by R. Jacklin and modifications were completed under the supervision of Dr. A. A. El Damatty. A paper co-authored by R. Jacklin, A. A. El Damatty and A. Dessouki will be submitted to the *Journal of Wind and Structures*

Chapter Four: Analysis and Optimization of a Retrofit System for Light-Framed Wood Structures under Wind Loading

The development and analysis of the numerical model were completed by R. Jacklin under the supervision of Dr. A. A. El Damatty. Drafts of the work were prepared by R. Jacklin and modifications were completed under the supervision of Dr. A. A. El Damatty. A paper co-authored by R. Jacklin and A. A. El Damatty will be submitted to *Journal of Structural Engineering.*

Chapter Five: Experimental Testing of a Retrofit System to Increase Uplift Capacity of Light-Framed Wood Structures

The experimental testing and the numerical analysis were completed by R. Jacklin under the supervision of Dr. A. A. El Damatty. Drafts of the work were prepared by R. Jacklin and modifications were completed under the supervision of Dr. A. A. El Damatty. A paper co-authored by R. Jacklin and A. A. El Damatty will be submitted to the *Engineering Structures.*

Acknowledgments

I would like to first thank Dr. El Damatty for his valuable guidance and expertise throughout the years of working under his supervision. I would also like to thank The Natural Science and Engineering Research Council of Canada (NSERC) and M. A. Steelcon Engineering Limited for the financial support of the research, Wilbert Logan and Ryan Tang for their assistance with the experimental program, Murray Morrison for sharing the experimental data, my family and friends for their support, and my sister Joella for her valuable editing services.

Table of Contents

Abstract ii

Co-Authorship Statement iii

Acknowledgments iv

Table of Contents v

List of Tables x

List of Figures xi

Chapter 1: Introduction 1

1.1 General 1

1.2 Background 4

1.2.1 Numerical and Experimental Studies of Structural Behaviour 4

1.2.2 Current Technology and Building Code Development 6

1.2.3 Retrofitting Technology 8

1.3 Objectives of Study 10

1.4 Thesis Structure 12

1.4.1 Finite-Element Modeling of a Light-Framed Wood Rood Structure 13

1.4.2 Parametric Study of Retrofit System for Light-framed Wood Structures under Uniform Uplift Load 13

1.4.3 Analysis and Optimization of a Retrofit System for Light-Framed Wood Structures under Wind Loading 14

1.4.4 Experimental Testing of a Retrofit System to Increase Uplift Capacity of Light-Framed Wood Structures 14

1.5 References 14

Chapter 2:Finite-Element Modeling of a Light-Framed Wood Roof Structure 17

2.1 Introduction 17

2.2 Description of the Conducted Experiment 21

2.3 Numerical Modeling of the Roof Structure 23
2.3.1 Interior Trusses 23
2.3.2 Gable Truss 24
2.3.3 Plywood Sheathing 25
2.3.4 Roof to Wall Connection 26
2.3.5 Roof Overhang 27
2.3.6 Boundary Conditions 27
2.3.7 Load Input Data 28
2.4 Validation of the Numerical Model 30
2.5 Analysis of Structural Behaviour 34
2.5.1 Analysis of the Tributary Area Method 34
2.5.2 Behaviour under Uniform and Non-uniform Load 36
2.5.3 Effect of Increased Gable End Stiffness on Sheathing Failures 40
2.6 Conclusions 41
2.7 References 42
Chapter 3: Parametric Study of Behaviour after Retrofitting Under Uniform Load 45
3.1 Introduction 45
3.2 Model Description 49
3.2.1 Roof Structure 49
3.2.2 Bearing Cables 51
3.2.3 External Cables 51
3.2.4 Rigid Bar 52
3.3 Typical Behaviour of the Structure with Retrofit System 52
3.3.1 Effect on Roof to Wall Connection Behaviour 53
3.3.2 Force Distribution in Retrofit System 56

3.3.3 Effect on Sheathing Deflection and Shear Force 57
3.4 Parametric Study under Uniform Pressure Distribution 58
3.4.1 Details of the Parametric Study 58
3.4.2 Results of Parametric Study 60
3.5 Conclusions 70
3.6 References 72
Chapter 4: Analysis and Optimization of a Retrofit System for Light-Framed Wood Structures under Wind Loading 73
4.1 Introduction 73
4.2 Model Description 77
4.2.1 General Structural Geometry, Elements and Properties 78
4.2.2 Time History Load Application 80
4.2.3 Roof to Wall Connection 81
4.2.4 Wall System 82
4.2.5 Numerical Model of Retrofit System 83
4.3 Numerical Results 84
4.3.1 Comparison to the Experimental Results 85
4.3.2 Analysis of the Plastic Deformation 89
4.4 Parametric Optimization under a Non-uniform pressure distribution 91
4.4.1 Design wind speed and loading 92
4.4.2 Design Variables 92
4.4.3 Design Constraints 92
4.4.4 Results 94
4.5 Assessment of Optimized Retrofit under Non-uniform Pressure Distributions ... 96
4.5.1 Assessment Under Selected 35mps Time History 96
4.5.2 Assessment under NBCC Pressure Distribution 100

4.6 Feasibility Analysis of Nylon Strap 102
4.6.1 General Discussion of Material Properties 102
4.6.2 Numerical Results 103
4.7 Conclusions 105
4.8 References 107
Chapter 5: Experimental Testing of a Retrofit System to Increase Uplift Capacity of Light-Framed Wood Structures 109
5.1 Introduction 109
5.2 Proposed Retrofit System 113
5.3 Experimental Design 116
5.3.1 Apparatus 117
5.3.2 Experimental Instrumentation 121
5.3.3 Procedure 123
5.4 Description of the Numerical Model of the Experiment 124
5.4.1 Truss System 124
5.4.2 RTW Connection 125
5.4.3 Retrofit System 125
5.4.4 Cable and Turnbuckle Numerical Properties 126
5.5 Experimental Results 126
5.5.1 Control Experiment 126
5.5.2 'Retrofit – New' Experimental Results 128
5.5.3 'Retrofit – Damaged' Experimental Results 134
5.6 Numerical Response and Behaviour 136
5.6.1 Load-Deflection Behaviour of Truss System 136
5.6.2 Force Distribution between Load Paths 138
5.7 Conclusions 142

5.8 References 144
Chapter 6: Conclusions and Future Research 146
6.1 Summary 146
6.2 Key Findings of the Current Work 146
6.3 Recommendations for Future Work 149
Curriculum Vitae 151

List of Tables

Table 2.1: Load case selection from 20m/s TLP experiment 29

Table 2.2: Load case selection from 25m/s TLP experiment 29

Table 2.3: Total uplift force transferred by the RTW connections of the east gable for load cases selected from 20m/s wind speed experiment..... 36

Table 2.4: Total uplift force transferred by the RTW connections of the east gable for load cases selected from 25m/s wind speed experiment..... 36

Table 3.1: Initially proposed dimensions for full-scale retrofit system 52

Table 3.2: Parametric study values 59

Table 4.1: Values considered for the design variables 92

Table 4.2: Demand to capacity ratios for the optimum solutions of the parametric study 95

Table 4.3: Maximum force and demand to capacity ratio for each component under 35mps time history loading 100

Table 4.4: Critical mean hourly wind velocities of numerical analysis (m/s) 104

Table 5.1: Initially proposed dimensions for full-scale retrofit system 116

Table 5.2: Summary of Experimental and Equivalent Full-scale properties 120

Table 5.3: Experimental critical applied load summary 135

List of Figures

Figure 1.1: Failure of roof sheathing above gable end, source: www.floridadisaster.org 3

Figure 1.2: Example of roof system failure after multiple RTW connection failures, source: www.Disastersafety.org 3

Figure 1.3: Elevation view of proposed retrofit system as applied to a gable-style roof 11

Figure 1.4: Elevation view of proposed retrofit system as applied to a gable-style roof 11

Figure 2.1: Full-scale experimental set-up with steel reaction frame 22

Figure 2.2: Plan view of pressure box distribution for the full-scale experiment 22

Figure 2.3: Plan view of structural skeleton of roof system 23

Figure 2.4: Elevation view and dimensions of interior Howe-style truss 24

Figure 2.5: Moment releases included in the finite-element model 24

Figure 2.6: Gable end trusses of numerical model with additional external RTW connections 25

Figure 2.7: RTW connection load-deflection relationship 27

Figure 2.8: Pressure distribution for load case 5 (units = Pa) 29

Figure 2.9: Pressure distribution for load case 12 (units = kPa) 30

Figure 2.10: Deflection of the RTW connections for load case 5 31

Figure 2.11: Deflection of the RTW connections for load case 12 32

Figure 2.12: Deflection of connection S-03 throughout load cases 1 to 12 33

Figure 2.13: Deflection of connection S-10 throughout load cases 1 to 12 33

Figure 2.14: RTW connection force for tributary area method and numerical model, load case 12 35

Figure 2.15: RTW deflections under equivalent uniform pressure distribution and realistic pressure distribution for load case 12 37

Figure 2.16: Selection cuts for analysis 38

Figure 2.17: Deflection profile of sheathing along section 1-1 under non-uniform and equivalent uniform pressure distribution for load case 12 38

Figure 2.18: Sheathing deflected profile along length of building at section 2-2 under non-uniform and equivalent uniform pressure distribution for load case 12 39

Figure 2.19: Predictions of uplift force per truss under non-uniform and equivalent uniform loading..... 40

Figure 3.1: Elevation view of structure with retrofit system 47

Figure 3.2: Elevation view of structure with retrofit system 47

Figure 3.3: Plan view of proposed retrofit system as applied to a gable-style roof..... 48

Figure 3.4: Plan view of structural skeleton 50

Figure 3.5: Elevation view and dimensions of Howe-style truss..... 50

Figure 3.6: Load deflection relationship for roof to wall connection 51

Figure 3.7: South elevation view with selected analysis points..... 53

Figure 3.8: Typical applied uniform pressure vs selected RTW connection deflection 54

Figure 3.9: RTW connection deflection along the length of structure under 1.2kPa of uniform pressure 56

Figure 3.10: Typical bending moment diagram of center rigid bar under 1.2kPa of uniform pressure 57

Figure 3.11: Deflected shape of sheathing located above the center truss with and without the retrofit system under 1.2kPa uniform pressure 57

Figure 3.12: Resulting shear forces at selected sheathing locations with and without retrofit system under 1.2 kPa of uniform pressure..... 58

Figure 3.13: Applied pressure vs selected RTW connection deflection for varying external cable diameters..... 61

Figure 3.14: Axial force in the bearing cables for varying external cable diameters under 1.6 kPa of uniform pressure 61

Figure 3.15: Applied pressure vs selected RTW connection deflection for varying bearing cable diameters..... 62

Figure 3.16: Axial force in the bearing cables for varying bearing cable diameters under 1.6 kPa of uniform pressure 63

Figure 3.17: Applied pressure vs selected RTW connection deflection for varying bar rigidities 64

Figure 3.18: Axial force in the bearing cables for varying bar rigidities under 1.6 kPa of uniform pressure 65

Figure 3.19: Applied pressure vs selected RTW connection deflection for insufficient initial external cable prestressing 66

Figure 3.20: Applied pressure vs selected RTW connection deflection for varying initial external cable prestressing 67

Figure 3.21: Axial force in the bearing cables for varying intial external cable prestressing under 1.6 kPa of uniform pressure 67

Figure 3.22: Applied pressure vs selected RTW connection deflection for varying external cable angle 68

Figure 3.23: Axial force in the bearing cables for varying external cable angles under 1.6 kPa of uniform pressure 69

Figure 3.24 Applied pressure vs selected RTW connection deflection for varying roof overhang lengths 70

Figure 4.1: Elevation view of proposed retrofit system as applied to a gable-style roof 76

Figure 4.2: Elevation view of proposed retrofit system as applied to a gable-style roof 76

Figure 4.3: Plan view of structural skeleton of roof system 79

Figure 4.4: Deflection of an experimental RTW connection during the 35m/s experiment... 80

Figure 4.5: Developed load deflection response for roof to wall connection 82

Figure 4.6: Shifted and damaged experimental behaviour with loading 85

Figure 4.7: Deflected shape of the structure under maximum global uplift pressure (Time Step 633) 86

Figure 4.8: Deflected shape of the structure under minimum global uplift pressure (Time Step 116) 86

Figure 4.9: Experimental and numerical RTW connection deflection for truss 3 88

Figure 4.10: Experimental and numerical RTW connection deflection for truss 9 88

Figure 4.11: Experimental and numerical RTW connection deflection for truss 15 88

Figure 4.12: Average magnitude of percent difference between experimental and numerical RTW connection deflections..... 89

Figure 4.13: Experimental results compared to the plastic and elastic analysis for the critical connection, S-03 90

Figure 4.14: Deflected shape of the structure after damaging load, Time = 15 sec 91

Figure 4.15: Deflected shape of the RTW connections under the maximum loading 97

Figure 4.16: Deflection of the RTW connection S-03 through the time history 98

Figure 4.17: Section cut for analysis of deflected shape of the sheathing 98

Figure 4.18: Deflected shape of the sheathing under maximum loading 99

Figure 4.19: Deflection of the RTW connections under 38m/s wind loading 101

Figure 5.1: Elevation view of proposed retrofit system as applied to a gable-style roof 113

Figure 5.2: Elevation view of proposed retrofit system as applied to a gable-style roof 114

Figure 5.3: Plan view of proposed retrofit system as applied to a gable-style roof..... 114

Figure 5.4: Elevation view of the experimental apparatus with retrofit system 117

Figure 5.5: Elevation view of Experimental and Full-Scale Systems 118

Figure 5.6: Plan view of experimental and full-scale systems..... 119

Figure 5.7: Experimental setup 122

Figure 5.8: Experimental setup 122

Figure 5.9: Plan view of experimental apparatus with naming convention..... 123

Figure 5.10: RTW connection stiffness for developed for numerical model 125

Figure 5.11: Failure of connection W1-L3 after sudden withdrawal during control experiment 127

Figure 5.12: Load-deflection relationship for each RTW connections during control experiment..... 128

Figure 5.13: RTW connection failure after application of retrofit system 129

Figure 5.14: Load-defection relationship for first connection failures during ‘Retrofit-New’ and Control experiments 130

Figure 5.15: Load-deflection relationship of RTW connections of the ‘Retrofit-New’ experiment..... 130

Figure 5.16: Vertical component of force in each load path..... 133

Figure 5.17: Axial force on cables of retrofit system vs. applied load 134

Figure 5.18: Axial force on external cables as external load applied 136

Figure 5.19: Load-deflection relationship for selected RTW connections, experimental results and numerical prediction..... 137

Figure 5.20: Tensile force on external cables vs. load applied..... 139

Figure 5.21: Experimental result and numerical prediction for force in RTW connections as load is applied 140

Figure 5.22: Close-up of sheathing damage at eve after completion of the experiment 141

Chapter 1

1 Introduction

1.1 General

The vast majority of structures in North America are residential. Light-framed wood construction is preferred in this region due to the low cost, the availability of materials and the ease of construction. Typical light-framed wood structures, which satisfy span and load limits, follow the prescriptive requirements of governing building codes to determine the member sizes and connection details. Most residential light-framed wood structures meet these guidelines; consequently, structural analysis is not needed for the design of these structures.

Past high speed wind events have exposed vulnerabilities in existing residential light-framed wood structures, with the resulting damage being a major source of economic loss. For example, the damage to light-framed wood structures represented a large portion of the US$20-25 billion of economic losses caused by Hurricane Andrew in 1992 (HUD, 1993), with approximately 95% of those losses resulting from failure of components of the roof system (Baskaran and Dutt, 1997). While light-framed wood structures preformed much better during Hurricane Katrina in 2005, the lack of a continuous load path from the roof to the foundation was still found to result in structural damage leading to economic loss (van de Lindt et al., 2007). Pielke et al (2008) presented a normalized analysis of hurricane damage over the last decade and found that increased population and infrastructure in coastal regions could increase the economic loss caused by future hurricanes unless mitigation strategies are implemented. The focus of this research is to

develop a mitigation technique that reduces the economic loss that result from damage to light-framed wood structures in extreme wind events.

A major source of the economic loss caused by damage to light-framed wood structures in extreme wind events, as identified by post hurricane damage reports, results from the lack of a continuous load path from the roof to the foundation. Under the loading of high speed wind, the roof system becomes subjected to uplift pressures generated in two ways. First, as the air separates from the roof structure, a negative pressure is applied to the roof sheathing. The second way by which roof uplift is generated occurs after a failure in the building envelope on the windward wall. High internal pressures are then generated, add to with the effect of the external negative pressure, resulting in large global roof uplift pressures acting on the roof system. Under this uplift loading, the sheathing-to-truss (STT) and the roof-to-wall (RTW) connections have been identified as weak links in the load path of the structure (FEMA, 1993; van de Lindt et al., 2007). Both types of connection rely on the withdrawal capacity of the nail to transfer the uplift forces to the foundation. Complete structural collapse can occur as a result of either failure mode, increasing economic loss and endangering the lives of the inhabitants. Figure 1.1 and Figure 1.2 show examples of damage resulting to light-framed wood structures from STT and RTW connection failures respectively.

Figure 1.1: Failure of roof sheathing above gable end, source: www.floridadisaster.org

Figure 1.2: Example of roof system failure after multiple RTW connection failures, source: www.Disastersafety.org

The failures of previous structures suggest that the behaviour of light-framed wood structures under uplift loading must be improved. As discussed below, past research has focused on: studying the load sharing behaviour of the structure using numerical and

experimental techniques, improving the strength of the individual connections with new technologies and more stringent building codes, and developing retrofitting systems to improve the strength of existing structures.

1.2 Background

1.2.1 Numerical and Experimental Studies of Structural Behaviour

In an attempt to better understand the behaviour of a light-framed wood structure, numerous experimental and numerical studies have been conducted. The recent focus has been full-scale, three-dimensional experimental and numerical work.

Morrison et al. (2012) loaded a full-scale structure built to the provisions of the Ontario Building Code with a realistic pressure distribution. The loading, which was developed from a wind tunnel study, was simulated using a system of 58 pressure bags, resulting in a spatially and temporally varying roof sheathing pressure. They found that the structure demonstrated significant load sharing, resulting in tributary area loads on the RTW connections that were significantly above the failure loads anticipated from experiments on individual toe-nail connections. Under the peak pressures of the realistic pressure distribution, the RTW connections were found to suffer permanent withdrawal, becoming increasingly damaged as the experimental loading progressed to higher wind velocities. This connection damage was confirmed in the individual connection testing completed by Morrison and Kopp (2011). The realistic wind loading applied during this study was unique, as previous studies had focused on the behaviour of the toe-nail connection under ramp loading. The testing of the individual connections found permanent withdrawal occurred under the peak loads. During the unloading and reloading phases after damage,

the stiffness of the connection remained similar to that of the initial stiffness of the connection.

Zisis and Stathopoulos (2012) studied the behaviour of an as-built, gable-style light-framed wood structure under environmental loading. The structure was implemented with load cells between the walls and foundation. Pressure taps on the structure and local weather monitoring stations provided information about the magnitude of the applied wind loading. The study found that approximately 30% of the total applied uplift force was transferred through the gable walls to the foundation. The experimental study was complemented with the dynamic analysis of a finite-element model consisting of frame, area and rigid link elements. Due to the energy dissipation within the structure, the wind load acting on the foundation was approximately 17 to 28% less experimentally than predicted by the numerical model.

Shivarudrappa and Nielson (2013) developed a finite-element model of a gable roof structure, validated using the experimental work of Datin and Prevatt (2013). Linear frame and shell elements were used with nonlinear link elements to capture the behaviour of the structure. The model was used to study the sensitivity of the distribution of the applied load at the RTW connections on the properties of the materials and connections within the structure. The sensitivity analysis found that the stiffness of the RTW connections had a large effect on the load sharing behaviour of the structure. Increasing the stiffness of the RTW connections reduced the amount of applied load shared to surrounding trusses. Increasing the bending stiffness of the sheathing was found to increase the load shared between the trusses. The study also found that the additional

RTW connections created along the gable end truss reduced the forces acting on the RTW connections of the next closest truss.

Li et al (1998) created a finite-element model of a truss system using the commercial software ETABS. The trusses were modeled using frame elements with increased bending stiffness for the top chord members to capture the partially composite behaviour created by the sheathing. The behaviour of the sheathing was captured using beam elements. The moment transferred by the gusset plate connection between truss members was neglected. The developed model showed good agreement with the experimental results presented in previous literature in terms of deflection, member axial force, and load distribution.

In general, numerical and experimental studies of full-scale light-framed wood structures have been completed to study their behaviour under uplift loading. The increased understanding of the load sharing behaviour will result in better design practices, thereby reducing the probability of failures in future structures.

1.2.2 Current Technology and Building Code Development

To address the capacity problems of the identified critical connections, product development has occurred. An example of this is the “HurriQuake” nail, developed to increase the capacity of the STT connection. The “HurriQuake” nail uses a harder shank than a standard air nail to increase the reliability of truss penetration. The “HurriQuake” nail also has a ring shank to increase withdrawal resistance, as well as a larger head diameter. When testing sheathing panels connected to wood members using this nail, the mean uplift capacity of the sheathing panels improved by 32% above that measured for

panels connected with 8d common nails (IHRC, 2012). Product development has also addressed the issue of the capacity of the RTW connection. The truss tie (hurricane clip) is a steel strap used to attach the truss to the top plate of the wall or the wall studs. This strap complements the toe-nail connection, removing the withdrawal demand placed on the nails. Available in many sizes, the tie can increase RTW connection uplift capacity to 7.6kN (Simpson Strong-Tie, 2008), approximately a 400% increase above that of a three, 16d toe-nail connection. Simpson Strong-Tie has developed steel ties for use throughout the structure to create a continuous load path from the roof to the foundation. The use of the "HurriQuake" nail and the steel straps to complement the nailed connections can provide an efficient solution to the problems caused by uplift loading for new structures; however, non-structural elements limit access to both the critical connections in existing structures, making these technologies difficult to apply as a retrofit.

The issues in the capacity of the critical connections have also been addressed by increasing the requirements of the building codes, which are constantly improving as research and the lessons learned from extreme wind events identify the vulnerabilities of the current version of the code. Major improvements were made to the South Florida Building Code following Hurricane Andrew, increasing the capacity of both of the critical connections discussed above. These changes were adopted locally in 1994 before becoming standard for the entire state of Florida in 2001 (Gurley et al., 2006). Building code changes have also occurred in Canada. For example, the most recent edition of the National Building Code of Canada (NRC, 2010) defined high wind areas, in which the capacity required for both the STT and the RTW connections are increased above that of the previous edition.

As code improvements are made, previously constructed buildings remain with known vulnerabilities. Structures built before 1994 in the coastal regions of the United States are extremely vulnerable to uplift forces caused by wind, as the majority use insufficient nails for the STT connection (Datin et al., 2011). Thus, recent changes of building codes, along with the known vulnerabilities of the structures constructed under previous editions of those codes, suggests that a retrofit system capable of improving the uplift behaviour of light-framed wood structures is needed.

1.2.3 Retrofitting Technology

While improved building codes have been found to reduce the number of failures resulting from high speed winds in new structures (Meloy et al., 2007), existing structures remain vulnerable. As a need has been identified, research has been conducted on the development of retrofit techniques for light-framed wood structures.

Past attempts to develop retrofit techniques that have been presented in the literature have focused on increasing the capacity of the individual critical connections. Datin et al (2011) tested a sprayed polyurethane foam adhesive applied from within the structure to the sheathing and truss members, reducing the withdrawal demand on the STT connections. The experimental work found that the foam adhesive was effective at increasing the uplift capacity of the roof sheathing by 250-300%. In another study, Canbek et al (2011) investigated the use of a fiber reinforced polymer (FRP) tie to create the RTW connection. Adhesives are used to bond the FRP tie to the top plate and the truss to create the RTW connection. This technology is intended to replace or improve the capacity of the current toe-nail or hurricane clip. The FRP tie provided 1.65 times increase in ultimate capacity when compared to a standard hurricane clip.

The previous two retrofit techniques require access to the critical connections for installation, which can be costly due to the non-structural elements that are typically installed in a residential home. Stewart et al (2003) presented an economic analysis of the vulnerability of existing residential structures. They estimated that the cost of increasing the hurricane resistance of a structure during construction ranges from 1-10% the cost of the structure. This cost increases to 15-50% to retrofit a current structure, a large cost that is a deterrent to many home owners.

Little technical research has been presented on a retrofit system which is economical, easy to apply, and effective without modification to the existing structure; however, patents have been issued on the subject. In general, these patents focus on a tension element placed over the structure that is attached to ground anchors. These systems also tend to include a pretensioning devise (ratchet or turnbuckle).

The patents issued for Bachynski (2007), Gaffney (1998), Gitlin and Maloney (1998), and Watson Jr. (2008) all contain a retrofit system with a very fine fabric mesh placed over the structure. The systems presented cover the entire roof of the structure, increasing the capacity of both the STT and RTW connections. These harness systems also focus on protecting the windows of the structure by continuing the fabric mesh to the ground to protect the structure from flying debris, thereby maintaining the integrity of the building envelope. While providing an effective retrofit system, the fine fabric mesh appears difficult to apply to a structure quickly, resulting in a permanently installed system.

The patents issued to Bimberg and Bimberg(1997) and Luzzi (1999) contain systems with individual tension elements that are placed over the roof and attached to anchoring

devices. In the system presented by Bimberg, a series of steel cables, connected to wooden bearing pads, are applied over the roof of the structure and independently connected to the ground. A more simple design is proposed by Luzzi. This patented system is simply a nylon ratchet strap that is placed over the roof of the structure and attached to the foundation using an anchoring device. While providing economic and easy-to-apply retrofit techniques, these systems provide few tension members along the roof, which can result in high local stresses on, and damage to, the fascia board of the structure. Few tension members along the length of the roof would also reduce the ability of the system to prevent failure of the sheathing. As the STT connection failure results in a large amount of economic loss during high speed wind events, a system which reduces the probability of this failure mode, while remaining inexpensive and easy to apply, is necessary.

1.3 Objectives of Study

The objective of this research is to analyze the behaviour of a proposed retrofit system using numerical and experimental techniques. The proposed system consists of a series of cables placed along the sheathing of the roof, identified as the bearing cables in Figure 1.3 and Figure 1.4. Along the eave of the structure, the bearing cables are attached to rigid bars. Cables containing a prestressing device, identified as the external cables in Figure 1.3 and Figure 1.4, connect the rigid bars to piles which are permanently installed in the ground. When a high speed wind warning is announced, the system can be easily applied to the roof of the building and attached to the piles. This system provides the uplift forces an alternate load path to the ground without travelling through the weak nailed connections within the structure. Figure 1.3 and Figure 1.4 show the retrofit idea

as applied to a gable-style roof. While similar in idea to the systems which have been patented in the past, the inclusion of the rigid bar reduces the number of required ground anchors. The rigid bar also works to provide a uniform distribution of force in the bearing cable elements, reducing magnitude of local bearing forces acting on the structure. The proposed system should provide improved capacity to both the STT and RTW connections while being an easy to apply, cost effective system.

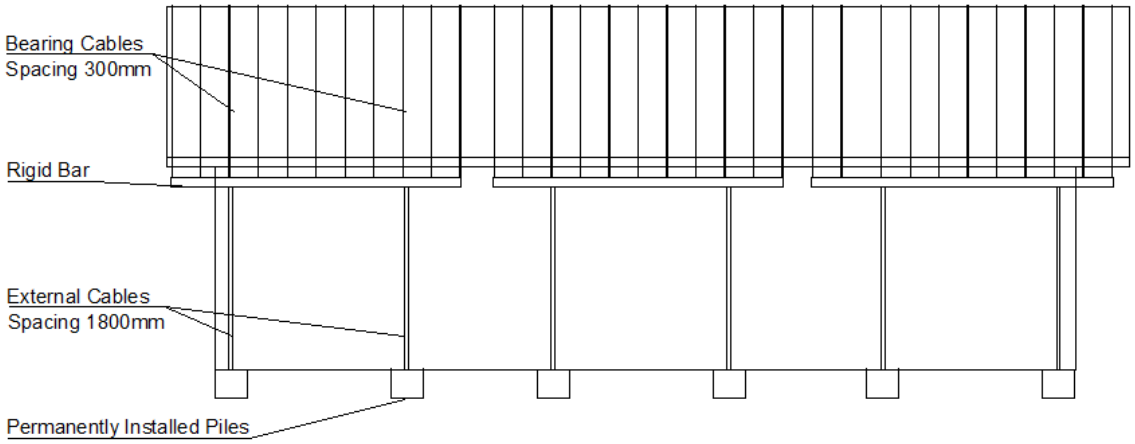

Figure 1.3: Elevation view of proposed retrofit system as applied to a gable-style roof

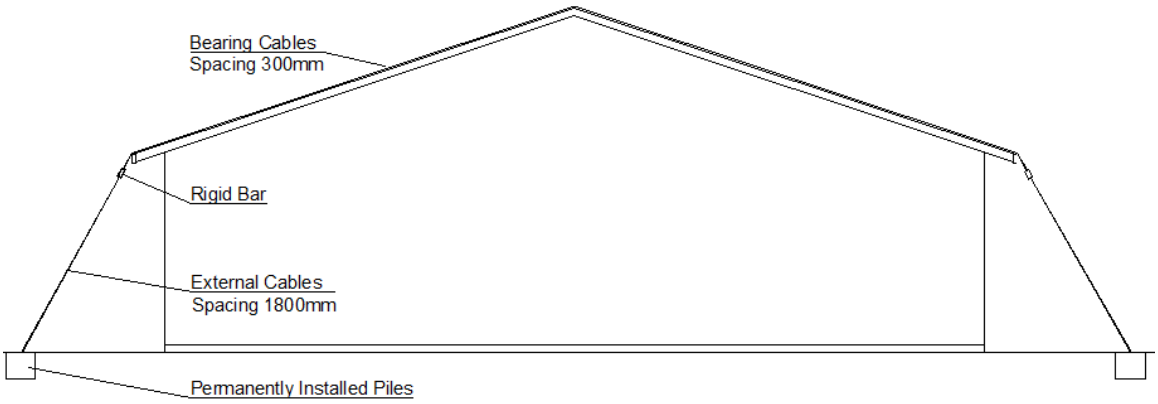

Figure 1.4: Elevation view of proposed retrofit system as applied to a gable-style roof

The adequacy of the retrofit system will be assessed as follows:

- Develop a three-dimensional, numerical model capable of capturing the behaviour of a light-framed wood structure under a realistic wind pressure. The model

should match the full-scale experimental results obtained by Morrison et al. (2012)

- Conduct an experimental program on a retrofitted section of a light-framed wood structure to assess the ability of the retrofit system to increase the uplift capacity of the roof structure.
- Use the experimental results to validate the assumptions of the numerical model in terms of capturing the load distribution between the truss and retrofit systems.
- Conduct a numerical parametric study to understand the relationship between the properties of the components of the retrofit system and the behaviour of the structure.
- Determine the effect that varying the dimensions of each retrofit system component has on the behaviour of the structure after retrofitting and the force distribution within the retrofit system.
- Optimize the retrofit system to provide a minimum weight while satisfying selected design constraints at a design wind speed.
- Assess the behaviour of the optimum retrofit system under multiple non-uniform pressure distributions.

1.4 Thesis Structure

This thesis has been prepared in the integrated article format. This chapter provides the motivation for the current work by discussing the vulnerability of light-framed wood structures under uplift loads. A review is completed on past numerical and experimental studies that focused on studying the behaviour of wood structures under uplift load. The strategies that have been implemented to mitigate the damage to these structures is also

presented, including the development of new connection technologies and retrofit techniques, as well as building code improvements. The objects of the thesis, which are addressed in the following chapters, are clearly defined. Chapter six provides a summary of the conclusions of this research, as well as suggestions for future work.

1.4.1 Finite-Element Modeling of a Light-Framed Wood Rood Structure

Chapter two focuses on understanding the behaviour of light-framed wood structures under uplift loading. A three-dimensional finite-element model capable of capturing the behaviour of a light-framed wood structure under a realistic pressure distribution is developed. The formulation of the numerical model is described, followed by validation with a recently conducted full-scale experiment. After validation, the model is used to analyze the behaviour of the truss system under realistic and equivalent uniform pressure distributions and to perform an assessment of the use of the tributary area method to calculate the withdrawal force resulting at each RTW connection.

1.4.2 Parametric Study of Retrofit System for Light-framed Wood Structures under Uniform Uplift Load

Chapter three uses a developed numerical model to complete a parametric study on the components of the retrofit system. This chapter begins with a description of the developed numerical model. The model is used to study the typical behaviour of the structure under a uniform pressure after application of the retrofit system. The results of the parametric study are presented, with a focus on the effect that variation of each design variable has on: a) the improvement of the structural behaviour resulting from application of the retrofit system and b) the distribution of forces in the retrofit system.

1.4.3 Analysis and Optimization of a Retrofit System for Light-Framed Wood Structures under Wind Loading

Chapter four begins by extending the developed numerical model of the light-framed wood structure to include plastic damage at the RTW connection. After validation of the model with the results of a full-scale experiment, the nonlinear model is used to assess the behaviour of the proposed retrofit system under multiple non-uniform pressure distributions. The components of the retrofit system are optimized to provide a minimum weight while satisfying structural design constraints at a design wind speed. The optimal system is then assessed under non-uniform pressure distributions to evaluate the increase in capacity of the structure after application of the retrofit system.

1.4.4 Experimental Testing of a Retrofit System to Increase Uplift Capacity of Light-Framed Wood Structures

Chapter five focuses on an experiment conducted to test the proposed system on a section of roof. The idea of the retrofit system is first introduced, with a summary of the numerical work previously completed. The results of the experiment are presented, with a focus on the behaviour of the truss system after application of the retrofit system, as well as the ability of the system to increase the capacity of the structure. The experimental results are then used to validate the assumptions of the numerical model to gain confidence in its adequacy.

1.5 References

Bachynski, M. (2007). *U.S Patent No. 20070022672*. Washington, DC: U.S. Patent and Trademark Office.

Baskaran, A. and Dutt, O. (1997). Performance of roof fasteners under simulated loading conditions. *Journal of Wind Engineering and Industrial Aerodynamics*, *72*(0), 389-400

Bimberg, U., and Bimberg, O. (1997), *U.S Patent No. 5623788.* Washington, DC: U.S. Patent and Trademark Office.

Canbek, C., Mirmiran, A., Chowdhury, A., and Suksawan, N. (2011). Development of Fiber-Reinforced Polymer Roof-to-wall Connection. *J. Compos. Constr., 15*(4), 644-652.

Datin, P. L., Prevatt, D. O., and Pang, W. (2011). Wind-uplift capacity of residential wood roof-sheathing panels retrofitted with insulating foam adhesive. *Journal of Architectural Engineering, 17*(4), 144-154

Department of Housing and Urban Development (HUD). (1993). *Assessment of Damage to Single-Family Homes Caused by Hurricanes Andrew and Iniki*. U.S., Office of Policy and Development and Research, HUD-0006262.

Federal Emergency Management Agency (FEMA). (1993). *Building Performance: Hurricane Iniki in Hawaii - Observations, Recommendations, and Technical Guidance.* Federal Emergency Management Agency.

Gaffney, G. (1998). *U.S Patent No. 5819477.* Washington, DC: U.S. Patent and Trademark Office.

Gitlin, H. M. and Maloney, Jr., J. W. (1998), *U.S Patent* No. 5791090, Washington, DC: U.S. Patent and Trademark Office.

Gurley, K., Davis, R.H., Ferrera, S.P., Burton, J., Masters, F., Reinhold, T., and Abdullah, M. (2006). Post 2004 hurricane field survey – an evaluation of the relative performance of the Standard Building Code and the Florida Building Code. *Proc. 2006 ASCE/SEI* Structures Congress, St. Louis, MO. 8.

International Hurricane Research Center (IHRC). (2012). *Hurricane loss reduction for housing in Florida: Roof Sheathing Fastener Stud*y. Florida International University, Miami, USA.

Li, Z., Gupta, R., and Miller, T. H. (1998). Practical approach to modeling of wood truss roof assemblies. *Practice Periodical on Structural Design and Construction, 3*(3), 119-124.

Luzzi, J. (1999). *U.S Patent No. 5881499.* Washington, DC: U.S. Patent and Trademark Office.

Meloy, N., Sen, R., Pai, N., and Mullins, G. (2007). Roof damage in new homes caused by hurricane charley. *Journal of Performance of Constructed Facilities, 21*(2), 97-107.

Morrison, M. J., Henderson, D. J., and Kopp, G. A. (2012). The response of a wood-frame, gable roof to fluctuating wind loads. *Engineering Structures, 41,* 498-509.

Morrison, M. J., and Kopp, G. A. (2011). Performance of toe-nail connections under realistic wind loading. *Engineering Structures*,*33*(1), 69-76.

National Research Council of Canada (NRC). (2010). *National Building Code of Canada (NBCC) 2010*. Ottawa, NRCC 53301

Pielke, R. A., Gratz, J., Landsea, C. W., Collins, D., Saunders, M. A., and Musulin, R. (2008). Normalized hurricane damage in the united states: 1900-2005. *Natural Hazards Review, 9*(1), 29-42.

Shivarudrappa, R., and Nielson, B. G. (2013). Sensitivity of load distribution in light-framed wood roof systems due to typical modeling parameters. *Journal of Performance of Constructed Facilities, 27*(3), 222-234

Stewart, M. G. (2003). Cyclone damage and temporal changes to building vulnerability and economic risks for residential construction. *Journal of Wind Engineering and Industrial Aerodynamics, 91*(5), 671-691

Simpson Strong-Tie Company Inc. (2011). *Technical Bulletin, Uplift Connectors, Truss-to-Wall Tiedowns (Spruce-Pine-Fir*). Pleasanton, California.

van de Lindt, J., Graettinger, A., Gupta, R., Skaggs, T., Pryor, S., and Fridley, K. (2007). Performance of wood-frame structures during Hurricane Katrina. *Journal of Performance of Constructed Facilities, 21*(2), 108-116.

Watson, Jr., A. (2006). *U.S. Patent No. 7392620*. Washington, DC: U.S. Patent and Trademark Office.

Zisis, I., and Stathopoulos, T. (2012). Wind load transfer mechanisms on a low wood building using full-scale load data. *Journal of Wind Engineering and Industrial Aerodynamics, 104-106*, 65-75

Chapter 2

2 Finite-Element Modeling of a Light-Framed Wood Roof Structure

2.1 Introduction

Residential light-framed wood structures are very common in North America due to the ease of construction, the low cost, and the availability of materials and labour. Construction using of repetitive wood members, sheathing panels, and non-structural elements results in a structure with a high degree of redundancy, as well as complex and indeterminate load paths. Typical residential wood structures, subject to span and live load limits, are not analyzed by an engineer. Instead member sizes and connections details follow the prescriptive requirements of the local governing building code. Past extreme wind events have exposed the vulnerability of this type of structure to the uplift loading that results from high winds, with the sheathing-to-truss (STT) connections and the roof-to-wall (RTW) connections being identified as the most critical connections in the load path (FEMA, 1993; Shanmugam et al., 2009). The damage that resulted to light-framed wood structures represented a large portion of the US$20-25 billion of economic loss that was caused by Hurricane Andrew in 1992 (HUD, 1993). Approximately 95% of this loss resulted from failures of materials of the roof system (Baskaran and Dutt,1997). While light-framed wood structures preformed much better during Hurricane Katrina in 2005, the lack of a continuous load path from the roof to the foundation was still found to result in structural damage leading to economic loss (van de Lindt et al., 2007).

As extreme wind events expose the vulnerabilities of existing structures, building codes change to improve the capacity of new structures. For example, the most recent edition of

the National Building Code of Canada defined high wind areas, in which the capacities required for both the STT and the RTW connections are increased above that of the previous edition (NRC, 2010). Recent changes have also occurred to the Florida Building Code. Major improvements were made to the South Florida Building Code following Hurricane Andrew. These changes were adopted locally in 1994 before becoming standard for the entire state of Florida in 2001 (Gurley et al., 2006). As building codes are improved, existing structures remain with known vulnerabilities, as they are built to the standard of an outdated code. Structures built before 1994 in the coastal regions of the United States are extremely vulnerable to the uplift forces caused by wind as the majority are constructed with insufficient nails for the STT connections (Datin et al., 2011). The large economic loss that has occurred, the frequent building code changes, and the vulnerability of existing structures all demonstrate the need to better understand the behaviour of light-framed wood structures in high speed wind events.

In an attempt to better understand the behaviour of light-framed wood structures under uplift loading, researchers have used a combination of experimental and numerical studies. Morrison et al. (2012) loaded a full-scale structure built to the provisions of the Ontario Building Code with a realistic pressure distribution. The loading, which was developed from a wind tunnel study, was simulated using a system of 58 pressure bags, resulting in a spatially and temporally varying roof sheathing pressure. They found that the structure demonstrated significant load sharing, resulting in tributary area loads on the RTW connections that were significantly above the failure loads anticipated from experiments on individual toe-nail connections. Under the peak pressures of the realistic pressure distribution, the RTW connections were found to suffer permanent withdrawal,

becoming increasingly damaged as the experimental loading progressed to higher wind velocities. This connection damage was confirmed in the individual connection testing completed by Morrison and Kopp (2011). The realistic wind loading applied during this study was unique, as previous studies had focused on the behaviour of the toe-nail connection under ramp loading. The testing of the individual connections found that permanent withdrawal occurred under the peak loads. During the unloading and reloading phases after damage, the stiffness of the connection remained similar to that of the initial stiffness of the connection.

Zisis and Stathopoulos (2012) studied the behaviour of an as-built, gable-style light-framed wood structure under environmental loading. The structure was implemented with load cells between the walls and foundation. Pressure taps on the structure and local weather monitoring stations provided information about the magnitude of the applied wind loading. The study found that approximately 30% of the total applied uplift force was transferred through the gable walls to the foundation. The experimental study was complemented with the dynamic analysis of a finite-element model consisting of frame, area and rigid link elements. Due to the energy dissipation within the structure, the wind load acting on the foundation was approximately 17 to 28% less experimentally than predicted by the numerical model.

Shivarudrappa and Nielson (2013) developed a finite-element model of a gable roof structure, which was validated using the experimental work of Datin and Prevatt (2013). Linear frame and shell elements were used with nonlinear link elements to capture the behaviour of the structure. The model was used to study the sensitivity of the distribution of the applied load at the RTW connections on the properties of the materials and

connections within the structure. The sensitivity analysis found that the stiffness of the RTW connections had a large effect on the load sharing behaviour of the structure. Increasing the stiffness of the RTW connections reduced the amount of applied load shared to surrounding trusses. Increasing the bending stiffness of the sheathing was found to increase the load shared between trusses. The study also found that the additional RTW connections created along the gable end truss reduced the forces acting on the RTW connections of the next closest truss.

Li et al. (1998) created a finite-element model of a truss system using the commercial software ETABS. The trusses were modeled using frame elements with increased bending stiffness for the top chord members to capture the partially composite behaviour created by the sheathing. The behaviour of the sheathing was captured using beam elements. The moment transferred by the gusset plate connection between truss members was neglected. The developed model showed good agreement with the experimental results presented in previous literature in terms of deflection, member axial force, and load distribution.

This chapter further investigates the behaviour of light-framed wood structures under the uplift loading of a realistic pressure distribution. A three-dimensional finite-element model is first developed to capture the behaviour of a full-scale experiment recently conducted by at The University of Western Ontario. After describing the components used to develop the numerical model, a comparison between the numerical prediction and experimental results in terms of the deflected shape at the RTW connections is presented to gain confidence in the numerical model. The model is then used to analyze the behaviour of the truss system under realistic and equivalent uniform pressure

distributions and to perform an assessment of the use of the tributary area method to calculate the withdrawal force resulting at each RTW connection.

2.2 Description of the Conducted Experiment

An experiment has been recently conducted at the Insurance Research Lab for Better Homes at the University of Western Ontario to study the behaviour of a light-framed wood structure under a realistic wind pressure distribution. The tested structure, shown in Figure 2.1, was built to the provisions of the Ontario Building Code and inspected to ensure that it matched the typical construction techniques of the area. A realistic pressure distribution was developed from a wind tunnel study and simulated using a system of 58 pressure bags, resulting in an applied pressure to the roof sheathing that varied in both time and space. The pressure bags ranged from 0.36 m^2 to 5.8 m^2 in area. As shown in Figure 2.2, the smallest bags were located at the windward edge of the structure, where the largest variation in the magnitude of pressure occurs for the selected wind angle. The magnitude of the realistic pressure distribution that was initially applied to the structure corresponded to a mean wind velocity of 20 m/s at roof height. The wind velocity was increased by 5 m/s until failure of the RTW connections, which occurred under the pressure corresponding to a 45 m/s wind velocity. As the pressures were applied, the resulting deflection at each RTW connection was recorded. Further details of the experimental procedure are available in Morrison (2010).

Figure 2.1: Full-scale experimental set-up with steel reaction frame (source: http://www.eng.uwo.ca/irlbh/)

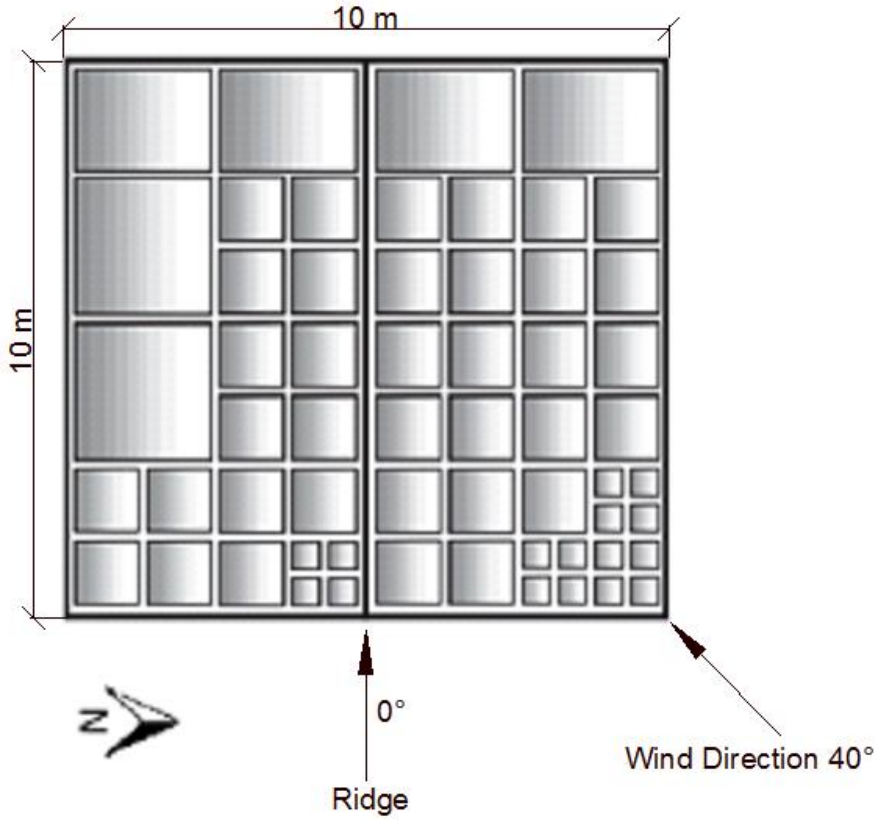

Figure 2.2: Plan view of pressure box distribution for the full-scale experiment (Source: Morrison, 2010)

2.3 Numerical Modeling of the Roof Structure

The experimental structure is numerically modeled using the finite-element program SAP 2000 (Computers and Structures, Inc., 2009). A plan view of the structural skeleton of the roof system is provided in Figure 2.3, followed by a description of the various components of the numerical model.

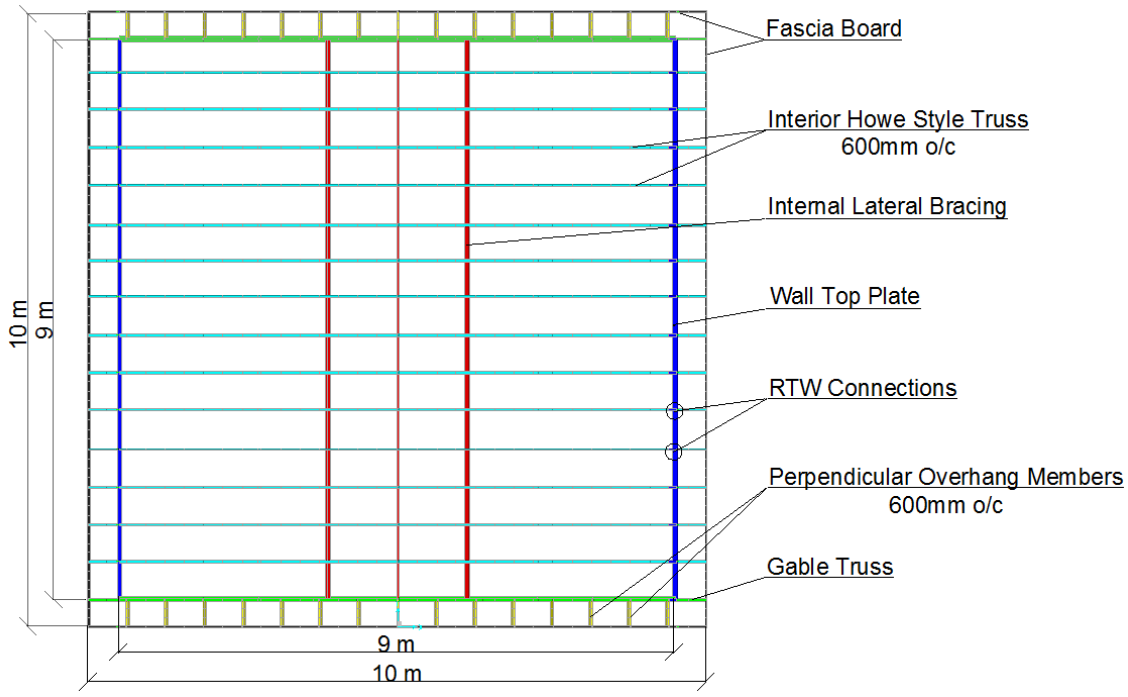

Figure 2.3: Plan view of structural skeleton of roof system

2.3.1 Interior Trusses

Linear frame elements are used to model the wood members of the truss system. The structure contains 14 interior, Howe-style trusses spaced at 600mm (2ft) centers with the dimensions shown in Figure 2.4. Top and bottom chords of the trusses are 39mm x 89mm (2x4) members. Interior webbing of the trusses are constructed of 39mm x 64mm (2x3) members. The material properties for the frame elements are provided by the Canadian Wood Design Manual (CWDM) (CWC and CSA, 2010) for SPF, No. 1/No. 2 lumber.

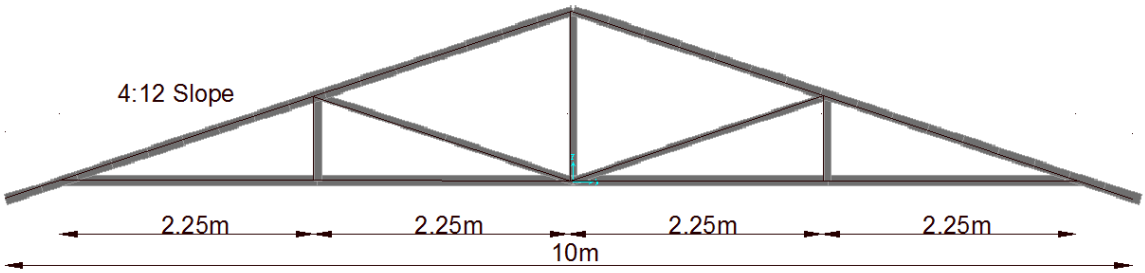

Figure 2.4: Elevation view and dimensions of interior Howe-style truss

Physical connections between the members within each truss are made with metal "gusset" plates. Li et al (1998) conducted numerical modeling of a wood truss system and concluded that, when compared to experimental literature, neglecting the moment transfer of the gusset plate connection resulted in a more accurate force distribution within truss members than a fully rigid, gusset plate connection. Moment is transferred through a gusset plate when the member is continuous through the connection, as is the case on the top and bottom chords of the truss. Figure 2.5 shows the locations of the moment releases applied to the numerical model to capture the behaviour of the truss described by Li et al (1998).

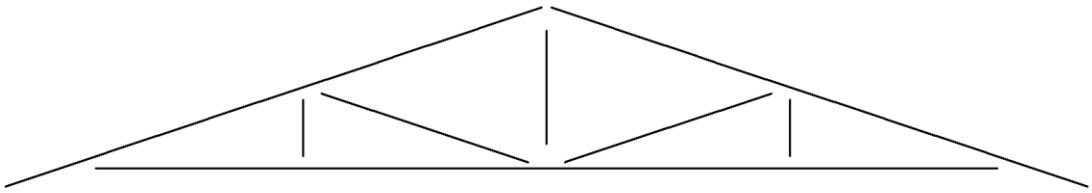

Figure 2.5: Moment releases included in the finite-element model

2.3.2 Gable Truss

The two exterior trusses, identified as the gable trusses in Figure 2.3, contain modifications when compared to the interior trusses. Each gable truss has additional vertical webbing for the support of the external sheathing. Also, as the gable truss is

continuously supported by an external wall, extra RTW connections are made along the length of the truss. These connections result in the gable truss having a higher stiffness than the interior trusses. As shown in Figure 2.6, additional vertical members are included in the numerical model of the gable trusses to match the experimental structure, with additional RTW connections at each location where a vertical member intersects the bottom chord of the truss. Similar to the numerical formulation of the interior trusses, moment releases are applied to each member of the gable trusses unless the member is continuous through the gusset plate connection.

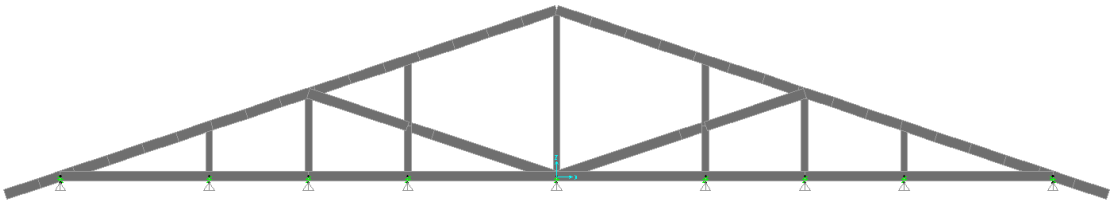

Figure 2.6: Gable end trusses of numerical model with additional external RTW connections

2.3.3 Plywood Sheathing

A total of 2112 shell elements are used to model the plywood sheathing of the roof. Shell elements have membrane and bending capabilities allowing them to deform in and out-of-plane, simulating the realistic behaviour of the sheathing. Each element has an approximate area of .05 m^2. The smallest pressure boxes in the full-scale experiment are represented by 8 area elements in the finite-element model.

Wood is an anisotropic material, with strength dependent on the direction of the grains. The stiffness of plywood sheathing is dependent on the layout of the grains of the plies. To account for this, a modification factor is used to reduce the bending stiffness of the sheathing in the direction perpendicular to the face grains to match the properties given

by the CWDM. For 12mm CSP plywood constructed with 4 plies, the bending stiffness is 9 times larger in the direction of the face grains than that in the direction perpendicular to the face grains (CWC and CSA, 2010). Thus, a factor of 0.11 is applied as an inertia multiplier to reduce the bending stiffness of the shell element in this weak axis.

The plywood sheathing increases the bending stiffness of the top chord of the truss as partially composite behaviour occurs and a "T" beam is created. To capture this behaviour, the center line of the shell elements have been offset from the centerline of the top chord of the truss. The nodes of the top chord are connected to the nodes of the sheathing using a body constraint to model composite behaviour.

2.3.4 Roof-to-Wall Connection

A multi-linear force-deflection relationship, used to simulate the behaviour of the toe-nail connection, is captured using a multi-linear elastic link element. A typical load-deflection relationship for a toe-nail connection, as shown in Figure 2.7, is used in the numerical model. This connection property has been adapted from the experimental work presented by Reed et al. (1997), and is based on the average of 16 tests. The load deflection curve has a high stiffness when subjected to a negative load, representing the truss bearing on the top plate of the wall. Under withdrawal loading, the connection has an initial stiffness of 550 kN/m, with an ultimate capacity of 1.8 kN.

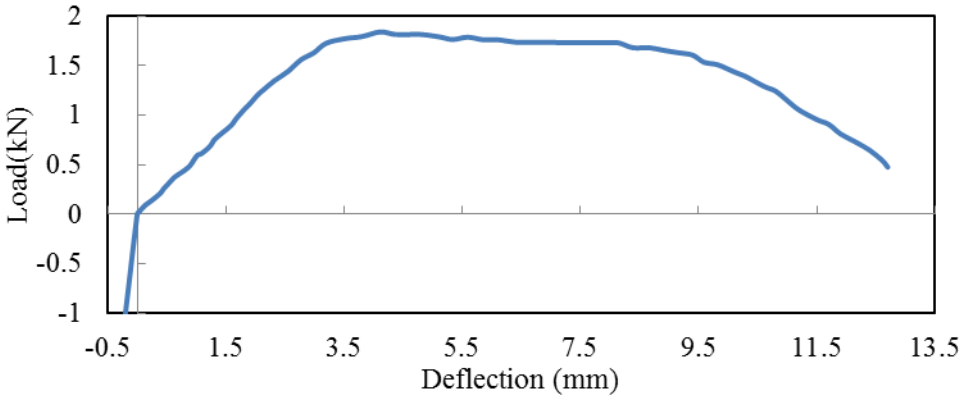

Figure 2.7: RTW connection load-deflection relationship (adapted from Reed et al. 1997)

2.3.5 Roof Overhang

The roof system overhangs the top plate of the walls by approximately 500mm in each direction. Figure 2.4 shows the construction method of the overhang in the direction parallel to the trusses. The top chord of the truss continues past the RTW connection by 500mm, supporting the sheathing. The numerical model includes a fascia board, shown in Figure 2.3, which is a 38mm by 89mm (2x4) member running perpendicular to the truss system, connecting the free end of the overhang of each truss.

A 500mm overhang is included at each gable end. The roof sheathing is supported by 38mm by 89mm (2x4) members connected perpendicular to the gable truss, identified as the perpendicular overhang members in Figure 2.3. A 38mm by 89mm (2x4) fascia board running parallel to the top chord of the truss is attached to the outer edge of each 38mm by 89mm (2x4) member. The fascia board supports the sheathing along the outermost edge of the overhang around the entire structure.

2.3.6 Boundary Conditions

It is assumed that the walls beneath the RTW connections have negligible effect on the deflections recorded experimentally as the members of the walls experience little axial

deformation under the magnitude of loading applied. The wall system is neglected and the boundary conditions of the numerical model are applied as deflection restraints immediately beneath the top plate of the exterior walls.

2.3.7 Load Input Data

The comparison between the experimental and numerical results is carried out by conducting quasi-static analysis. The natural period of the structure is well below the critical periods of the loading, as such, the dynamic effect should have negligible effect on the behaviour of the truss system. The nonlinear behaviour of the tested structure is found to occur mostly at the RTW connections, where permanent, nonlinear damage occurs as the peak pressures are applied. Before application of the first damaging peak pressure, the behaviour of the connection can be approximated as linear elastic (Morrison and Kopp, 2011). As such, the load cases considered for this analysis are selected before the first damaging peak pressure so that nonlinear behaviour of the RTW connections is not anticipated and quasi-static analysis is justifiable. Each selected load case is assessed under a snap shot of the non-uniform pressure distribution, assuming no initial deflection. To validate the numerical results at higher wind levels, after nonlinear damage to the RTW connections has occurred, time-history analysis becomes necessary.

Twelve load cases have been selected from the experiment before damage occurred. The loading of the selected time steps results in the largest global uplift forces applied to the structure before the connections sustain damage. Table 2.1 and Table 2.2 show the time steps selected from the full-scale experiment to validate the finite-element model. The global uplift force acting on the structure is larger than the dead load of the roof (approximately 15kN) for each selected pressure distribution.

Table 2.1: Load case selection from 20m/s TLP experiment

Load Case	1	2	3	4	5	6
Time in TLP test (sec)	57.10	96.96	279.32	361.48	651.76	755.46
Global Uplift Force (kN)	-21.3	-21.9	-22.3	-27.8	-22.0	-28.9

Table 2.2: Load case selection from 25m/s TLP experiment

Load Case	7	8	9	10	11	12
Time in TLP test (sec)	47.76	75.92	95.66	102.66	132.38	166.72
Global Uplift Force (kN)	-30.2	-30.8	-34.5	-30.2	-30.7	-32.4

Two pressure distributions, load case 5 and load case 12, are shown below in Figure 2.8 and Figure 2.9, respectively. The distribution of pressure in load case 5 shows a strong positive pressure in the windward corner, with a nearly uniform negative pressure applied over the remainder of the structure. The distribution of pressure in load case 12 shows a negative pressure applied over the entire roof system with stronger pressures above the east gable end. Load case 12 results in the largest experimental deflections for the critical connection before nonlinear damage initiates.

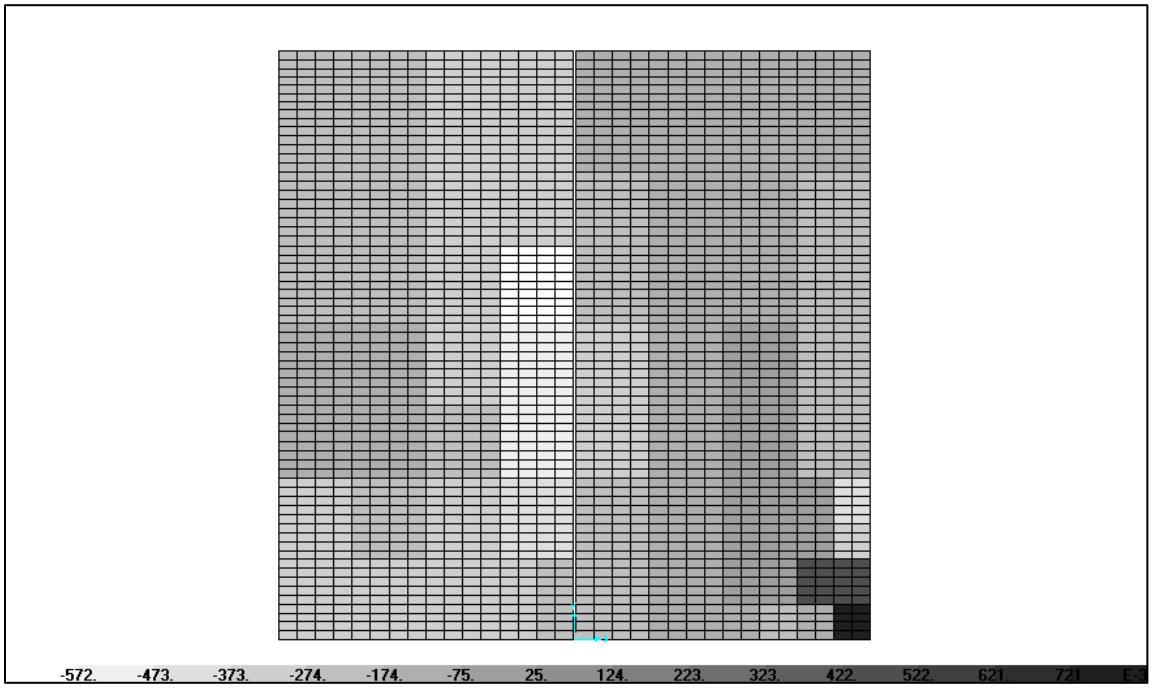

Figure 2.8: Pressure distribution for load case 5 (units = Pa)

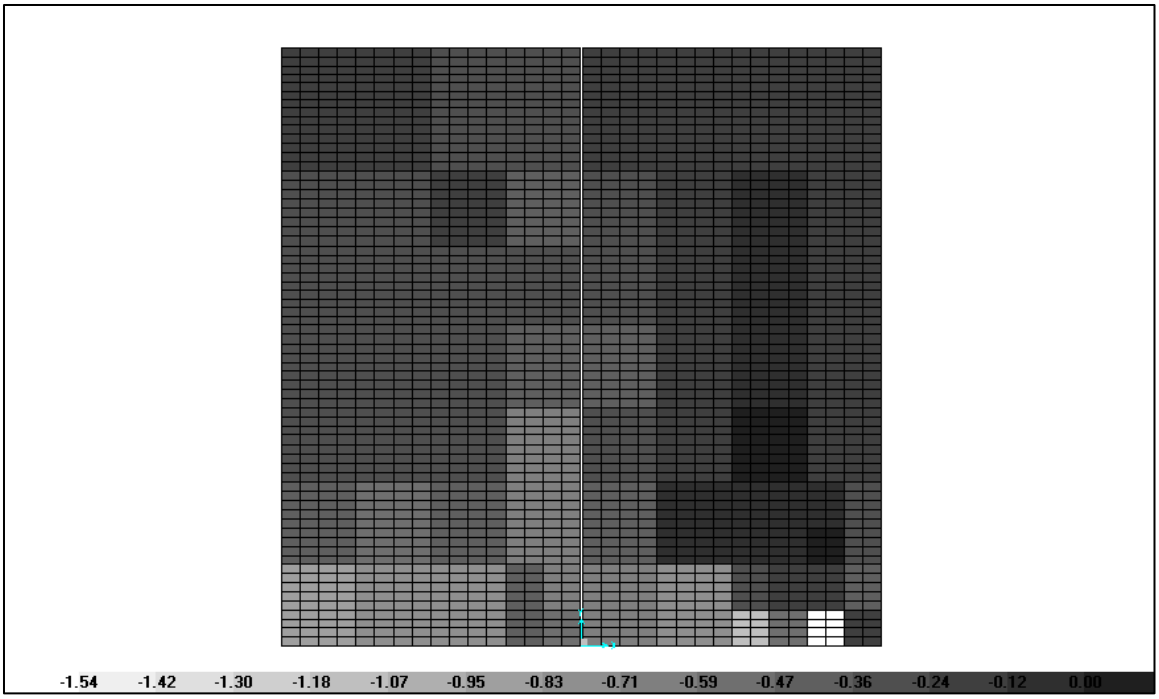

Figure 2.9: Pressure distribution for load case 12 (units = kPa)

2.4 Validation of the Numerical Model

The validation of the finite-element model includes a comparison between the numerical predictions and the experimental full-scale test results in terms of deflection values at the RTW connections. Each RTW connection is labeled as either a north or south link, followed by the truss number. The windward corner is labeled connection N-01, with numbers increasing along the length of the structure. Overhangs are labeled connections N/S-01 and N/S-18. The gable ends are connections N/S-02 and N/S-17. The critical connection during the experiment is identified as S-03.

For validation of the numerical model, the prediction of the deflected shape of the roof should be similar to the full-scale experimental results. Variation of individual connection magnitudes along the length is expected due to the variability of the toe-nail connection properties. The deflection of the RTW connections along the north and south walls is presented for load cases 5 and 12 in Figure 2.10 and Figure 2.11, respectively.

In terms of the deflected shape of the RTW connections along the length building, the prediction of the numerical model shows good agreement with the experimental results. For load case 5, in which the applied pressure is most uniformly distributed, the numerical model predicts a nearly uniform deflected shape along the building. The experimental results show more variability in the deflection of each connection. The average deflection for the south side connections when the roof is subjected to the applied pressure of load case 5 is 0.4mm for both the numerical prediction and the experimental results. For the deflection of the north connections presented in Figure 2.10, the numerical prediction and experimental results match very well in terms of average, with both having a value of 0.2mm.

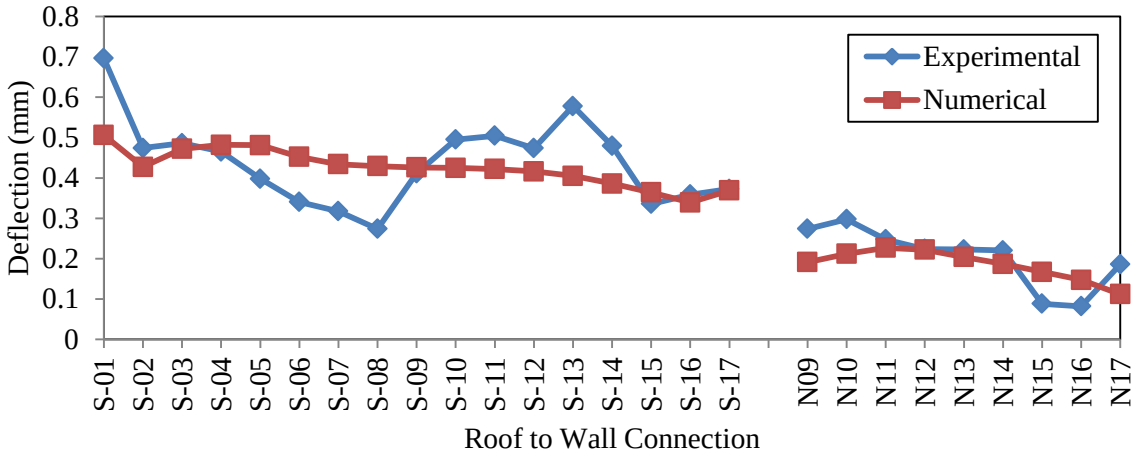

Figure 2.10: Deflection of the RTW connections for load case 5

Figure 2.11 shows the RTW connection deflection obtained under the applied pressure of load case 12. Under this applied loading, the numerical prediction matches the experimental results very well in terms of magnitude of deflection along the length of the structure. Also, there is strong agreement in the trend of deflection for the connections near the east gable on the south side. Both the numerical prediction and experimental results predict that connection S-02, located on the gable truss, experiences less

deflection than the surrounding connections. This local minimum results from the increased stiffness of the gable truss due to the additional RTW connections. Both the numerical prediction and experimental results agree that the global maximum occurs at connection S-01, with a local maximum occurring at connection S-03. After the local maximum at connection S-03, the numerical prediction and the experimental results show a relatively linear reduction in deflection along the length of the structure.

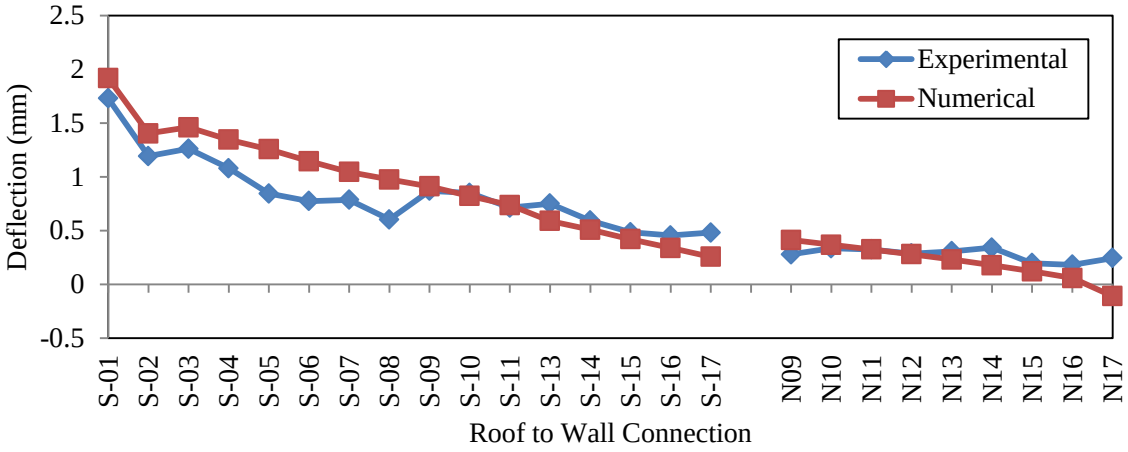

Figure 2.11: Deflection of the RTW connections for load case 12

The numerical prediction shows strong agreement with the experimental results for magnitude of deflection in the north-west section of the house. However, the model is unable to predict the general trend of deflection for the north connections near the east gable end. The experimental results showed a small negative deflection for these RTW connections. The numerical model is not able to capture this behaviour as the RTW connection is stiff in the negative direction to model bearing.

During the full-scale experiment, connection S-03 was determined to be the critical link, as it was the location of failure. Therefore, it is important that the model matches the behaviour at this connection. The deflection of the connection corresponding to the

center truss, S-10 is also presented to validate the model behaviour throughout the twelve selected pressure distributions. The numerical predictions and the experimental results for the deflection of connections S-03 and S-10 throughout the selected load cases are plotted in Figure 2.12 and Figure 2.13.

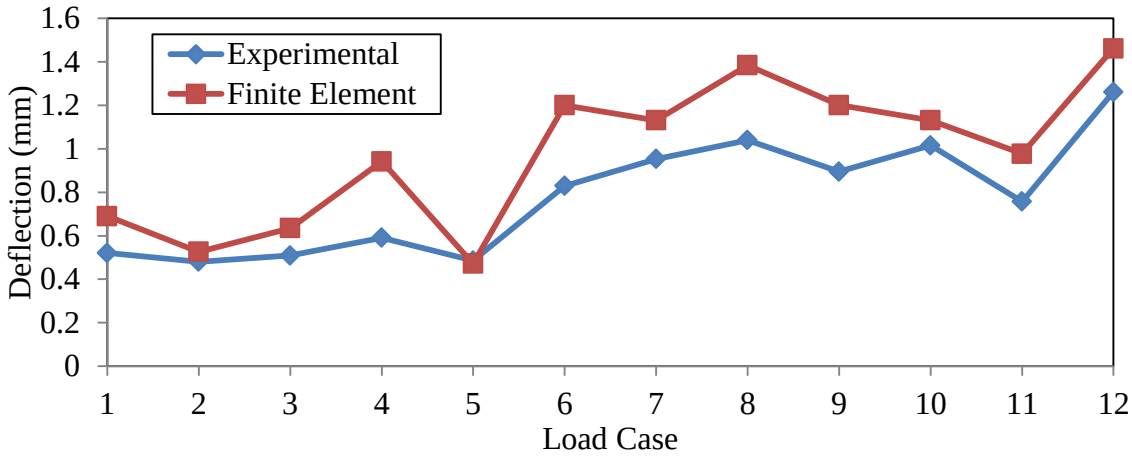

Figure 2.12: Deflection of connection S-03 throughout load cases 1 to 12

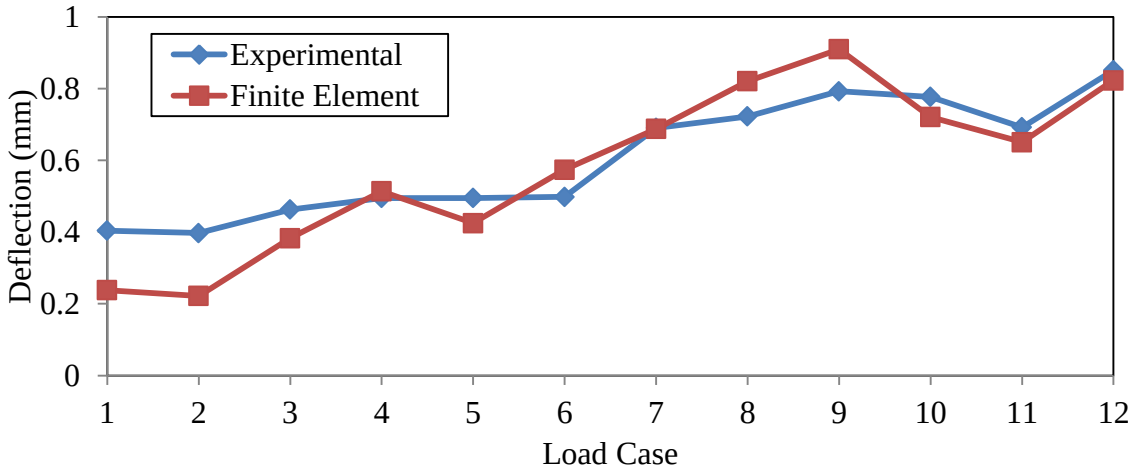

Figure 2.13: Deflection of connection S-10 throughout load cases 1 to 12

The numerical model tends to overestimate the deflection at connection S-03 by an average of 26% when compared to the experimental results. While the model overestimates slightly the deflection at this link, the trend through the load cases is

matched very well. The numerical prediction of connection S-10 shows very strong agreement with the experimental results, with an average percent difference of 14%.

In the author's opinion, the general trend of the deflected shape predicted by the finite-element model reasonably matches the experimental results. Considering the variability of the stiffness of a toe-nail connection, the error found is acceptable.

2.5 Analysis of Structural Behaviour

2.5.1 Analysis of the Tributary Area Method

The tributary area method is commonly used to evaluate the forces acting at the RTW connections. A pressure applied to the sheathing is converted into an equivalent line load acting on the nearest supporting trusses. Each truss is assumed to act independently to transfer the resulting line load to the RTW connections. The width of the tributary area of each truss is half the span to the next truss, roughly 600mm (2ft) for the studied structure. The gable ends have approximately 20% larger tributary area than the interior trusses as they support the entire overhang. The numerical model is used to assess the adequacy of this approach when applied to wood roofs subjected to non-uniform pressure distributions.

Figure 2.14 compares the force at the RTW connections predicted by each analysis method under the pressure distribution of load case 12. The tributary area method greatly overestimates the force at connections N-03 and S-03, predicting more than double the force withheld by the RTW connection than the numerical analysis prediction. The load sharing that occurs to the gable end reduces the peak load that is predicted on this connection. The numerical model predicts load sharing between the connections on the

interior of the structure, since a much more linear distribution of force on the connections occurs along the length of the structure when compared to the tributary area method. The load sharing distributes the pressure over multiple connections, reducing the demand on the individual connections that have the highest tributary area force prediction, while increasing the demand on the connections predicted to withstand lower load levels.

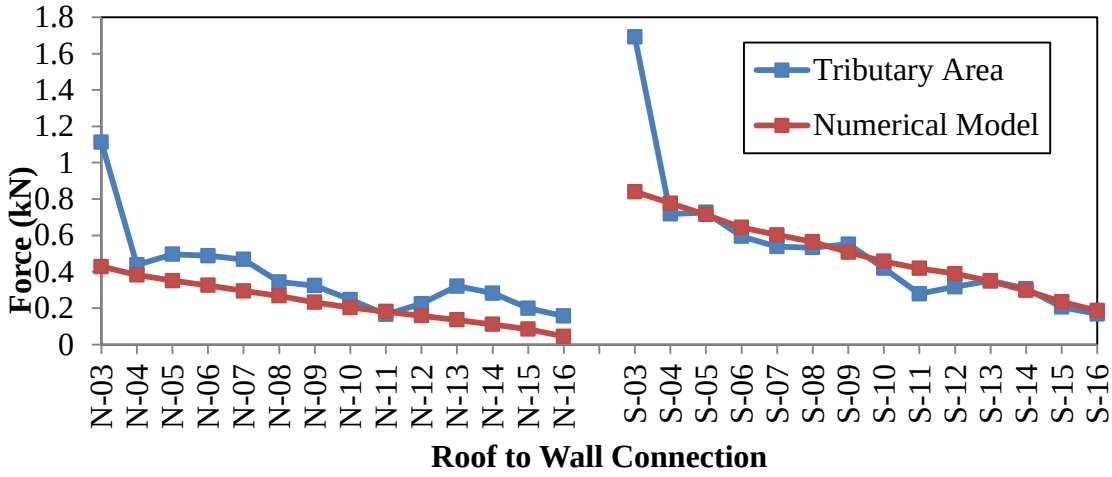

Figure 2.14: RTW connection force for tributary area method and numerical model, load case 12

The numerical model tends to predict smaller forces in the connections on the interior trusses of the structure due to the increased load transferred through the gable ends. For the selected pressure distribution, the force in every north connection is overestimated by the tributary area method.

Table 2.3 and Table 2.4, which report the uplift force withheld by the RTW connections of the east gable truss for all 12 selected load cases, show that the numerical model predicts that the gable truss transfers much more uplift load to the walls than predicted by the tributary area method. The largest difference between the two analysis methods is under the pressure distribution applied in load case 5, where the tributary area method predicts that the dead load of the east gable truss is larger than the applied uplift load.

Due to the load sharing demonstrated under this pressure distribution, the numerical model predicts that an uplift force is transferred to the walls by the RTW connections of the gable end. For the load cases analyzed from the 25m/s experiment, the numerical model predicts that the gable end transfers 46% to 94% more uplift force than the tributary area method prediction.

Table 2.3: Total uplift force transferred by the RTW connections of the east gable for load cases selected from 20m/s wind speed experiment

Load Case	1	2	3	4	5	6
Tributary Area Prediction (kN)	2.2	1.7	1	2.9	-0.1	3.7
Finite-Element Prediction (kN)	3.1	2.4	2.3	4.4	1	5.1
Percent Increase	45%	45%	135%	54%	1158%	38%

Table 2.4: Total uplift force transferred by the RTW connections of the east gable for load cases selected from 25m/s wind speed experiment

Load Case	7	8	9	10	11	12
Tributary Area Prediction (kN)	2.8	2.8	2.3	2.8	2.8	3.9
Finite-Element Prediction (kN)	4.6	4.8	4.5	4.5	4.2	5.6
Percent Increase	64%	70%	94%	61%	51%	46%

The tributary area method is not capable of capturing either the load sharing that occurs in the truss system or the effect of the increased stiffness of the gable end truss. The tributary area method is most accurate in sections of the house with a uniform truss stiffness without large variation in loading from truss to truss. The inability of the tributary area method to capture the effect of the gable truss results in a very conservative force approximation for the critical connection.

2.5.2 Behaviour under Uniform and Non-uniform Load

The purpose of this section is to compare the house behaviour under a spatially varying wind load to that of an equivalent uniform pressure to gain further insight into the load

sharing behaviour of the structure. Using a weighted average based on the area of each experimental pressure box, an equivalent uniform pressure is calculated for each side of the structure. The equivalent uniform pressure matches the realistic pressure distribution in terms of global uplift applied to the structure. This average pressure is then applied to the numerical model for comparison with the spatially varying pressure. Load case 12 is selected for this analysis. The equivalent uniform pressure applied for this load case is -.38 kPa on the south (leeward) side and -0.23 kPa on the north (windward) side.

Figure 2.15 compares the RTW connection deflections of the structure under the realistic pressure distribution to that of the equivalent uniform pressure. Both load cases result in a similar average deflection, differing by only 5%. The peak value under the realistic pressure distribution is much higher than under the equivalent uniform loading. Both deflection and withdrawal force at the critical connection, S-03, are 80% higher under the loading of the realistic pressure distribution than under the loading of the equivalent uniform load.

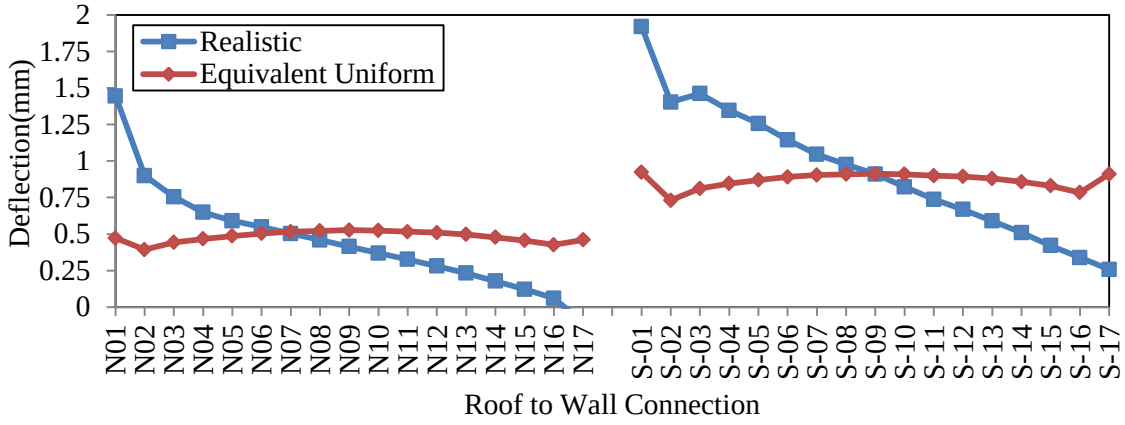

Figure 2.15: RTW deflections under equivalent uniform pressure distribution and realistic pressure distribution for load case 12

Figure 2.16 shows the location of the two section cuts used to draw the deflection profile of the structure under the selected pressure distributions. Section 1-1 is used to present

the deflection of the top chord member of the critical truss on the leeward side of the structure. Section 2-2 is used to present the deflected shape of the sheathing along the length of the structure between the RTW connection and the nearest interior web member of the truss.

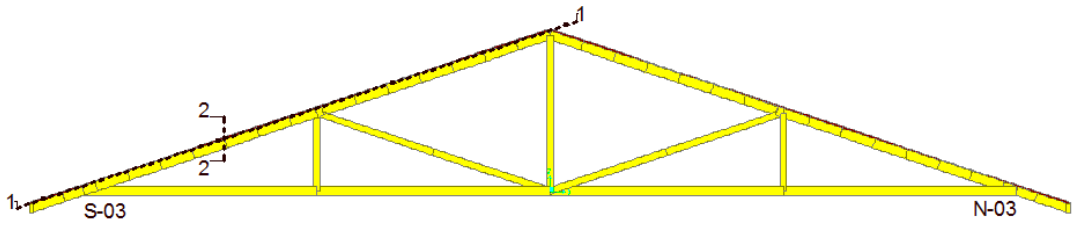

Figure 2.16: Selection cuts for analysis

As shown in Figure 2.17, the perpendicular deflection of the sheathing along the south, top chord member of the critical truss is much lower under the equivalent uniform loading than under the realistic pressure distribution, which has higher pressures acting near the eave. The maximum deflection under the realistic pressure distribution is more than double that of the equivalent uniform pressure distribution.

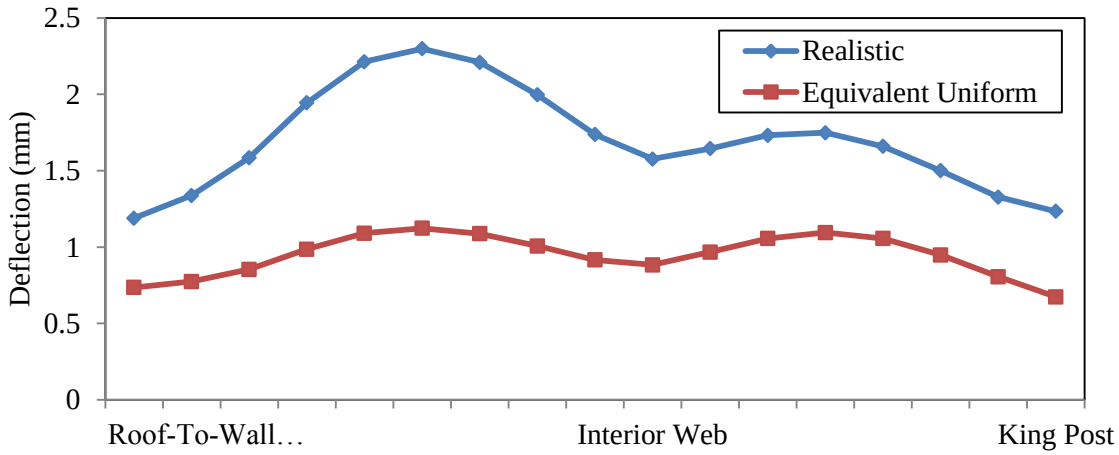

Figure 2.17: Deflection profile of sheathing along section 1-1 under non-uniform and equivalent uniform pressure distribution for load case 12

Figure 2.18 presents the perpendicular deflection of the sheathing along the length of the structure at section 2-2. Local maxima occur in the sheathing between each truss. It is again found that the maximum deflection is nearly twice as large under the realistic pressure distribution than under the equivalent uniform loading.

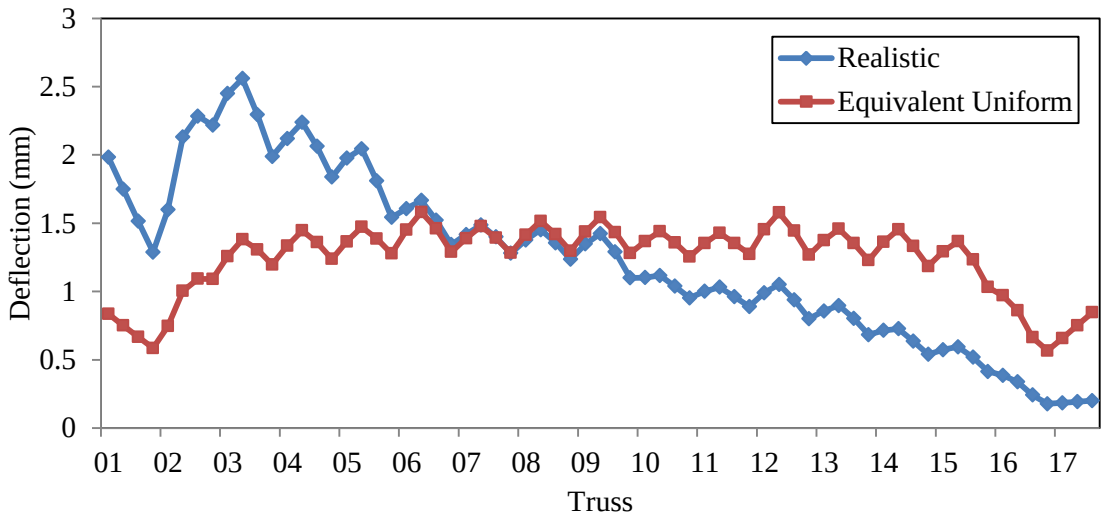

Figure 2.18: Sheathing deflected profile along length of building at section 2-2 under non-uniform and equivalent uniform pressure distribution for load case 12

Figure 2.19 presents the total uplift force transferred by the RTW connections of each truss under the realistic and equivilent uniform pressure distributions. Under the realistic pressure distribution applied in load case 12, the east gable transfers 34% of the total global uplift pressure to the walls. Under the equivalent uniform pressure distribution, only 16% is transferred to the walls by the east gable end. The application of the peak pressure near the gable truss in the realistic pressure distribution allows for a larger percentage of force transfer to occur through the strong, gable truss, thereby reducing the forces on the interior RTW connections.

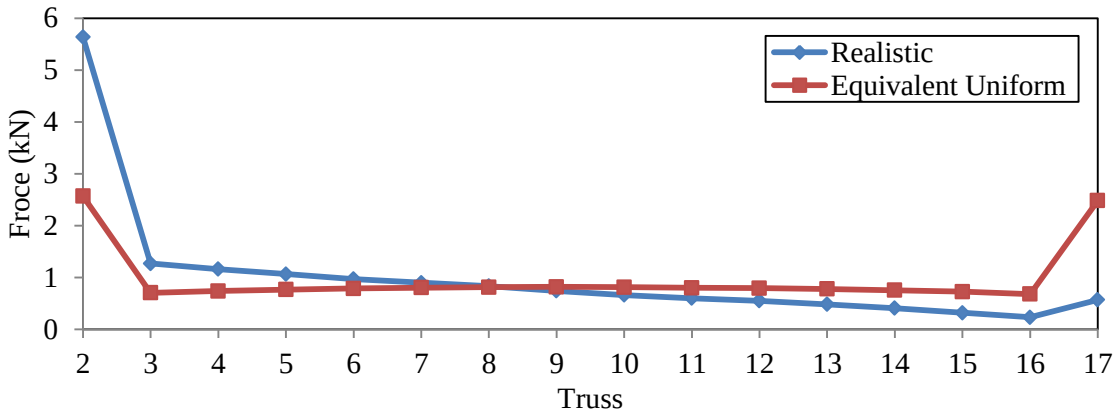

Figure 2.19: Predictions of uplift force per truss under non-uniform and equivalent uniform loading

The equivalent uniform pressure underestimates the maximum deflections in both the sheathing and the RTW connections. The load sharing that occurs in the structure is not sufficient to create a similar behaviour between the realistic pressure distribution and an equivalent uniform loading.

2.5.3 Effect of Increased Gable End Stiffness on Sheathing Failures

The STT connections are critical near the edges of the building where the largest pressures result from high speed winds. The results of the numerical model have identified the stiffness of the gable end to be a large factor in the uplift behaviour of the structure. The numerical model suggests extra force will be transferred by the sheathing-to-gable truss connections, increasing the vulnerability of these already critical connections.

The deflected shape of the sheathing under the non-uniform pressure distribution in Figure 2.18 shows that the typical local maxima on the interior of the structure occur directly between two trusses. The local maximum between the gable truss and the first interior truss occurs closer to the interior truss than the gable truss. This location of local

maximum indicates that more force is transferred through the connections of the sheathing to the more stiff gable truss. The overhang of the structure works as a cantilever and will also have a lower stiffness than the gable end truss. The differential stiffness in the critical location will result in the connections of the sheathing to the gable truss withstanding much more force than anticipated.

The increased demand could result in progressive overloading of the connections and removal of the roof sheathing, which has been identified as the most common failure in wood homes during high speed wind events. The effect of differential stiffness of the truss system has yet to be studied in the analysis of the failure of the roof sheathing. As the numerical model suggests unequal force transfer by the sheathing connections in this critical area, more analysis should be completed on this topic.

2.6 Conclusions

A finite-element model of the roof system of a light-framed wood structure is developed using the software SAP 2000. The model simulates the full-scale experiment conducted under simulated wind loading at the Insurance Research Lab for Better Homes. Frame, area and link elements are used to model the roof of the structure.

The validation of the numerical model is conducted by comparing the deflections along the length of the roof obtained numerically and experimentally under multiple realistic pressure distributions. The comparison between the full-scale test results and the finite-element analysis shows good agreement in magnitude of deflection and trend of the deflected shape. In the author's opinion, discrepancies are acceptable.

In a comparison to the numerical results, the tributary area method has not provided an accurate prediction of the loads acting on the RTW connections along the length of the structure. The tributary area method is shown to be not capable of capturing either the load sharing that occurs in the truss system or the effect of the increased stiffness of the gable end truss. The numerical model predicts that a large amount of load sharing occurs to the gable truss. For loading applied from the 25m/s experiment, the gable truss carries between 46-94% more uplift numerically than the tributary area prediction depending on the pressure distribution. Load sharing to the gable is larger when peaks are applied closer to the gable.

A comparison of the structural behaviour under a realistic pressure distribution and an equivalent uniform pressure distribution shows that the load sharing that occurs in a wood structure is not sufficient to create a similar behaviour between the two load cases.

The behaviour in the numerical model suggests that the differential stiffness of the truss system around the gable end will increase the vulnerability of the sheathing to truss connections in the critical location. A further investigation should be completed on the effect of the increased stiffness of the gable end and the effect of this on the withdrawal failure of the STT connections.

2.7 References

Baskaran, A., and Dutt, O. (1997). Performance of roof fasteners under simulated loading conditions. *Journal of Wind Engineering and Industrial Aerodynamics*, *72*, 389-400.

Canadian Wood Council (CWC), and Canadian Standards Association (CSA). (2010). *Wood design manual, 2010 :The complete reference for wood design in Canada*. Ottawa: Canadian Wood Council

Computers and Structures, Inc. (2009). SAP 2000 V. 14: Integrated Software for Structural Analysis and Design. Berkley, California, USA.

Datin, P. L., and Prevatt, D. O. (2013). Using instrumented small-scale models to study structural load paths in wood-framed buildings. *Engineering Structures, 54*, 47-56.

Datin, P. L., Prevatt, D. O., and Pang, W. (2011). Wind-uplift capacity of residential wood roof-sheathing panels retrofitted with insulating foam adhesive. *Journal of Architectural Engineering, 17*(4), 144-154.

Department of Housing and Urban Development (HUD). (1993). *Assessment of Damage to Single-Family Homes Caused by Hurricanes Andrew and Iniki.* U.S., Office of Policy and Development and Research, HUD-0006262.

Federal Emergency Management Agency (FEMA). (1993). *Building Performance: Hurricane Iniki in Hawaii - Observations, Recommendations, and Technical Guidance.* Federal Emergency Management Agency.

Gurley, K., Davis, R.H., Ferrera, S.P., Burton, J., Masters, F., Reinhold, T., and Abdullah, M., (2006). Post 2004 hurricane field survey – an evaluation of the relative performance of the Standard Building Code and the Florida Building Code. *Proc. 2006 ASCE/SEI Structures Congress*, St. Louis, MO. 8.

Li, Z., Gupta, R., and Miller, T. H. (1998). Practical approach to modeling of wood truss roof assemblies. *Practice Periodical on Structural Design and Construction, 3*(3), 119-124.

Morrison, M. J. (2010). *Response of a Two-Story Residential House Under Realistic Fluctuating Wind Loads*. (PhD Thesis). London, Ont.: Department of Engineering, The University of Western Ontario.

Morrison, M. J., Henderson, D. J., and Kopp, G. A. (2012). The response of a wood-frame, gable roof to fluctuating wind loads. *Engineering Structures, 41*, 498-509.

Morrison, M. J., and Kopp, G. A. (2011). Performance of toe-nail connections under realistic wind loading. *Engineering Structures, 33*(1), 69-76.

National Research Council of Canada (NRC). (2010). *National Building Code of Canada 2010*. Ottawa, NRCC 53301

Reed, T. D., Rosowsky, D. V. and Schiff, S. D. (1997). Uplift capacity of light-frame rafter to top plate connections. *Journal of Architectural Engineering*, *3*(4), 156-163.

Shanmugam, B., Nielson, B. G., and Prevatt, D. O. (2009). Statistical and analytical models for roof components in existing light-framed wood structures. *Engineering Structures, 31(*11), 2607-2616.

Shivarudrappa, R., and Nielson, B. G. (2013). Sensitivity of load distribution in light-framed wood roof systems due to typical modeling parameters. *Journal of Performance of Constructed Facilities, 27*(3), 222-234

van de Lindt, J., Graettinger, A., Gupta, R., Skaggs, T., Pryor, S., and Fridley, K. (2007). Performance of wood-frame structures during Hurricane Katrina. *Journal of Performance of Constructed Facilities, 21*(2), 108-116.

Zisis, I., and Stathopoulos, T. (2012). Wind load transfer mechanisms on a low wood building using full-scale load data. *Journal of Wind Engineering and Industrial Aerodynamics, 104-106,* 65-75

Chapter 3

3 Parametric Study of Behaviour after Retrofitting Under Uniform Load

3.1 Introduction

Residential, light-framed wood structures built under the provisions of governing building codes have been a major source of economic loss during past high speed wind events. Much of the economic loss is due to structural damage resulting from the lack of a continuous load path capable of transferring the uplift pressures, which arise from high speed winds, from the roof to the foundation (van de Lindt et al., 2007). Post hurricane damage reports (HUD, 1993; FEMA, 1993) have identified the sheathing-to-truss (STT) connection and the roof-to-wall (RTW) connection as critical connections in the uplift load path. Building codes have addressed these vulnerabilities by improving the required capacity for these connections. The capacity of the STT connection has been improved by reducing the distance between connections, increasing the diameter and length of penetration of the nail, and/or by specifying a ring or spiral shank nail. The capacity of the RTW connection is improved by increasing the number of nails per connection, increasing the length of the nail, and/or using of a steel clip to compliment the toe-nail connection. Building code changes have occurred as recent as 2010, when the National Building Code of Canada (NRC, 2010) increased the required capacity of both critical connections in high wind areas.

Improved building codes reduce the probability of failure in new structures. However, the non-structural elements typically installed in light-framed wood homes limit the access to the critical connections, making current technologies difficult to apply to existing

structures. Stewart et al (2003) presented an economic analysis of the vulnerability of existing residential structures to hurricane loading. They estimated that the cost of increasing the hurricane resistance of a structure during construction ranges from 1-10% of the cost of the structure. This cost increases to 15-50% when retrofitting a current structure; a deterrent to many home owners. With many structures built to the provisions of outdated versions of governing building codes, a retrofit system is needed to improve the structural behaviour of light-framed wood structures in high speed wind events.

This study focuses on a retrofit system that is economical, easy to apply and effective without modification to the existing structure. The proposed system begins with a series of cables that are placed along the sheathing of the roof, identified as the bearing cables in Figure 3.1, Figure 3.2 and Figure 3.4. Along the eaves of the structure, the bearing cables are attached to rigid bars. Cables then connect the rigid bars to piles, which are permanently installed in the ground. When a warning of high speed winds is announced, the system can be easily applied to the roof of the building. This system provides the uplift forces an alternate load path to the ground, reducing the demand placed on the weak, nailed connections within the structure.

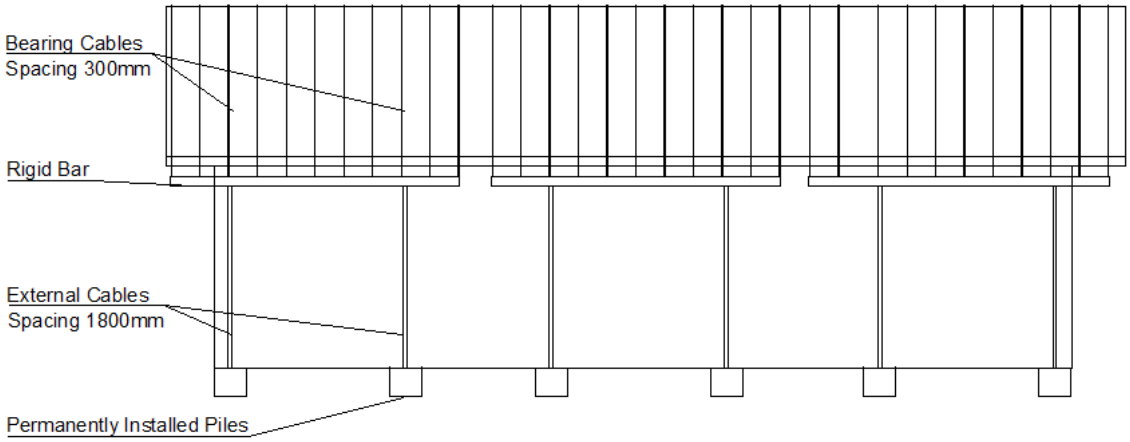

Figure 3.1: Elevation view of structure with retrofit system

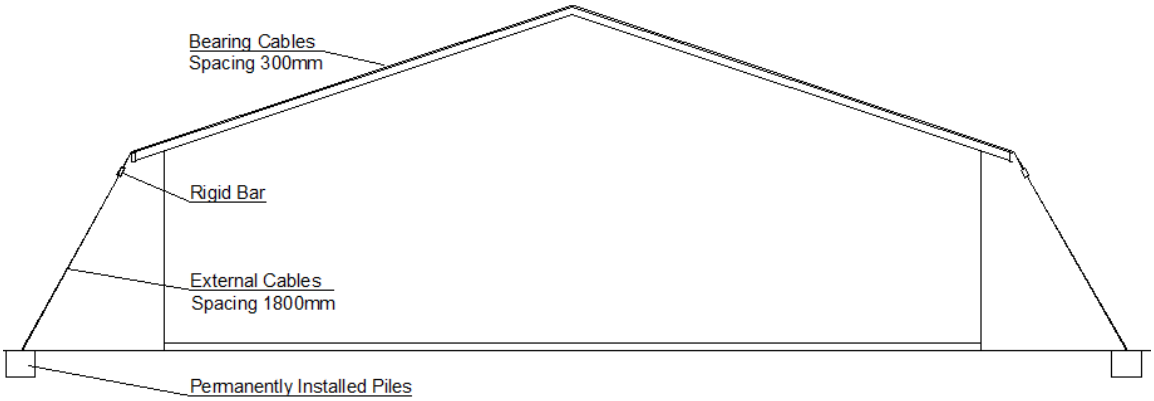

Figure 3.2: Elevation view of structure with retrofit system

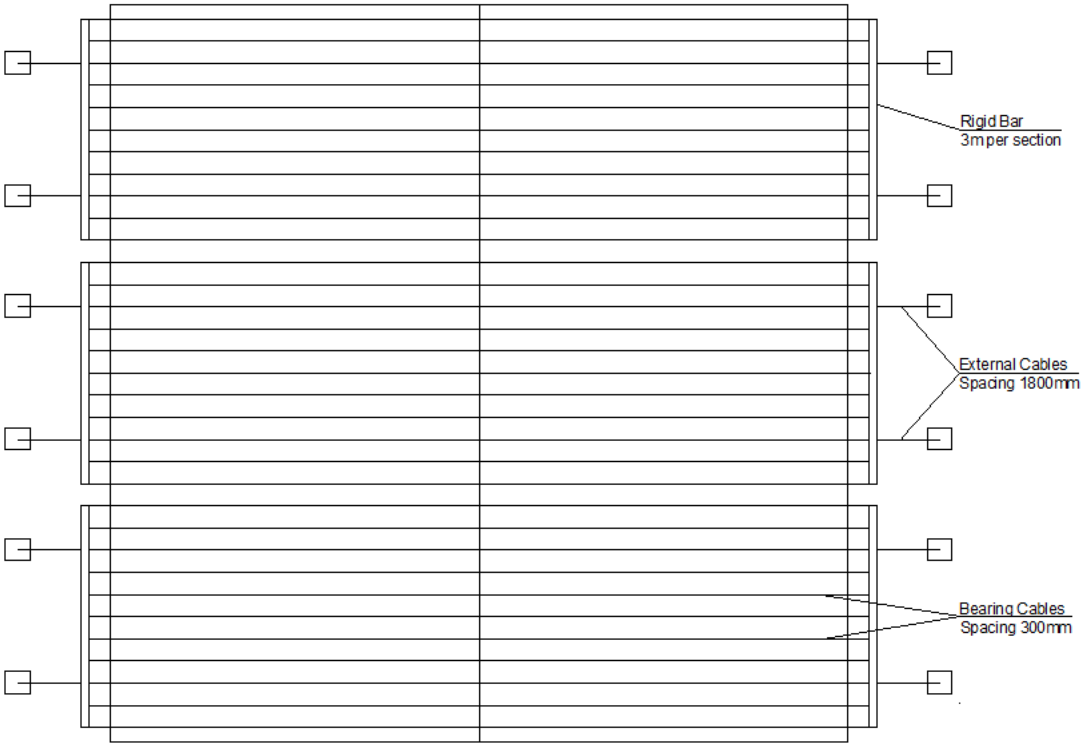

Figure 3.3: Plan view of proposed retrofit system as applied to a gable-style roof

The focus of this work is to study the behaviour of the retrofit system using numerical tools. First, a finite-element model of the roof system of a light-framed wood structure has been developed to accurately capture the behaviour under a realistic wind pressure in the commercial software, SAP2000 (Computers and Structures, Inc., 2009). The dimensions of the modeled house correspond to those of a full-scale experiment that was recently conducted at the Insurance Research Lab for Better Homes (Morrison et al. 2012). Built to the provisions of the Ontario Building Code, the structure matched the typical construction techniques of the area. A spatially and temporally varying realistic pressure distribution was applied to the structure while recording the corresponding deflections at the RTW connections. These results were used to validate the numerical model of the roof structure. Applying selected snapshots of the realistic pressure

distribution to the numerical model results in a similar deflection profile along the length of the roof system to that of the test structure (Jacklin and El Damatty, 2012).

This chapter focuses on extending the validated numerical model to include the retrofit idea. The chapter begins with a description of the developed numerical model. The model is used to study the typical behaviour of the structure under a uniform pressure after application of the retrofit system. The numerical model is then used to conduct a parametric study to determine the effect of varying the components of the retrofit system. The parametric study results are presented, with a focus on the effect of each design variable on: a) the improvement of the structural behaviour resulting from application of the retrofit system and b) the distribution of force in the retrofit system.

3.2 Model Description

3.2.1 Roof Structure

The roof structure of a typical, gable-style, light-framed wood home is modeled using the commercial finite-element program SAP2000 (Computers and Structures, Inc., 2009). Frame, shell and multi-linear elastic link elements are used to model the truss, sheathing and RTW connections respectively. The plan dimensions of the roof are approximately 9m by 9m, consisting of 16 Howe-style trusses spaced on 600mm (2ft) centers, as shown in the plan view of the structural skeleton in Figure 3.4. The trusses have a 4/12 slope and a 9m clear span, as shown in . To accurately model the anisotropic behaviour of the roof sheathing (12.5mm Canadian softwood plywood (CSP)) inertia multiplies are used to reduce the bending rigidity in the direction perpendicular to the face grains. The material properties of the truss and area elements match the properties suggested by the Canadian

Wood Design Code (CWC and CSA, 2010) for SPF No.1/No.2 lumber and CSP plywood respectively. Figure 3.6 shows the load deflection relationship used to model the withdrawal behaviour of the RTW connection, which has been adapted from the experimental work presented by Reed et al. (1997).

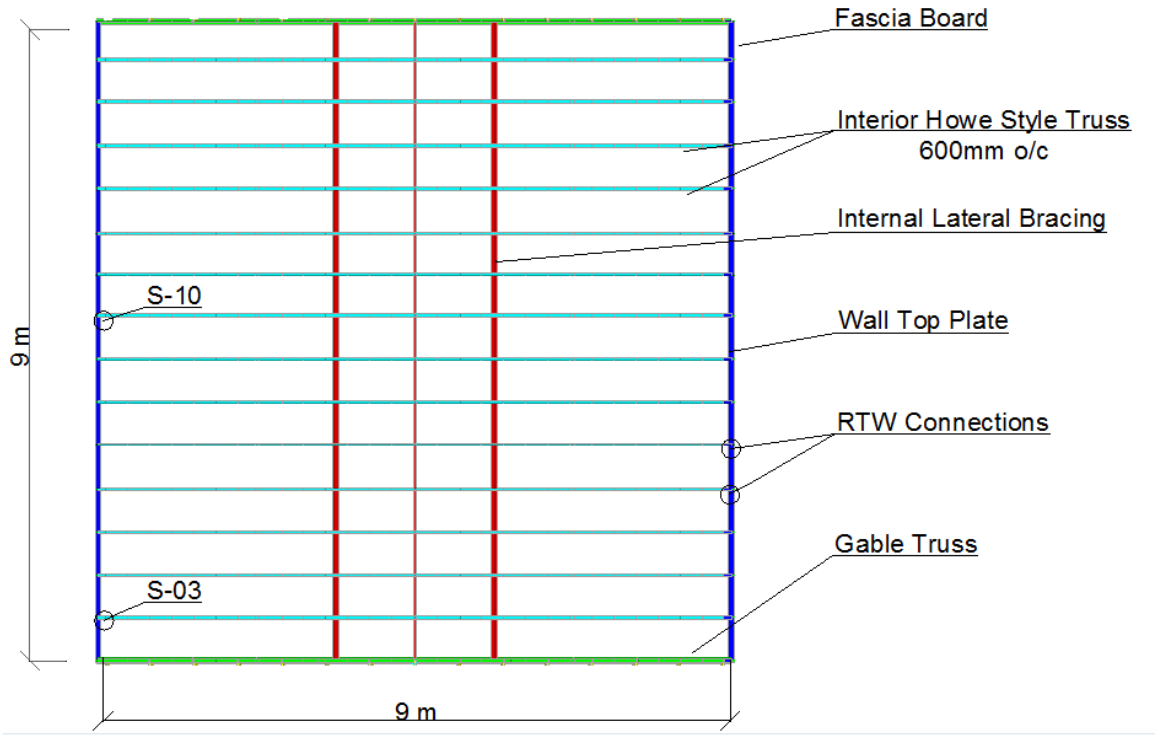

Figure 3.4: Plan view of structural skeleton

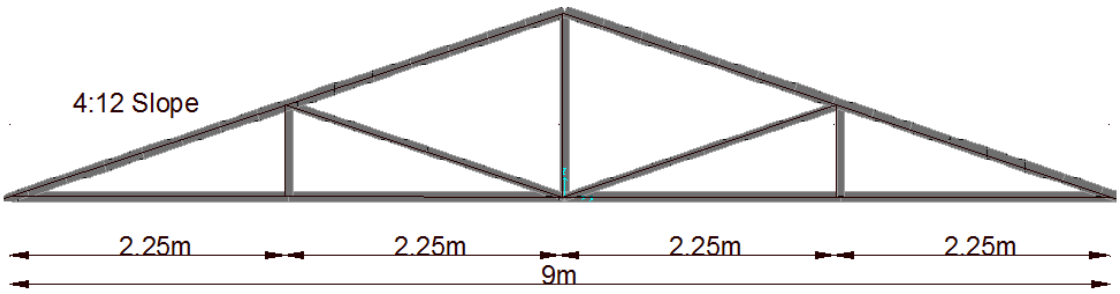

Figure 3.5: Elevation view and dimensions of Howe-style truss

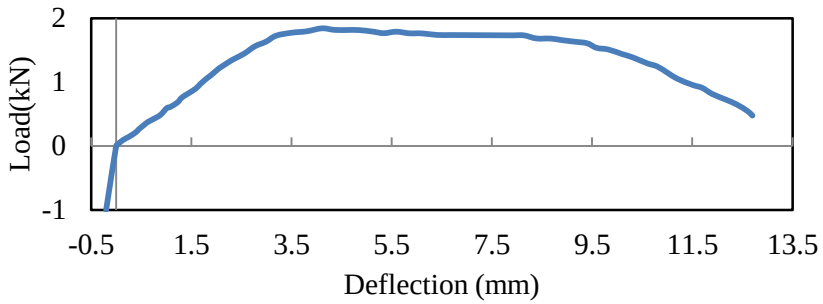

Figure 3.6: Load deflection relationship for roof to wall connection

3.2.2 Bearing Cables

The numerical model of the roof structure is extended to include the retrofit system. The bearing cables are modeled using nonlinear cable elements. To capture the interaction between the cable and the roof sheathing, a constraint is used to simulate bearing. Nodes of the cable elements are set to have compatible displacements with the nodes of the sheathing in the axis perpendicular to the sheathing. The frictional force developed between the retrofit system and roof is neglected, therefore, no compatibility in displacement in the in-plane direction of the sheathing is assumed. In total, 660 cable elements are used to model the 33 bearing cables of the retrofit system. Spacing for the cables is 300mm (1ft) on center. The cables are assumed to be a steel cross section with a yield strength of 350 MPa and a modulus of elasticity of 200GPa.

3.2.3 External Cables

The external cables are also modeled using cable elements, which have the same steel properties as the bearing cables. Two external cables attach each 3m (10ft) section of rigid bar to the permanently installed piles. The span between external cables is 1800mm (6ft), creating two 600mm (2ft) cantilever sections per rigid bar. This external cable spacing reduces maximum deflection of the rigid bar, thereby reducing the required bending rigidity necessary to create a uniform distribution of axial force in the bearing

cables. The external cables of the initially proposed retrofit system make an angle of 30° with the wall of the structure. The height of the structure is assumed to be 2.5m, resulting in an external cable length of 2.6m. A pin restraint is used to model the piles, restricting deflection at this location.

3.2.4 Rigid Bar

The rigid bars are modeled using frame elements. The initial cross section selected for the rigid bar is a hollow aluminum tube, 102mm by 52mm with a 6mm wall (2”x4”x1/4”). The strong axis of the rigid bar is oriented such that it is in-line with the cables. Three, 3m (10ft) sections of rigid bar are needed to retrofit the modeled structure, shown in Figure 3.1. Each rigid bar is attached to 11 bearing cables. The material property of 6061-T6 aluminum is used, which has a yield strength of 250MPa and a modulus of elasticity of approximately 70GPa.

3.3 Typical Behaviour of the Structure with Retrofit System

The behaviour of the structure is first examined using the initially proposed section properties presented in Table 5.1. Nonlinear static analysis is used. First, the structure is analyzed under the dead load and cable prestressing load, which represents the initial conditions for the uplift load. A uniform uplift pressure is then applied incrementally, using an increment of 0.2 kPa per step.

Table 3.1: Initially proposed dimensions for full-scale retrofit system

Retrofit System Component	**Initial Dimension**
Bearing cables	3mm steel cable
External cables	6mm steel cable
Initial prestressing force	1 kN to each external cable
Rigid Bar	Aluminum, Hollow Rectangular Section 102mm by 51mm with 6mm wall

The elevation view of the full-scale, retrofitted structure in Figure 3.7 shows the location of the elements selected to present the results in this paper. The center RTW connection is selected to present the applied pressure to deflection relationship as it demonstrates the maximum response under a uniform pressure. The maximum axial force in each bearing cable is presented for the bearing cables connected to the center rigid bar section, labeled cables 1 to 11 in Figure 3.7. This axial force demonstrates the distribution of force in the retrofit system. Three locations, S1, S2 and S3 in Figure 3.7, are selected to show the effect of the retrofit system on the sheathing of the structure. S1 and S2 are located at the center truss, where the deflections resulting from a uniform loading are largest. Point S3 is located above the gable truss; the location of maximum shear force acting in the sheathing for the unmitigated structure.

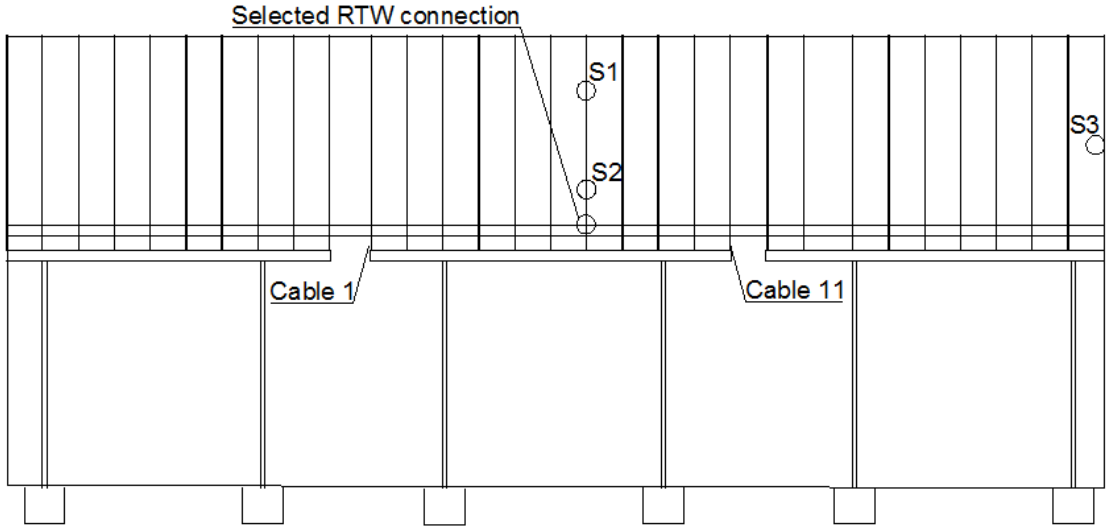

Figure 3.7: South elevation view with selected analysis points

3.3.1 Effect on Roof to Wall Connection Behaviour

After application of the retrofit system, the applied pressure to deflection relationship of the selected RTW connection, Figure 3.8, demonstrates four distinct phases of behaviour.

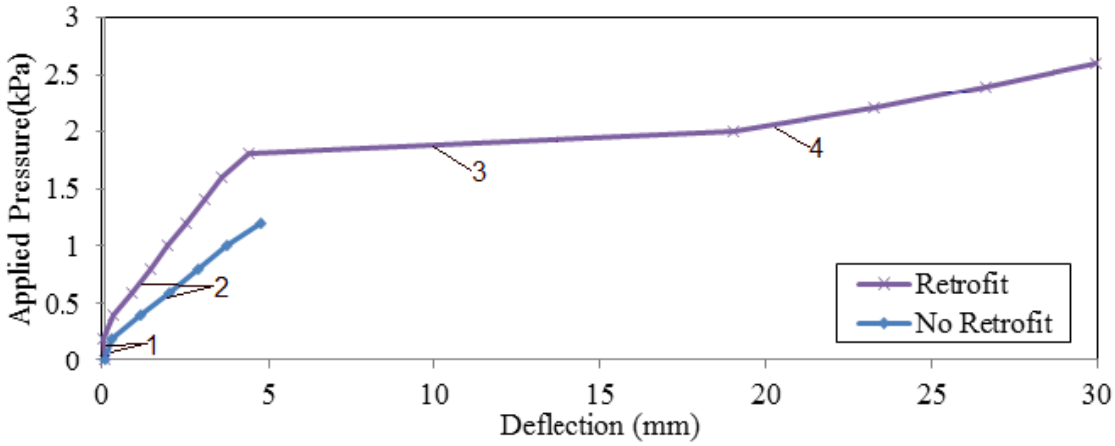

Figure 3.8: Typical applied uniform pressure vs selected RTW connection deflection

During the first phase, deflection of the truss system does not occur as the initial prestressing force in the retrofit system and the dead load of the structure are larger than the applied uplift forces. RTW connection deflection has not initiated and the force transferred to the retrofit system is minimal. This phase of the pressure deflection relationship of the RTW connection occurs with and without the retrofit system.

The second phase begins after the dead load and initial prestressing load are overcome by the applied pressure and the truss system begins to deflect. During this phase, the pressure deflection relationship of the RTW connection is linear before and after application of the retrofit system. The retrofit system increases the slope of this pressure deflection relationship as the retrofit system relieves some of the force from the RTW connections. The initially proposed retrofit system, with component sizes presented in Table 5.1, increases the slope in the linear range by 57% above that of the bare structure, contributing to the increased capacity of the structure.

The third phase begins with RTW connection failure. Large displacements occur to transfer the force from the overloaded connection to the retrofit system. As the first connection fails, the remaining RTW connections progressively fail. Failure of the

connection is demonstrated by the nearly horizontal slope of the pressure deflection relationship of the connection. The initially proposed retrofit system increases the uniform pressure at which RTW connection failure begins from 1.2kPa to 1.8kPa.

The fourth phase begins after complete withdrawal of the RTW connections. The pressure deflection relationship at the selected RTW connection regains stiffness, and the truss system deflects with a slope dependent on the properties of the retrofit system. Without application of the retrofit system, the truss system becomes unstable as the connections progressively fail. Retrofitting provides a load path for uplift forces after RTW connection failure and the system remains stable. The retrofit system changes the failure mode of the connection from a sudden withdrawal followed by instability, to a ductile failure with the ultimate capacity dependent on the strength of the components of the retrofit system.

After application of the retrofit system, the deflected shape along the length of the structure remains similar, as shown under 1.2kPa of uniform pressure in Figure 3.9. The retrofit system is effective at reducing the deflection of the RTW connections, as the average deflection is reduced by a factor of 2. A similar reduction is found on the axial force acting on the connections.

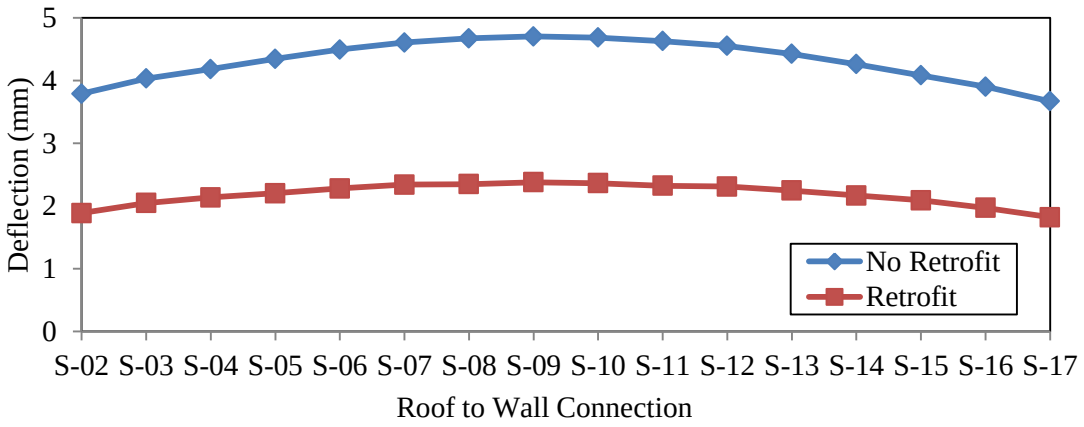

Figure 3.9: RTW connection deflection along the length of structure under 1.2kPa of uniform pressure

3.3.2 Force Distribution in Retrofit System

Figure 3.10 shows the typical bending moment along the length of the center rigid bar resulting from 1.6 kPa of uniform pressure applied to the structure. The external cables are connected to the rigid bar at cable-03 and cable-09. The orientation of the strong axis is in line with the cables of the system, which, when tightened, create a straight line from the eave of the structure to the permanently installed piles. Figure 3.10 shows that the rigid bar experiences negligible moment in the weak axis, demonstrating that all forces transferred through the rigid bar act in the plane of the cables. A hollow rectangular section will provide an efficient design for rigid bar, as it would provide a high strong axis bending rigidity to weight ratio.

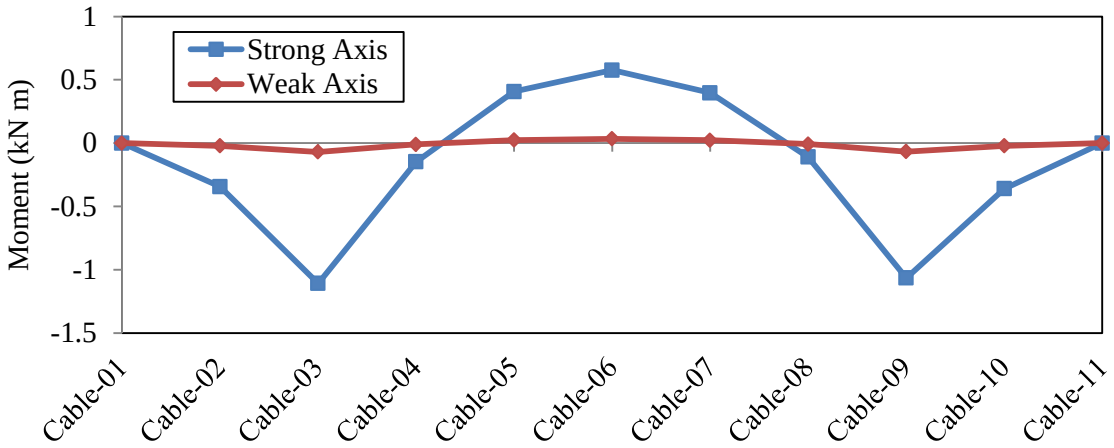

Figure 3.10: Typical bending moment diagram of center rigid bar under 1.2kPa of uniform pressure

3.3.3 Effect on Sheathing Deflection and Shear Force

Figure 3.11 presents the deflected shape of the sheathing located above the center truss with and without the retrofit system applied at 1.2 kPa of uniform pressure. The top chord of the truss maintains a similar deflected shape before and after the application of the retrofit system. The reduction in the sheathing deflection after application of the retrofit system is caused by the reduction in the rigid body deflection of the truss.

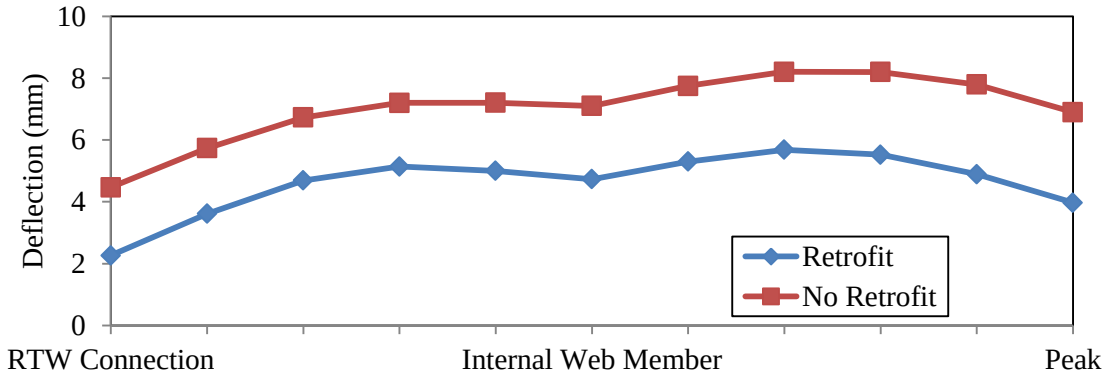

Figure 3.11: Deflected shape of sheathing located above the center truss with and without the retrofit system under 1.2kPa uniform pressure

Figure 3.12 presents the shear force per unit length acting on the sheathing at the selected points with and without the retrofit system applied at 1.2 kPa of uniform pressure. This shear force provides an approximation of the magnitude of the withdrawal force applied

to the STT connections in these locations. The retrofit system has little impact on the shear force in the sheathing for the points selected on the center truss, points S1 and S2 of Figure 3.7. The retrofit system reduces the shear force acting on the sheathing located above the gable end, point S3 of Figure 3.7. The gable truss contains extra RTW connections, as it is continuously supported by an external wall. The extra connections increase the load transferred through this truss, resulting in larger shear forces on the sheathing at this location. By reducing the load transferred to the gable truss, the retrofit system reduces the shear demand on the sheathing at the critical location by approximately 50%.

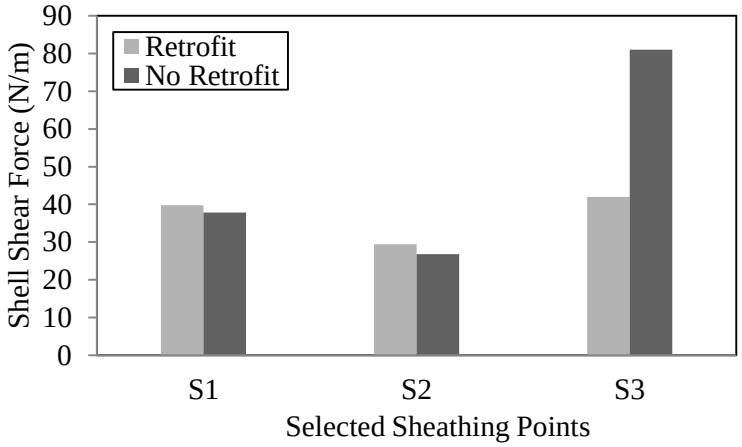

Figure 3.12: Resulting shear forces at selected sheathing locations with and without retrofit system under 1.2 kPa of uniform pressure

3.4 Parametric Study under Uniform Pressure Distribution

3.4.1 Details of the Parametric Study

This parametric study focuses on the ability of the retrofit system to prevent failure of the RTW connections. Thus, the results are presented for the first two phases of behaviour discussed above, before progressive failure of the RTW. In this range of loading, the ultimate capacities of the components of the retrofit system are not critical. Each retrofit system configuration studied demonstrates similar failure behaviour when the ultimate

capacities are considered; as the RTW connection progressively fail and the force is transferred from the overloaded connections to the retrofit system, either the bearing cables or the external cables exceed their ultimate capacity. The ultimate capacity of the rigid bar is not critical as the bending rigidity required to create a nearly uniform distribution of force in the bearing cables provides sufficient bending and shear capacities at all load levels.

Table 3.2 presents the properties varied in the parametric study. For this parametric study, inertia multipliers are used in the finite-element model to increase the bending rigidity of the rigid bar. This will show the effect of varying bar rigidity while neglecting the effect of increasing the self-weight of the rigid bar. For each case, two results are investigated: a) the applied pressure to deflection relationship at the center RTW connection and b) the axial force in the cables of the center rigid bar. The location of the selected analysis points are presented earlier in Figure 3.7. The applied pressure to deflection relationship shows the effect varying the parameter has on the ability of the retrofit system to prevent failure. The maximum bearing forces resulting on the structure and the total force transferred through the retrofit system can be determined with the distribution of axial force in the cables of the center rigid bar.

Table 3.2: Parametric study values

Parameter	**Sizes Considered (Default underlined)**
External Cable Diameter	3, **6**, 12, 18 mm
Bearing Cable Diameter	1, 2, **3**, 6, 12 mm
External Cable Prestressing Force	**1**, 3, 5 kN
Bar Rigidity Relative to Initial	I/32, I/16, **I** ,4I
Angle of External Cables with House	60,45,**30**,15,0
Overhang Distance (house parameter)	**0mm**, 250mm, 500mm

3.4.2 Results of Parametric Study

3.4.2.1 External Cable Diameter

Increasing the diameter of the external cable is effective at increasing the ability of the retrofit system to prevent structural failure. Figure 3.13 presents the pressure-deflection relationship for the selected RTW connection for varying external cable diameters. The applied pressure at which connection deflection begins is independent of cable diameter. Increasing the external cable diameter changes the slope of the pressure deflection relationship in the linear range. After application of the retrofit system, the slope in the linear range is increased by between 31-118% above that of the original structure.

Increasing the external cable diameter does not increase the effectiveness of the retrofit system without bound. Figure 3.13 shows that increasing the external cable diameter from 12mm to 18mm does not change the pressure deflection relationship of the RTW connection. When the stiffness of the external cables is much larger than the stiffness of the bearing cables, deflection is governed by the stiffness of the bearing cables. Further increasing of the external cable size becomes ineffective at changing the behaviour of the system.

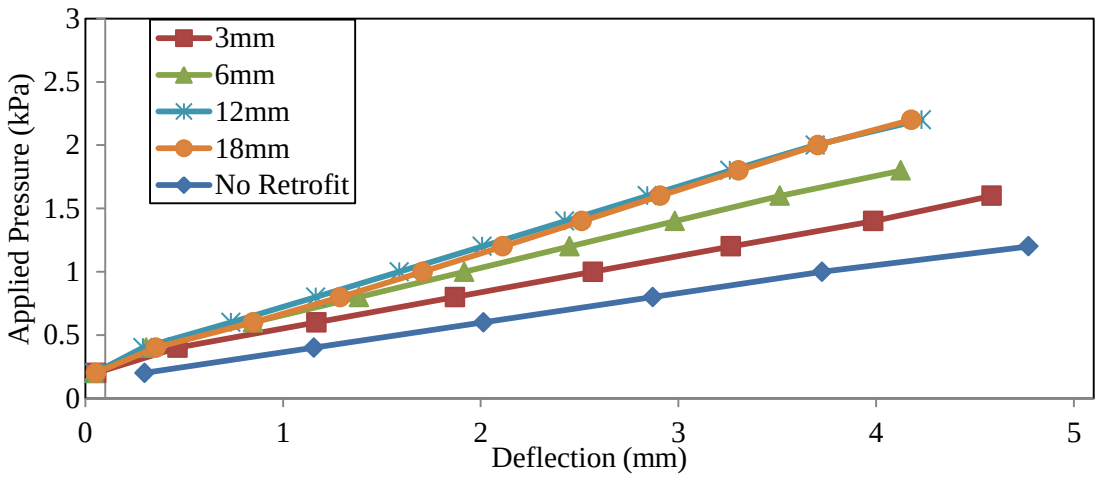

Figure 3.13: Applied pressure vs selected RTW connection deflection for varying external cable diameters

Figure 3.14 presents the axial force in the selected bearing cables for varying external cable diameters. Increasing the external cable diameter increases the total amount of force transferred through the retrofit system, but has little effect on the distribution of force in the bearing cables. The ratio between the maximum and minimum axial force is constant for the selected external cable diameters under the applied pressure.

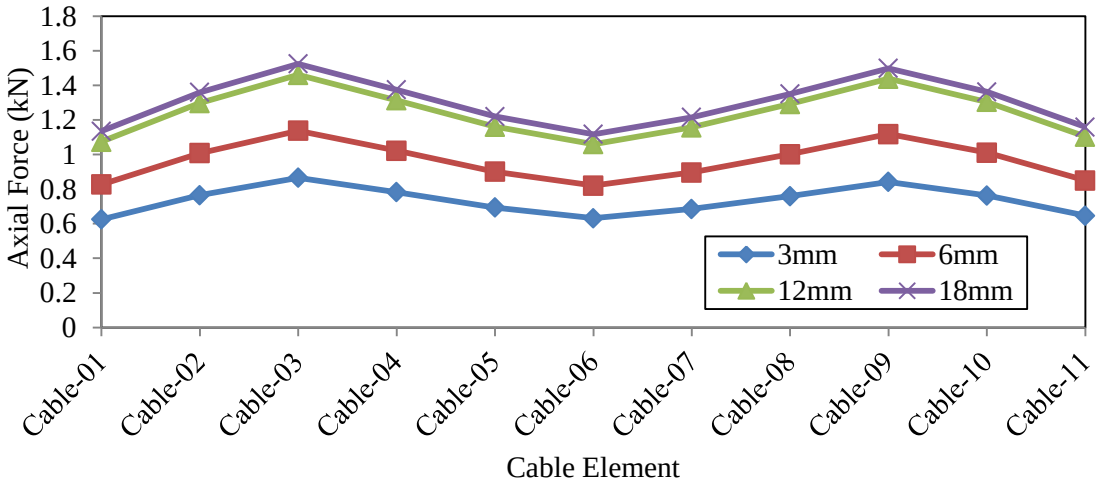

Figure 3.14: Axial force in the bearing cables for varying external cable diameters under 1.6 kPa of uniform pressure

3.4.2.2 Bearing Cable Diameter

Increasing the diameter of the baring cables is effective at increasing the ability of the retrofit system to prevent failure of the RTW connections. As is shown in Figure 3.15, the selected retrofit systems increase the slope of the pressure deflection relationship by 21-108% above that of the original structure.

Similar to increasing the external cable diameter, as the stiffness of the bearing cables becomes much larger than that of the external cables, a further increase in diameter is ineffective at changing the behaviour of the truss system. This is shown in Figure 3.15 by the nearly identical slopes of the pressure deflection relationship of the 6mm and 12 mm bearing cable diameters.

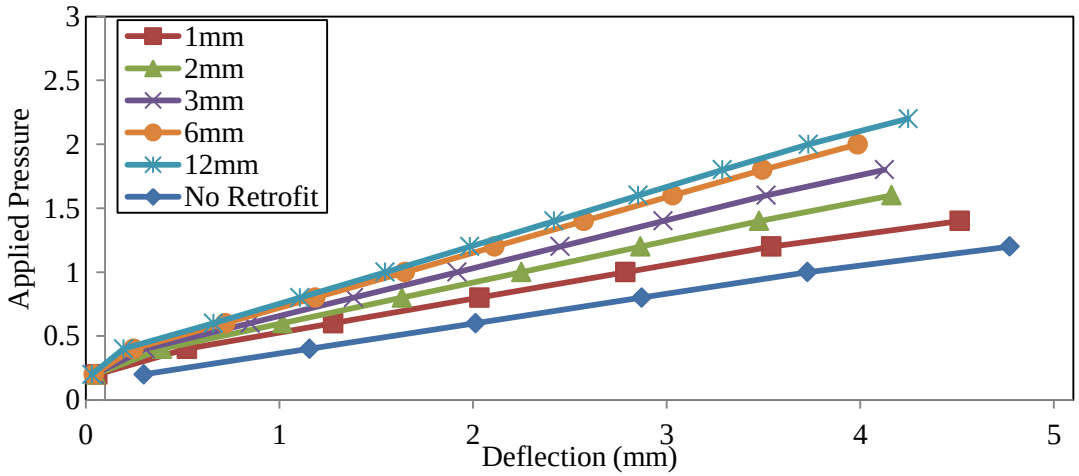

Figure 3.15: Applied pressure vs selected RTW connection deflection for varying bearing cable diameters

Figure 3.16 shows that as the diameter of the bearing cables is increased, the axial force in the retrofit system becomes less uniform. A larger diameter bearing cable results in more force transfer through the retrofit system; however, much of this increase occurs in the members located above the external cable connections. For larger cable diameters, this increase in axial force causes larger midspan deflections in the rigid bar, resulting in

a lower axial force in the center bearing cable (cable-06). As the bearing cable diameter is increased, a more rigid bar becomes necessary to maintain a uniform distribution of axial force in the retrofit system.

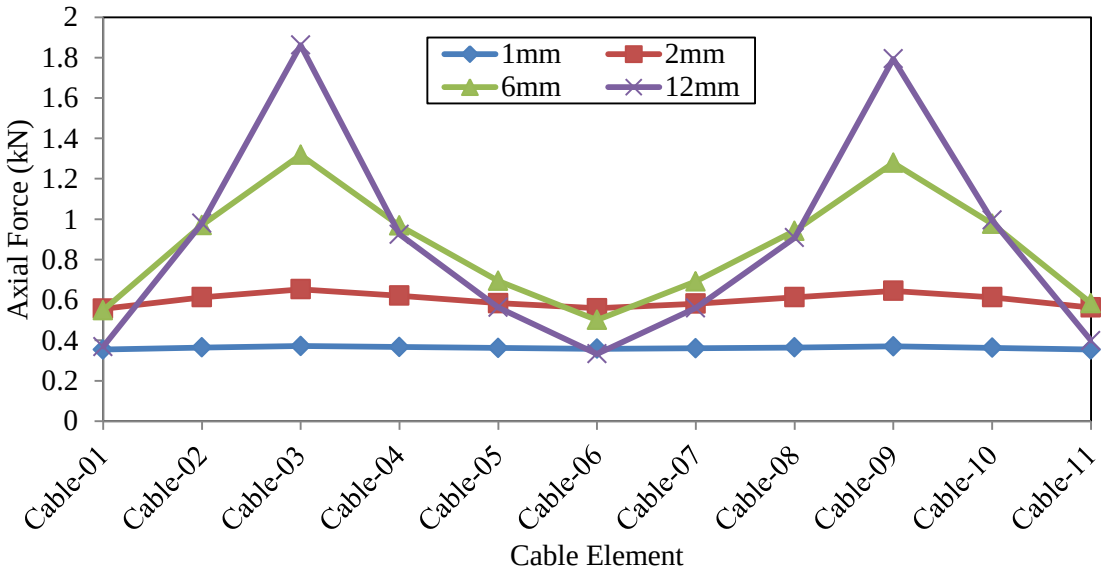

Figure 3.16: Axial force in the bearing cables for varying bearing cable diameters under 1.6 kPa of uniform pressure

3.4.2.3 Effect of Bar Rigidity

Figure 3.17 shows the applied pressure to deflection relationship of the center RTW connection for varying bar rigidities. As the bending rigidity of the bar is increased, the retrofit system increases the slope of the pressure deflection relationship of the RTW connection in the linear range by 34-64%. This range is much smaller than those found for increasing diameters of the external cables and the bearing cables. Increasing bar rigidity is not an effective way to increase the ability of the retrofit system to prevent failure of the truss system.

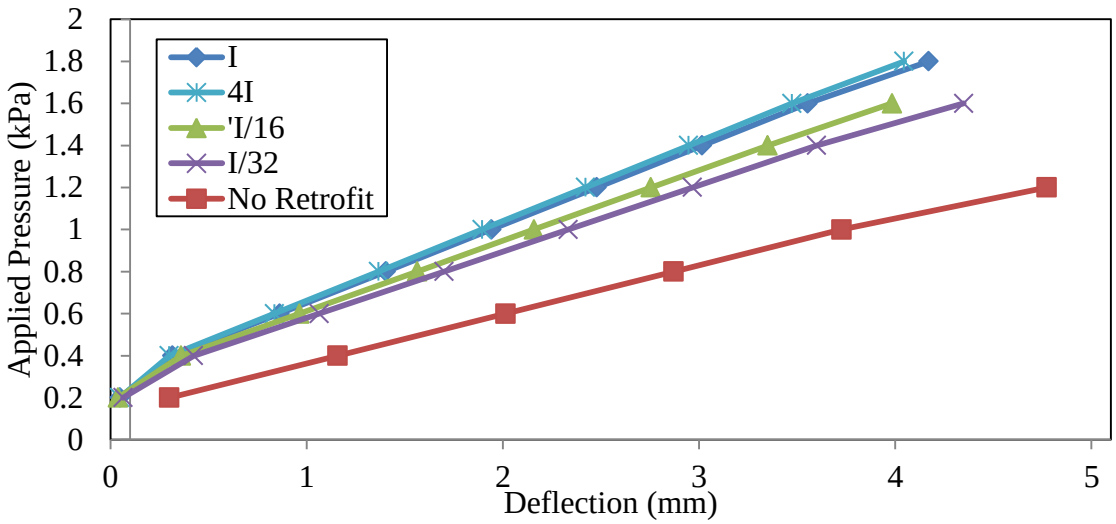

Figure 3.17: Applied pressure vs selected RTW connection deflection for varying bar rigidities

The function of the rigid bar is to create a uniform distribution of axial force in the bearing cables. As shown in Figure 3.18, increasing the bar rigidity results in a perfectly uniform distribution of axial force in the bearing cables. While the bar rigidity does not provide the most efficient way to increase the failure load of the truss system, the uniform distribution created by a more rigid bar reduces the maximum axial force in the bearing cables, thereby reducing the maximum bearing load on the structure. The opposite result occurs for bars with a low bending rigidity, as much higher loads are transferred through the bearing cables that are closest to the external cable connections. The load sharing that occurs in the truss system, transfers the uplift forces to the location of the more stiff bearing cable elements. This results in a larger maximum bearing load of the retrofit system on the structure, even though the system as a whole is less effective.

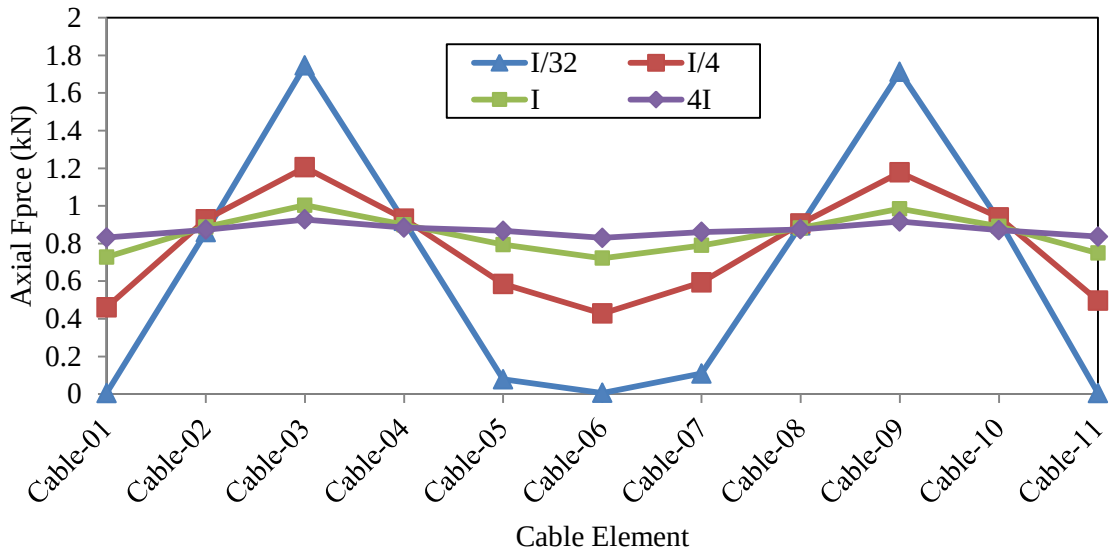

Figure 3.18: Axial force in the bearing cables for varying bar rigidities under 1.6 kPa of uniform pressure

3.4.2.4 Effect of Prestressing

As discussed in the analysis of the typical bending moment of the rigid bar, all forces are transferred in line with the external cables. The initial prestressing force applied to the external cables must be sufficient to create the alternate load path. Initial slack in the retrofit system caused by the self-weight of the components must be removed before the retrofit system becomes effective at relieving force from the structure. If this initial slack is not removed, deflection of the truss system will occur before the retrofit system becomes effective. As shown in Figure 3.19, when initial slack is present in the retrofit system, the slope of the pressure deflection relationship for the RTW connection is the same as the truss system without retrofitting. After deflection of the truss system, the retrofit system becomes taut, creating the alternative load path. The slope of the pressure deflection relationship then increases to match that of the linear range of the retrofit system that has been prestressed to a sufficient level. With initial slack, connection failure occurs at a much lower pressure than an equivalent system with sufficient

pretensioning. This is due to the initial force that is transferred through the RTW connections before the retrofit system becomes effective.

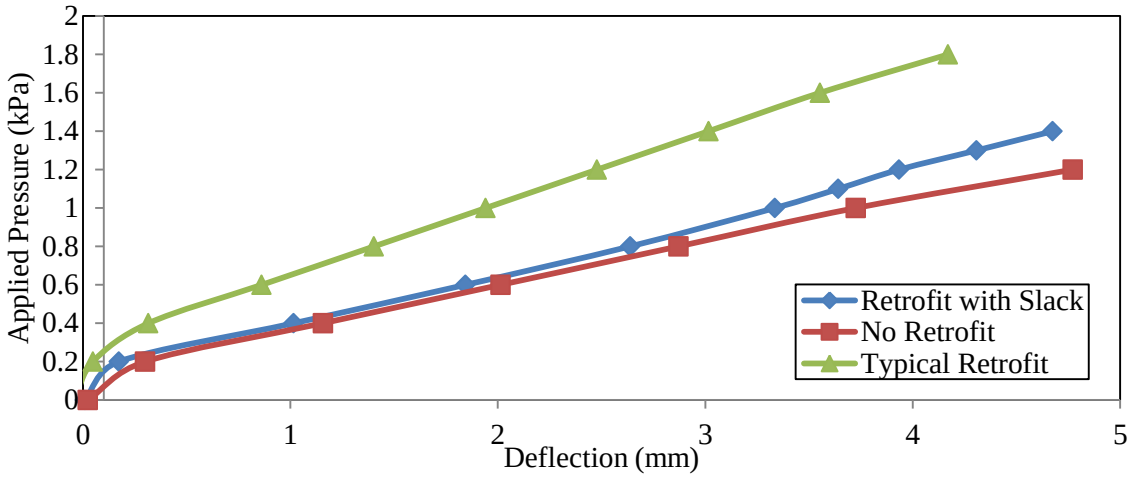

Figure 3.19: Applied pressure vs selected RTW connection deflection for insufficient initial external cable prestressing

Figure 3.20 presents the pressure deflection relationship as the prestressing force is varied. The prestressing force has little effect on the slope of the pressure deflection relationship of the RTW connection in the linear range. The prestressing force increases the load at which deflection begins, shifting the linear range of the pressure deflection relationship to higher applied pressures and increasing the pressure at which connection failure begins.

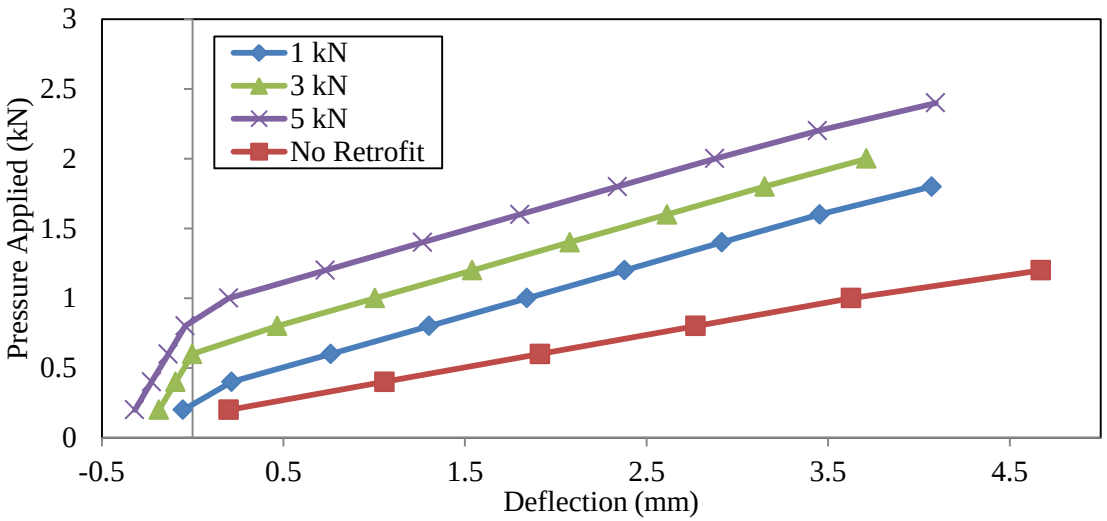

Figure 3.20: Applied pressure vs selected RTW connection deflection for varying initial external cable prestressing

The initial prestressing has little effect on the distribution of axial force in the bearing cables. The prestressing force increases the amount of force in the cables, shifting the distribution to higher loads. The ratio between the maximum and minimum cable axial force remains the same as the initial prestressing force is increased.

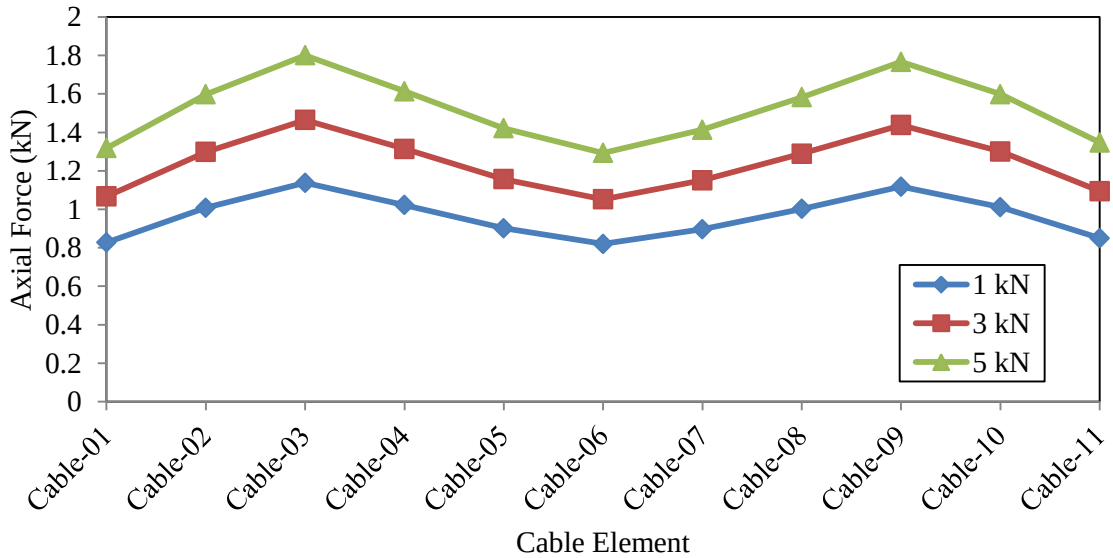

Figure 3.21: Axial force in the bearing cables for varying intial external cable prestressing under 1.6 kPa of uniform pressure

3.4.2.5 Angle of External Cables

The angle between the external prestressing cables and the wall of the structure is varied. The rigid bar is rotated to keep the strong axis of the aluminum bar in line with the cables. The length of the bearing cables overhanging the structure is constant. The external cable elements vary in length as the angle changes.

Decreasing the angle of the external cables increases the effectiveness of the retrofit system, as shown in Figure 3.22. For the studied angles, the slope of the pressure deflection relationship in the linear range increases by 10-100% over that of the original structure. It can be noticed in Figure 3.22 that the retrofit system is relatively ineffective when the angle of the external cables is 60°, as application results in an increase in the slope in the linear range of only 10% over that of the original structure. A reduction in angle from the initially proposed retrofit system (30°) to vertical (0°) increases the slope in the linear range by 26%. Decreasing the angle reduces the length of the external cables. This reduction in length increases the axial stiffness of the external cables, and thereby, enhances the effectiveness of the retrofit system.

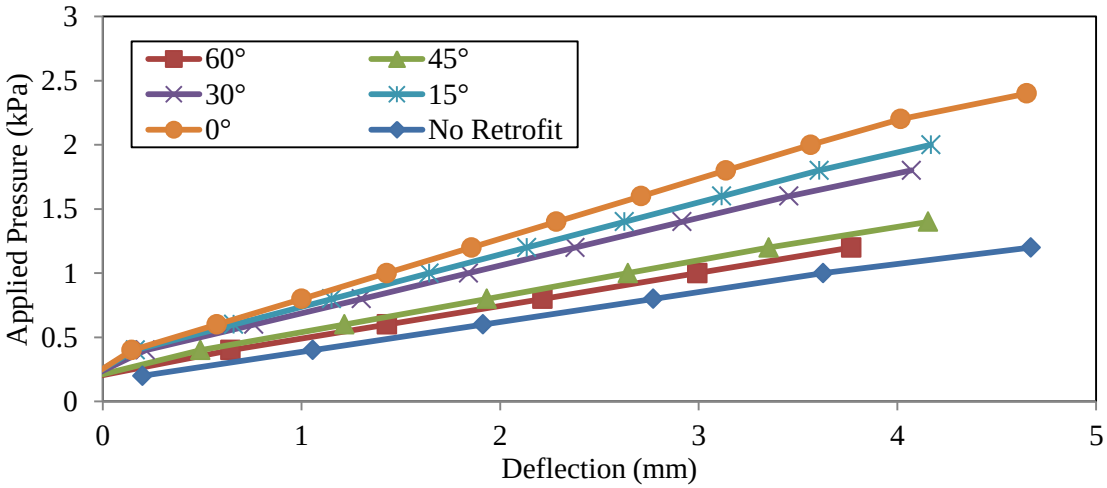

Figure 3.22: Applied pressure vs selected RTW connection deflection for varying external cable angle

Figure 3.23 shows that the angle of the external cables affects the distribution of axial force in the bearing cables. As shown in the parametric study involving varying external cable diameters, the increase in external cable stiffness does not affect the distribution of axial force. The strong axis remains in line with the cables and the bar rigidity has not changed. Thus, decreasing the angle has a similar effect on the axial force distribution as increasing the diameter of the bearing cables. Decreasing the angle increases the force transferred by bearing at the eave of the structure, resulting in higher axial forces in the cable members near the external cable connections. In general, decreasing the angle of the external cables results in more efficient use of the components of the retrofit system.

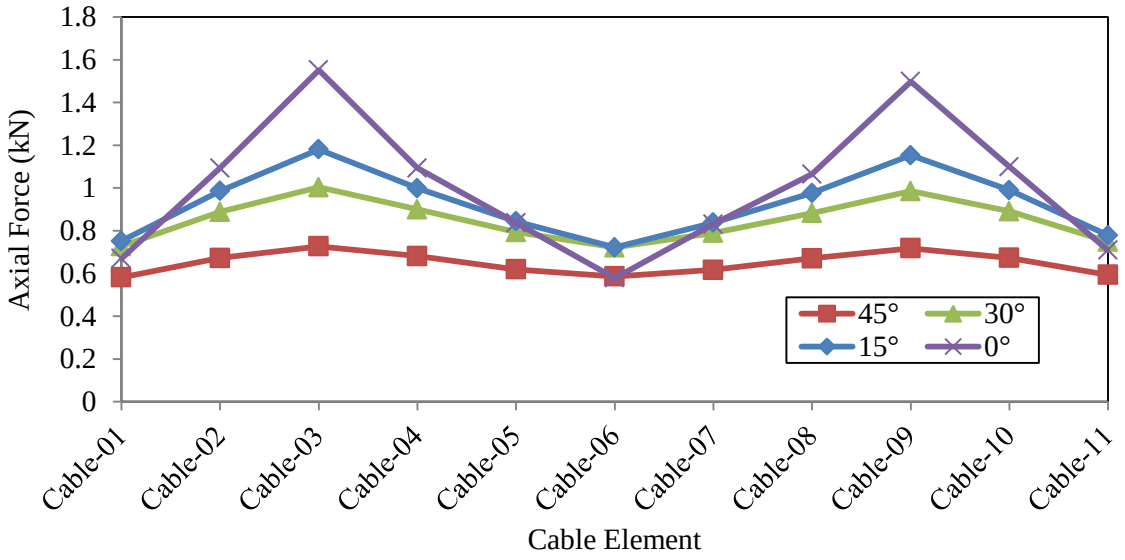

Figure 3.23: Axial force in the bearing cables for varying external cable angles under 1.6 kPa of uniform pressure

3.4.2.6 Effect of the Overhang

Most residential wood structures are constructed with an overhang, therefore, it is important to understand the effect of the overhang on the behaviour of the retrofit system. When applied to a structure without an overhang, the location that the retrofit system bears on the truss system is located immediately above the RTW connection. If an

overhang is present, the bearing location is offset from the connection by the distance of the overhang. The bending deflection that occurs in the overhang reduces the amount of force transferred to the retrofit system. Figure 3.24 presents the pressure deflection relationship for varying overhang lengths. As the distance of the overhang is increased from no overhang to a 500mm overhang, the slope of the linear range of the pressure deflection relationship is reduced by nearly 40%.

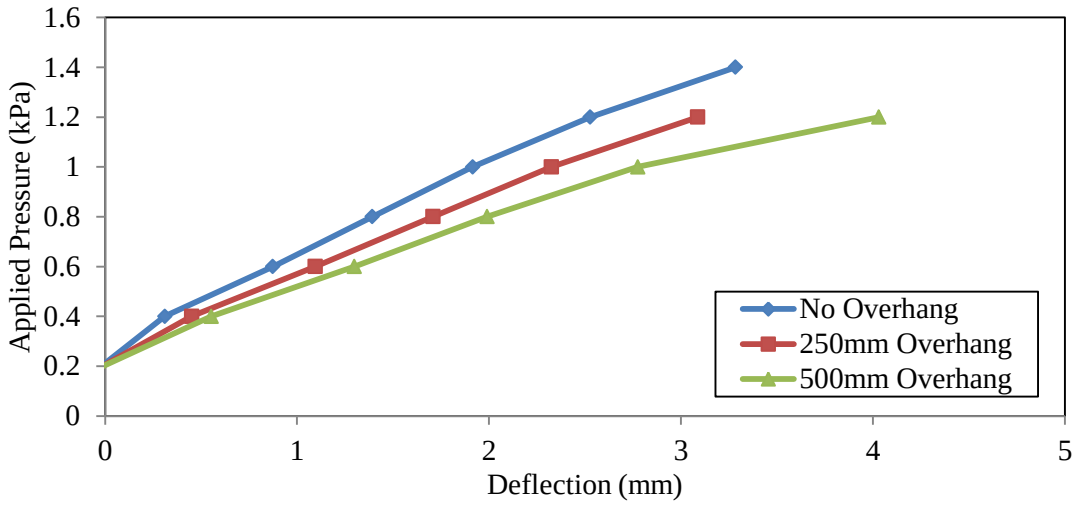

Figure 3.24 Applied pressure vs selected RTW connection deflection for varying roof overhang lengths

3.5 Conclusions

A parametric study is conducted to identify the effect each component of the retrofit system has on the behaviour of the structure and the distribution of forces in the retrofit system. The typical retrofit system is effective at reducing deflections at the RTW connections and reducing the shear force in the plywood sheathing at the critical location. The following results are obtained from the parametric study:

- The diameter of the external cables, the diameter of the bearing cables and the angle of the external cables have a large effect on the slope of the pressure

deflection relationship of the RTW connections, while the bar rigidity and initial prestressing force were found to have little effect.

- The bearing cable diameter, the bar rigidity and the angle of the external cables affect the distribution of axial force in the bearing cables, while the external cable diameter and initial prestressing force have little effect.

- Increasing the initial prestressing force increases the effectiveness of the retrofit system by increasing the load at which deflection starts to be pronounced.

- Reducing external cable angle and increasing the initial prestressing force are found to increase the effectiveness of the retrofit system without increasing component sizes. An optimal retrofit system design will lie on constraints placed on the feasible range of these design variables.

- The system becomes less effective as the overhang of the structure increases due to the deflection that occurs between the point of bearing and the RTW connection.

In general, increasing the stiffness of a design variable increases the effectiveness of the retrofit system. If a component becomes much more stiff than other components of the retrofit system, further increasing the size of that component is ineffective at changing the behaviour of the structure. A balance must be found between the bending rigidity of the rigid bars, the diameter of the bearing cables and the diameter of the external cables to provide an optimal retrofit system design.

3.6 References

Canadian Wood Council (CWC), and Canadian Standards Association (CSA). (2010). *Wood design manual, 2010 :The complete reference for wood design in Canada*. Ottawa: Canadian Wood Council

Computers and Structures, Inc.(2009). SAP 2000 V. 14: Integrated Software for Structural Analysis and Design. Berkley, California, USA.

Department of Housing and Urban Development (HUD). (1993). *Assessment of Damage to Single-Family Homes Caused by Hurricanes Andrew and Iniki*. U.S., Office of Policy and Development and Research, HUD-0006262.

Federal Emergency Management Agency (FEMA) (1993). *Building Performance: Hurricane Iniki in Hawaii - Observations, Recommendations, and Technical Guidance*. Federal Emergency Management Agency.

Jacklin, R., and El Damatty, A. A. (2012). Numerical and experimental study of retrofit system to increase uplift capacity of light-framed wood roofs. *Annual Conference of the Canadian Society for Civil Engineering 2012, June 6-9*, 3. pp. 2440-2449

Morrison, M. J., Henderson, D. J., and Kopp, G. A. (2012). The response of a wood-frame, gable roof to fluctuating wind loads. *Engineering Structures, 41*, 498-509.

National Research Council of Canada (NRC). (2010). *National Building Code of Canada 2010*. Ottawa, NRCC 53301

Reed, T. D., Rosowsky, D. V. and Schiff, S. D. (1997). Uplift capacity of light-frame rafter to top plate connections. *Journal of Architectural Engineering, 3*(4), 156-163..

Stewart, M. G. (2003). Cyclone damage and temporal changes to building vulnerability and economic risks for residential construction. *Journal of Wind Engineering and Industrial Aerodynamics*, 91(5), 671-691

van de Lindt, J., Graettinger, A., Gupta, R., Skaggs, T., Pryor, S., and Fridley, K. (2007). Performance of wood-frame structures during Hurricane Katrina. *Journal of Performance of Constructed Facilities, 21*(2), 108-116.

Chapter 4

4 Analysis and Optimization of a Retrofit System for Light-Framed Wood Structures under Wind Loading

4.1 Introduction

The vast majority of structures in North America are residential. Of these structures, light-framed wood construction is preferred due to the low cost, the availability of materials, and the ease of construction. Typical light-framed wood structures, which satisfy span and load limits, follow the prescriptive requirements of governing building codes to determine the member sizes and connection details. Most light-framed wood structures for residential use meet these guidelines; consequently, structural analysis and design are not needed. Past high speed wind events have exposed vulnerabilities in existing residential light-framed wood structures, with the resulting damage being a major source of economic loss. For example, the damage to light-framed wood structures represented a large portion of the US$20-25 billion of economic losses caused by Hurricane Andrew in 1992 (HUD, 1993), with approximately 95% of the losses resulting from failure of materials of the roof system (Baskaran and Dutt, 1997). Much of the structural damage results from the lack of a continuous load path capable of transferring the uplift loading, which results from high speed winds, from the roof to the foundation (van de Lindt et al., 2007). Post hurricane damage reports (FEMA, 1993) have identified the sheathing-to-truss (STT) connection and the roof-to-wall (RTW) connection as critical connections in the uplift load path of light-framed wood structures.

As vulnerabilities are identified, building codes are updated to improve the capacity of the critical connections. Major improvements were made to the South Florida Building

Code following Hurricane Andrew. These changes were adopted locally in 1994 before becoming standard for the entire state of Florida in 2001 (Gurley et al., 2006). Code changes have also occurred in the most recent edition of the National Building Code of Canada (NBCC) (NRC, 2010). A high wind area is now defined in which both critical connections require a larger capacity than under the previous edition of the building code.

While improved building codes have been found to reduce the number of failures resulting from high speed winds in new structures (Meloy et al., 2007), the structures built to the provisions of outdated versions remain vulnerable. For example, structures built before 1994 in the coastal regions of the United States are extremely vulnerable to the uplift forces caused by wind as the majority use insufficient nails for the STT connection (Datin et al., 2011). The non-structural elements installed in a residential wood structure limit access to critical connections, making it difficult to apply current technologies to existing structures. Stewart et al (2003) presented an economic analysis of the vulnerability of existing residential structures. They estimated that the cost of increasing the hurricane resistance of a structure during construction ranges from 1-10% of the cost of the structure. This cost increases to 15-50% for a retrofit of a current structure, a deterrent to many homeowners. This large cost suggests that a retrofit system is needed to improve the behaviour of these structures under uplift loading.

Past attempts to develop retrofit techniques have focused on increasing the capacity of the individual critical connections. Datin et al (2011) tested a sprayed polyurethane foam adhesive, applied from within the structure to the sheathing and truss members, to reduce the withdrawal demand on the STT connections. The experimental work found that the foam adhesive was effective at increasing the uplift capacity of the roof sheathing by

250-300%. In another study, Canbek et al (2011) investigated the use of a fiber reinforced polymer (FRP) tie to create the RTW connection. Adhesives bond the FRP tie to the top plate and the truss to create the RTW connection. This technology is intended to replace or improve the capacity of the current toe-nail or hurricane clip connection. The FRP tie provided a 65% increase in ultimate capacity when compared to a standard hurricane clip. While both the polyurethane adhesive and the FRP tie are effective at improving the uplift behaviour of the structure, access to the critical members is needed for application. Little research has been presented on a retrofit system that is economical, easy to apply, and effective without modification to the existing structure, which is the focus of this research.

The proposed system consists of a series of cables placed along the sheathing of the roof, identified as the bearing cables in Figure 1.3 and Figure 1.4. Along the eave of the structure, the bearing cables are attached to rigid bars. Cables containing a prestressing device, identified as the external cables, connect the rigid bars to piles that are permanently installed in the ground. When a warning of high speed winds is announced, the system can be easily applied to the roof of the building and attached to the piles. This system provides the uplift forces an alternate load path to the ground without travelling through the weak nailed connections within the structure. Figure 1.3 and Figure 1.4 show the retrofit idea as applied to a gable-style roof.

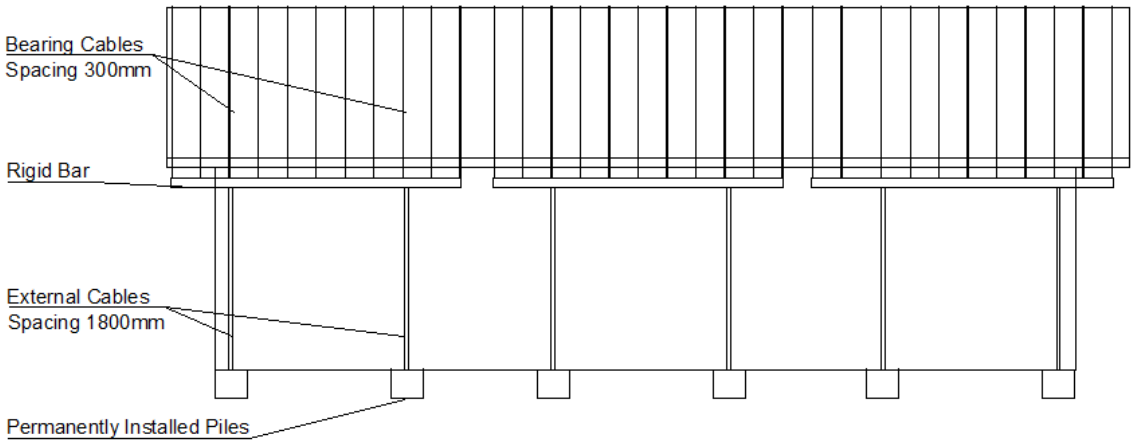

Figure 4.1: Elevation view of proposed retrofit system as applied to a gable-style roof

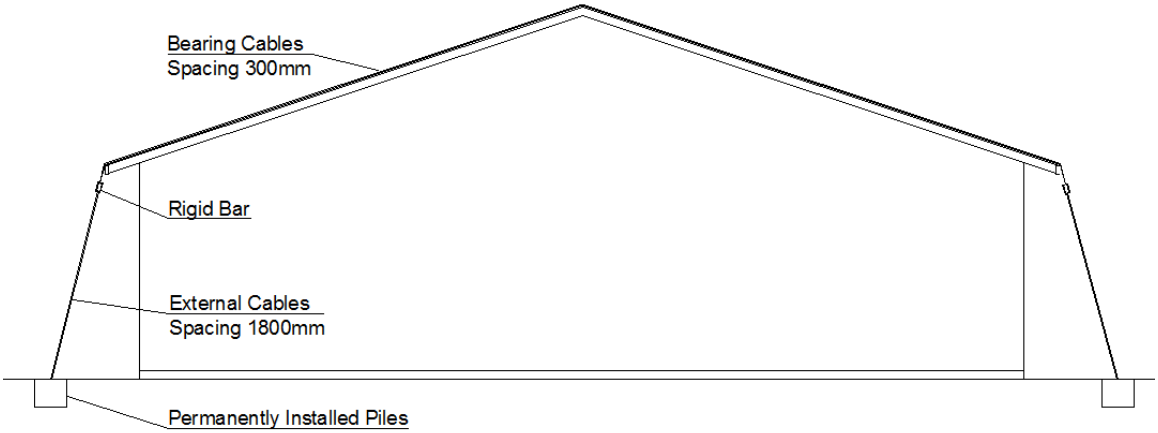

Figure 4.2: Elevation view of proposed retrofit system as applied to a gable-style roof

This chapter begins by developing a numerical model of a typical wood structure that includes plastic damage at the RTW connection. After validation of the model with the results of a full-scale experiment, the nonlinear model is used to assess the behaviour of the proposed retrofit system under non-uniform pressure distributions. The components of the retrofit system are optimized to minimize the weight of the system, while satisfying structural design constraints at a design wind speed. The optimal system is then assessed under non-uniform pressure distributions to evaluate the increase in capacity of the structure after application of the retrofit system.

4.2 Model Description

A finite-element model of the roof of a typical light-framed wood structure has been developed using the commercial software SAP2000 (Computers and Structures, Inc. 2009). The dimensions of the modeled house match those of a full- scale experiment recently conducted at the Insurance Research Lab for Better Homes at The University of Western Ontario. The test structure was built to the provisions of the Ontario Building Code and inspected to ensure that it matched the typical construction techniques of the area. A realistic pressure distribution was developed from a wind tunnel study and simulated using a system of 58 pressure bags, resulting in an applied pressure to the roof sheathing that varied in both time and space. The deflection at each of the RTW connections was recorded. The experiment applied a realistic pressure distribution beginning at a mean velocity of 20m/s, increasing the velocity by 5m/s until failure of the RTW connection, which occurred under the pressure of the 45m/s wind velocity. Further details of the experimental procedure and results are available in Morrison et al. (2012).

The numerical analysis presented in the earlier work focused on the behaviour of the experimental roof structure when the RTW connections remained in the linear elastic range. Applying selected snapshots of the realistic pressure distribution to the numerical model resulted in a similar deflection profile along the length of the structure to that of the test structure. However, the linear analysis was limited to the 25m/s mean wind velocity experimental loading, resulting in small magnitudes of deflection at the RTW connections. When numerical analysis of the experimental pressures corresponding to higher wind velocities was completed, the numerical model became ineffective at predicting the deflected shape of the roof structure due to the nonlinear damage that

occurred at the RTW connection. To capture the nonlinear behaviour demonstrated experimentally, a time history loading and a nonlinear RTW connection are developed for the model. The following section presents a description of the various components of the numerical model.

4.2.1 General Structural Geometry, Elements and Properties

The plan dimensions of the roof are approximately 10m by 10m. As shown in the plan view of the structural skeleton in Figure 2.3, the structure consisting of 16 Howe-style trusses spaced on 600mm (2ft) centers. The trusses have a 4/12 slope and a 9m clear span. Frame and shell elements are used to model the truss and sheathing respectively. The material properties of the frame and area elements match the properties suggested by the Canadian Wood Design Code (CWC and CSA, 2010) for SPF No.1/No.2 lumber and CSP plywood respectively. To accurately model the anisotropic bending behaviour of the roof sheathing, inertia multipliers are used to reduce the bending rigidity in the direction perpendicular to the face grains.

The two exterior trusses, identified as the gable trusses in Figure 2.3, contain modifications when compared to the interior trusses. Each gable truss has additional vertical webbing for the support of the external sheathing. Also, as the gable truss is continuously supported by an external wall, additional RTW connections are made along the length of the truss. These connections result in the gable trusses having a greater stiffness than the interior trusses when subjected to uplift loading.

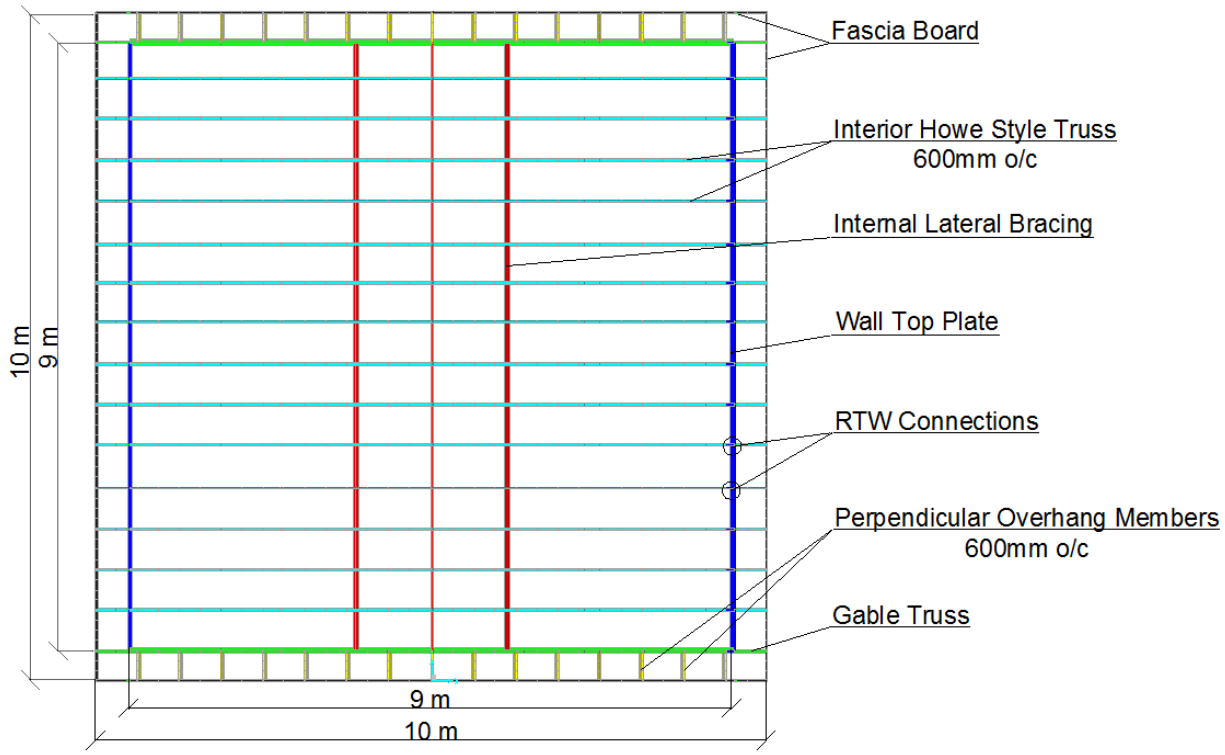

Figure 4.3: Plan view of structural skeleton of roof system

The roof system overhangs the top plate of the walls by approximately 500mm in each direction. Parallel to the trusses, the top chord of the truss continues past the RTW connection by 500mm, supporting the sheathing. The numerical model includes a fascia board, shown in Figure 2.3, which is a 38mm by 89mm (2x4) member running perpendicular to the truss system, connecting the free end of the overhang of each truss. A 500mm overhang is also included at each gable end. The roof sheathing is supported by 38mm by 89mm (2x4) members connected perpendicularly to the gable truss, identified as the perpendicular overhang members in Figure 2.3. A fascia board running parallel to the top chord of the truss is attached to the outer edge of each 38mm by 89mm (2x4) member. The fascia board supports the sheathing along the outermost edge of the overhang around the entire structure.

4.2.2 Time History Load Application

The developed linear elastic numerical model is not accurate at predicting the deflected shape of the structure for experimental loading corresponding to higher wind velocities. Plastic deformation occurs at the RTW connections, indicating that the deflected shape of the structure is dependent on previous loading. To capture this behaviour in the numerical model, a time history load must be applied to the structure.

Twenty seconds of the 35m/s experimental loading is selected for analysis. The selected interval, highlighted in Figure 4.4, contains both the maximum and minimum global roof uplift pressures applied during the 35m/s experimental pressure trace. The majority of the RTW connection damage resulting from the 35 m/s experimental loading occured in this interval. The time history load is applied as 1000 static time steps in which the initial conditions of each step are the load, displacement, and stiffness values of the previous step.

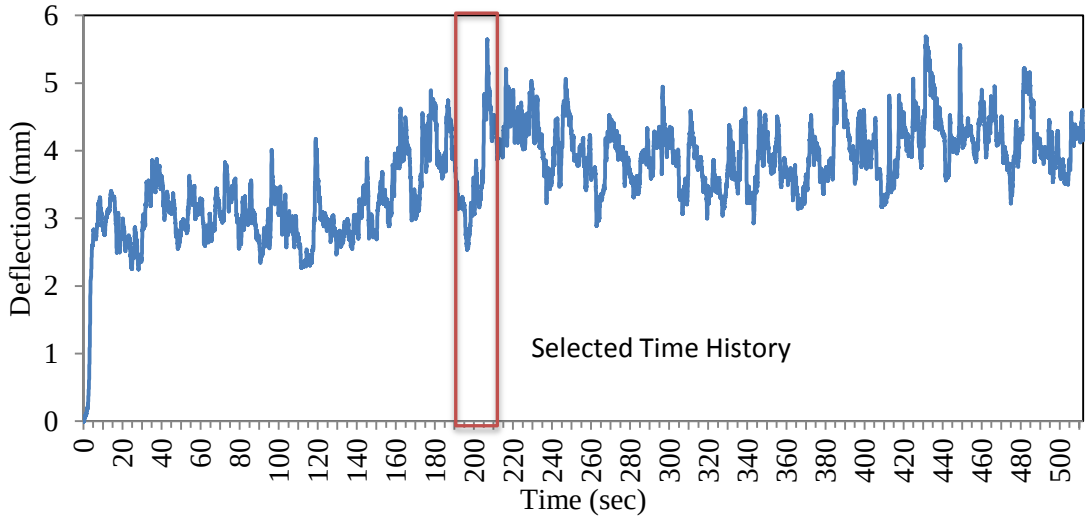

Figure 4.4: Deflection of an experimental RTW connection during the 35m/s experiment

4.2.3 Roof to Wall Connection

The nonlinear RTW connection developed for the numerical model is adapted from the experimental work conducted by Morrison and Kopp (2011). Unlike previous experimental studies, which focus on the behaviour of the connection under a ramp loading, the experimental load applied to the connection simulated a realistic wind pressure. When tested with a realistic loading, the RTW connection suffered permanent withdrawal under the peak gust pressures. During the unloading and reloading phases after damage, the stiffness of the connection remained similar to that of the initial stiffness of the connection.

The numerical model combines two link elements to capture the behaviour of the RTW connection. A nonlinear gap element is used to model the bearing behaviour of the truss on the top plate. This element has a stiffness that is an order of magnitude larger than the initial withdrawal stiffness of the RTW connection, preventing negative deflection under compression loads. The gap element has no effect on the stiffness of the connection under tension loading. This element is necessary to prevent negative deflection of the truss system under the deal load of the structure, allowing for realistic initial conditions for the retrofit system.

To capture the withdrawal behaviour described by Morrison and Kopp (2011), a multi-linear plastic link element is selected assuming a kinematic hysteresis loop. A multi-linear load deflection curve is adapted from the experimental results presented by Morrison and Kopp (2011). The initial stiffness of the connection is 1650kN/m. Damage begins as the connection is loaded above 2.3kN in withdrawal as the deflection follows the second slope of the load deflection relationship presented in Figure 4.5. After the

connection is loaded above this damaging load, the unloading and reloading of the connection follow the initial slope. Above 12mm of deflection, it is assumed that connection failure has occurred and the RTW connection withstands zero force. Figure 4.5 presents the load deflection curve resulting from the combination of the two elements.

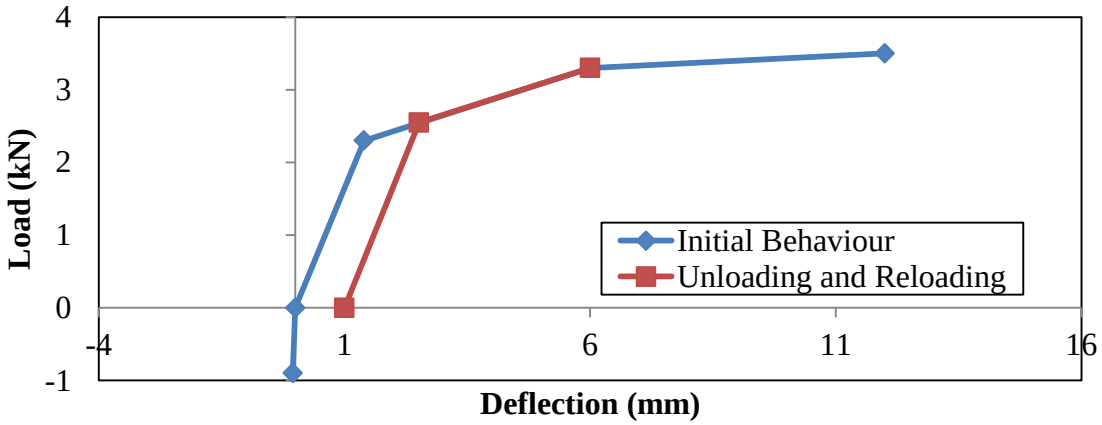

Figure 4.5: Developed load deflection response for roof to wall connection

4.2.4 Wall System

The effect of the wall system on the vertical deflection of the RTW connection is neglected in the numerical model. The axial deformation of the stud wall in the experimental structure is negligible under the magnitude of loading applied. It is assumed that any vertical deflection that occurs in the wall system is caused by the initial movement of the interior nailed connections.

Although neglected in the vertical loading, the behaviour of the wall system under lateral loading is captured in the numerical model. The behaviour of the walls under lateral loading can be idealized as shear walls connected by a rigid diaphragm, as demonstrated by the experimental work of Paevere et al. (2003) and Phillips et al. (1993), who have found that the diaphragm action demonstrated by the roof structure behaves much closer to a rigid diaphragm than a flexible diaphragm. A rigid diaphragm is assumed at the

height of the top plate of the wall, where linear springs are attached to external restraints to capture the in-plane stiffness of the shear walls. This in-plane, racking stiffness is a linear approximation of the experimental results presented by Kasal et al (1994). The structure contains two, 2.4m (8') stories. Each side of the structure is assumed to contain two shear wall sections per story, each of which is 4.8m (16') long. The stiffness is developed assuming that each wall is constructed of 38mm by 89mm (2x4) studs, internal drywall sheathing and external plywood sheathing.

4.2.5 Numerical Model of Retrofit System

The numerical model of the full-scale structure is extended to include the proposed retrofit system. The behaviour of the rigid bars is modeled using linear frame elements. Cable elements are used to capture the highly nonlinear behaviour of the bearing and external cables. The stiffness of the slender cables is dependent on the initial layout of the retrofit system, which is specified in the software. Pretensioning of the retrofit system is simulated by applying strain loading to the external cables, ensuring an initially taut system.

To simulate the interaction between the bearing cables and the roof sheathing, the nodes of the cable elements are set to have compatible displacements with the nodes of the sheathing in the axis perpendicular to the sheathing. The constraint has no effect on displacements in the plane of the sheathing. By specifying a constraint on displacement in the axis perpendicular to the sheathing, the numerical model captures the effect of the cable bearing on the truss while neglecting the frictional forces between the sheathing and the retrofit system.

4.3 Numerical Results

The validation of the finite-element model includes a comparison of the numerical predictions to the full-scale experimental results in terms of the deflection at the RTW connections. The comparison is presented along the length of the structure at selected time steps and through the time history at selected RTW connections.

Each connection is labeled as either a north or south link, followed by the truss number, ranging from 1 to 18. The windward corner is labeled connection N-01, with numbers increasing along the length of the structure. Overhangs are labeled connections N/S-01 and N/S-18. The gable ends are labeled connection N/S-02 and N/S-17.

The realistic pressure distribution of the selected time history is applied to the numerical model. The numerical results are modified so that the numerical and experimental RTW connection deflection results match under the loading of the first time step. The difference between the experimental results and the numerical prediction is calculated for each RTW connection under the loading of the first time step. This initial difference at each RTW connection is then added to the results of the numerical model for the remaining 999 time steps. The initial difference between the numerical and experimental deflection is assumed to be the result of the initial deflection of the nailed connections within the walls of the structure or permanent withdrawal of the RTW connection that occurred in earlier experimentation.

Figure 4.6 presents a comparison of the load deflection behaviour of the RTW connection resulting from applying the assumption described above when the experimental connection has suffered 1mm of permanent withdrawal. As discussed earlier, the

experimental results presented by Morrison and Kopp (2011) found that after the permanent withdrawal that occurs under a realistic wind load, damaged RTW connections have a similar stiffness to that of the undamaged connection. By shifting the results of undamaged numerical model to match the deflection of the damaged experiment, the load deflection behaviour of the connections match until the structure is loaded to the level where the connections suffer further damage. Above this level, some error is expected; however, given the variability of the properties of the RTW connection, especially in the nonlinear range, this error is accepted.

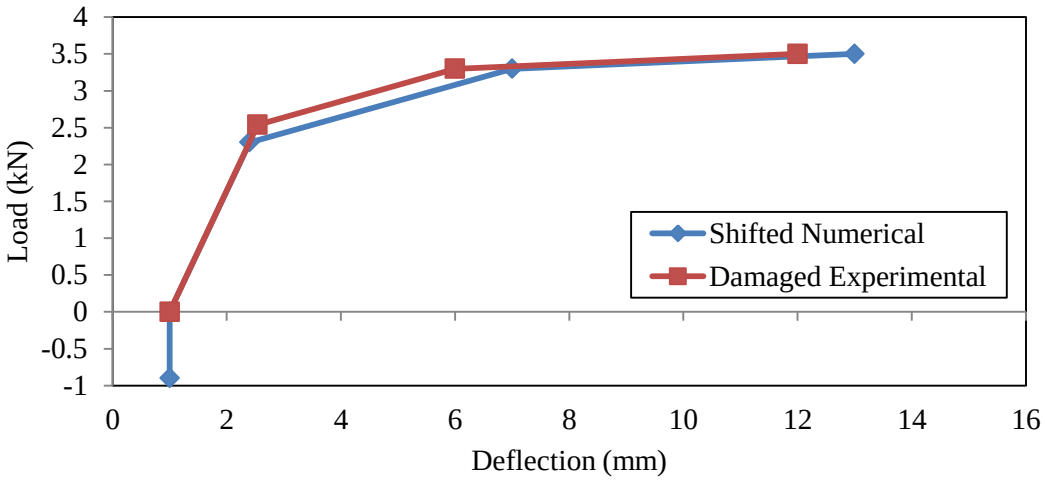

Figure 4.6: Shifted and damaged experimental behaviour with loading

4.3.1 Comparison to the Experimental Results

Figure 4.7 presents the deflection of the RTW connections for the time step corresponding to the maximum global roof uplift pressure. The numerical model is able to match the experimental results accurately, resulting in an average percent difference of 5%. The maximum magnitude of difference between experimental and numerical RTW connection deflections at this time step is 0.3mm. The model accurately predicts both the magnitude and shape of the structure for every RTW connection under this loading.

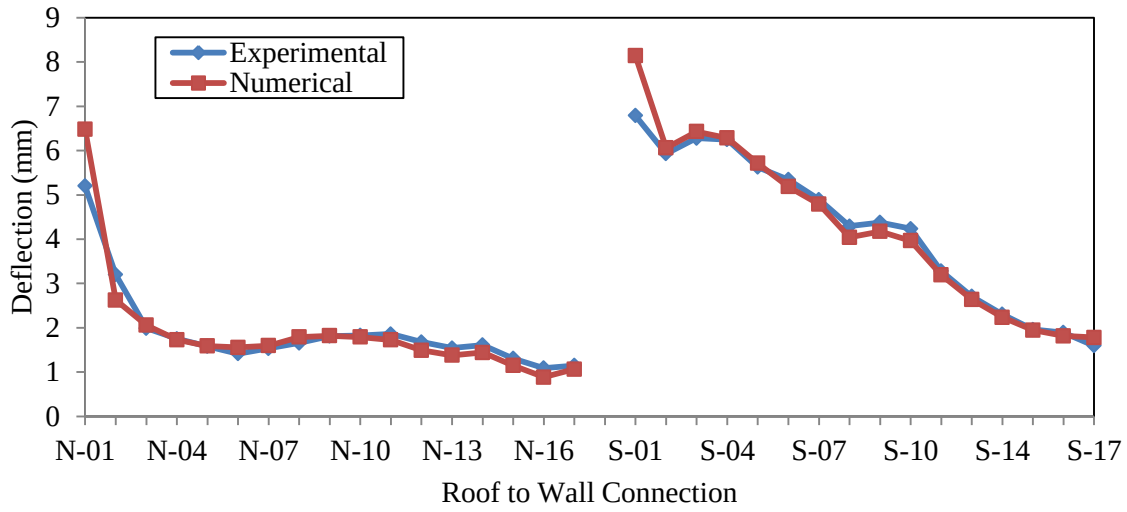

Figure 4.7: Deflected shape of the structure under maximum global uplift pressure (Time Step 633)

Figure 4.8 shows the deflection of the RTW connections under the minimum global roof uplift applied during the selected time history. The deflected shape of the experimental structure matches the numerical prediction for both the north and south connections; however, the numerical model tends to overestimate the deflection of the south connections. The maximum magnitude of error under this loading is 0.5mm at connection S-10, which is an 18% difference.

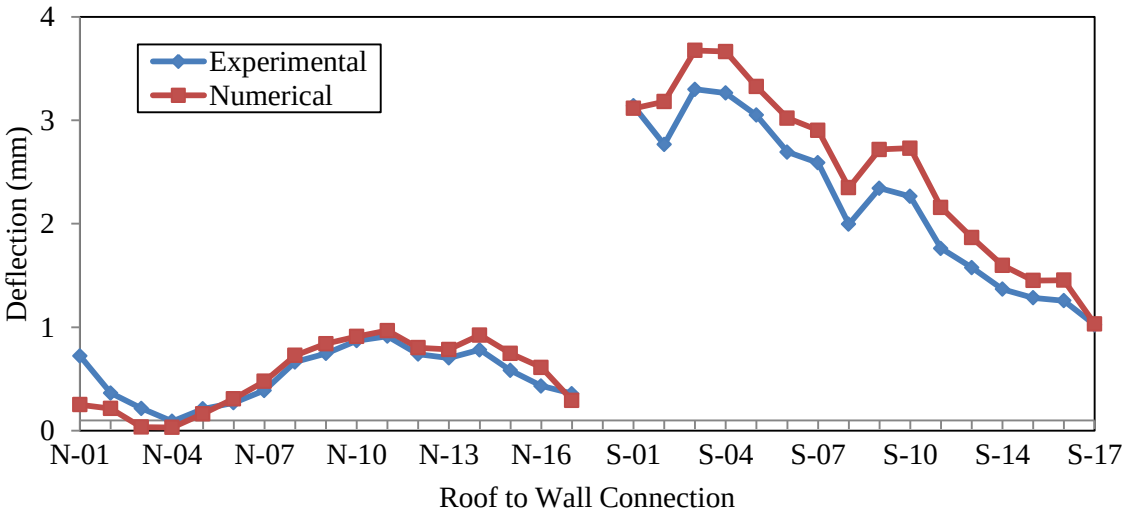

Figure 4.8: Deflected shape of the structure under minimum global uplift pressure (Time Step 116)

Figure 4.9 through Figure 4.11 show the deflection of selected RTW connections throughout the time history. Each connection presented shows the same trend as discussed above. The numerical model provides a better prediction of the deflection when the structure is loaded above the initial deflection. The numerical prediction tends to predict deflections larger than the experimental results around the global minimum uplift pressure.

Considering the variability of the stiffness of each connection, the numerical model provides a strong prediction of the deflection of each connection through time. Truss 3 represents the truss that the largest uplift pressures are applied. The numerical model shows very strong agreement with the experimental results for both the north and south connections for this truss. The prediction of the range of deflection for the north and south side connections on this truss are within 9% and 15% of that of the experimental results respectively. Connection S-09 shows the largest magnitude of difference in range in the data, with a 1.1mm difference between the experimental and numerical work, a 40% difference. As the pressure varies with time, the numerical model provides a strong approximation of the increase and decrease of the deflection of the RTW connection throughout the structure.

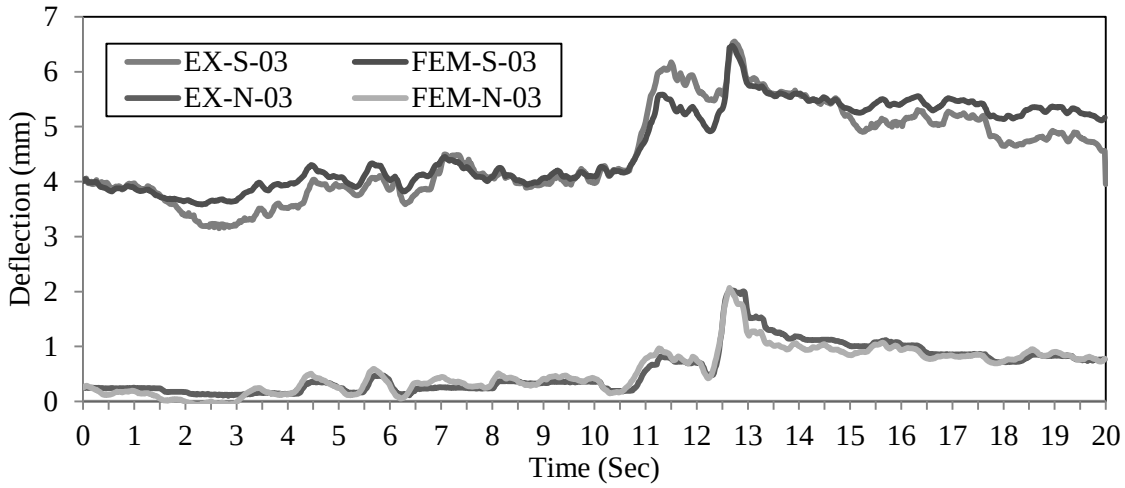

Figure 4.9: Experimental and numerical RTW connection deflection for truss 3

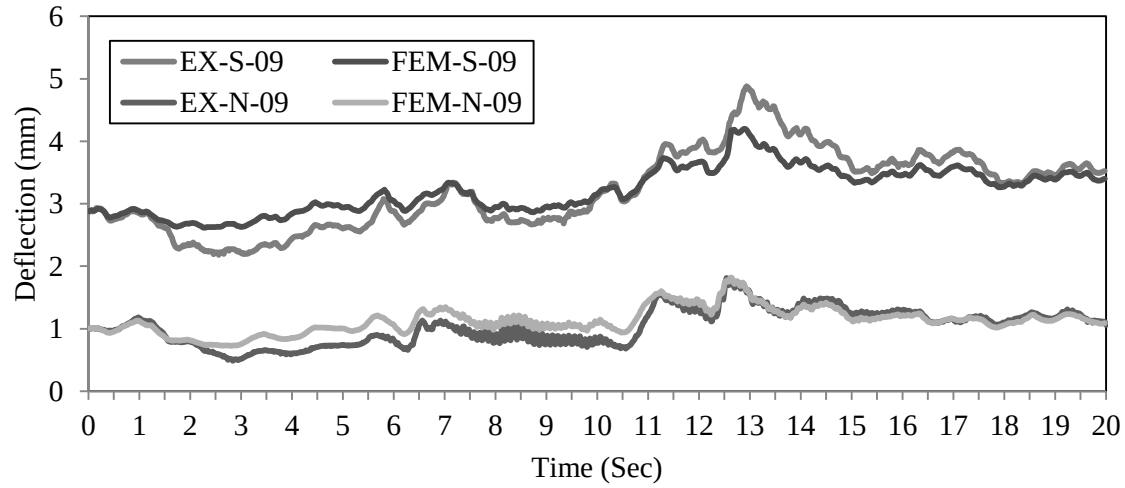

Figure 4.10: Experimental and numerical RTW connection deflection for truss 9

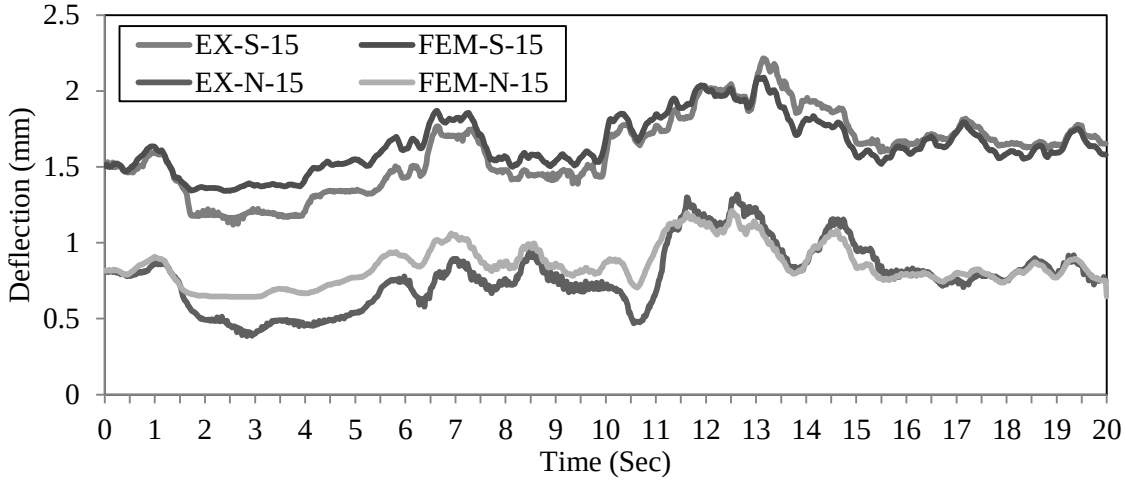

Figure 4.11: Experimental and numerical RTW connection deflection for truss 15

Figure 4.12 confirms the strong prediction of the numerical model, showing that the average magnitude of percent difference between the experimental and numerical RTW connection deflection throughout the time history remains below 10% for each south side connection. The model shows strong agreement with the experimental results for the interior trusses to which the largest pressures are applied, s-03 to s-07, as the magnitude of the percent difference through time remains below 6% for these connections.

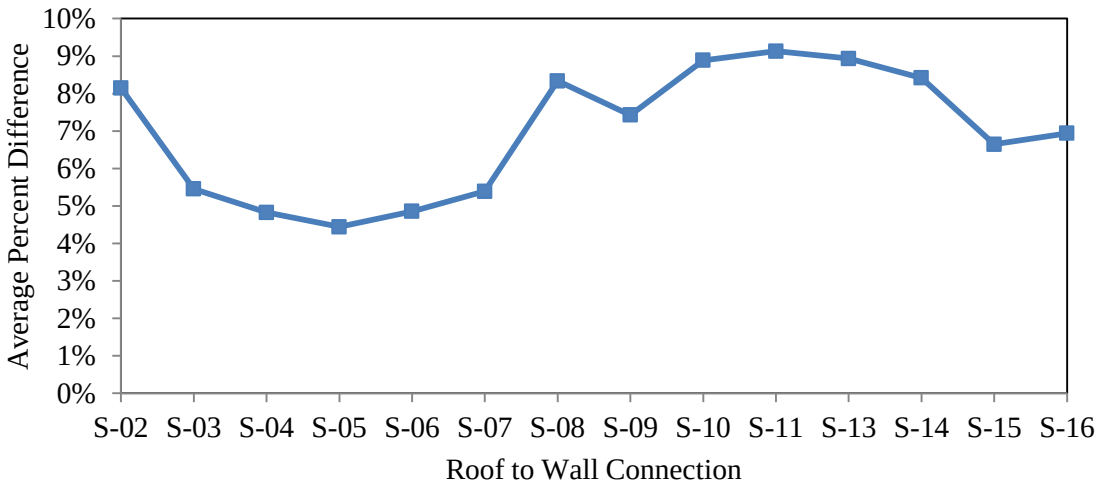

Figure 4.12: Average magnitude of percent difference between experimental and numerical RTW connection deflections

4.3.2 Analysis of the Permanent Nail Withdrawal

The selected realistic pressure distribution is analyzed using an equivalent elastic numerical model, where each step is independent of the previous loading, to determine the magnitude of plastic deformation that occurs. As shown in Figure 4.13, which presents the deflection of the critical RTW connection around the damaging peak pressure, the numerical model capable of capturing the plastic deformation of the RTW connection provides a better approximation of the experimental results after damage than the elastic model. The connection is first damaged under the pressure applied at 11.3 seconds of the time history, after which the models with the plastic and elastic

connections are no longer equal. After the maximum global uplift pressure is applied to the structure at 12.6 seconds, the critical connection suffers approximately 2mm of permanent withdrawal.

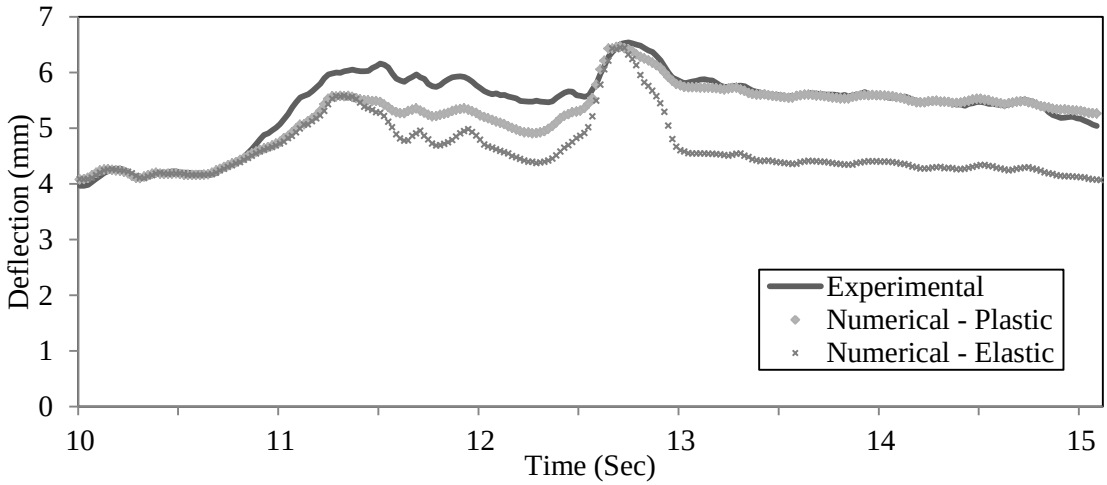

Figure 4.13: Experimental results compared to the plastic and elastic analysis for the critical connection, S-03

The deflection of the RTW connections along the length of the structure after the damaging peak pressure is presented in Figure 4.14. The plastic damage that occurs to the RTW connections creates a difference in deflection in connections N-02 to N-07 and S-2 to S-10. The plastic deformation that occurs during the damaging peak results in an inaccurate model if the structure is assumed to be elastic. The accurate results of the plastic numerical model confirm that a time history loading is necessary to accurately predict the deflection of the RTW connections of a light-framed wood structure under high speed wind loading.

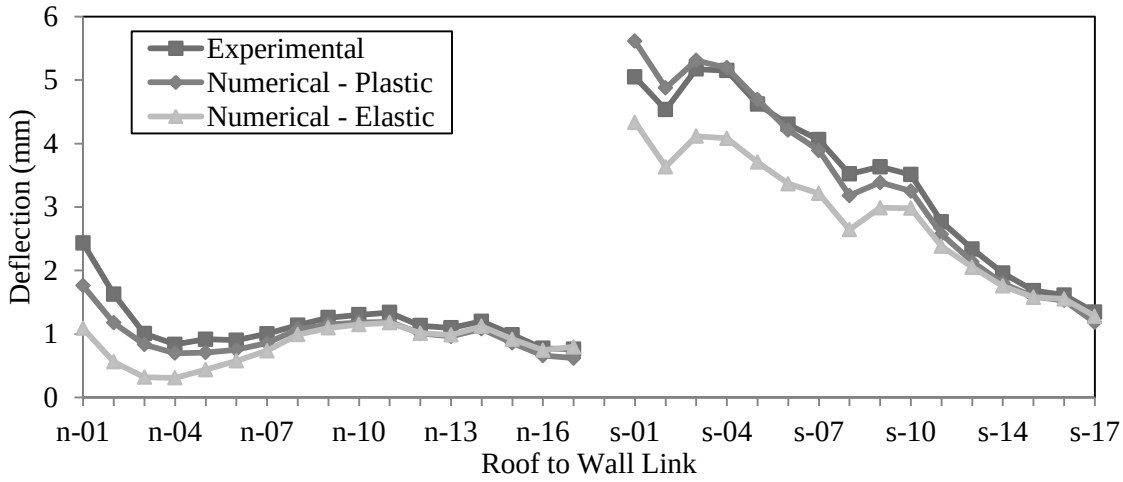

Figure 4.14: Deflected shape of the structure after damaging load, Time = 15 sec

Considering the variability in the stiffness of the RTW connections, the developed numerical model shows very strong agreement with the experimental results. Applying the assumption that the initial difference between the experimental and numerical results is caused by the initial slip of the interior nailed connections, the developed model provides an accurate prediction of the experiment. A numerical model that includes a plastic RTW connection dependent on the previously applied loading is found to provide a more accurate approximation of the experimental behaviour than an equivalent elastic structure.

4.4 Parametric Optimization under a Non-uniform pressure distribution

A discrete parametric study is completed to determine the properties of the retrofit system with the minimum weight that is capable of satisfying selected structural design constraints under a design wind load. Steel and aluminum sections tend to have a cost proportional to weight; therefore, minimal weight will also provide an approximation of the retrofit configuration with minimum cost. Minimizing the weight will also be beneficial for the ease of application of the system. Details of the parametric study are

provided below, including the design wind speed, the design variable and the design constraints.

4.4.1 Design wind speed and loading

A 45 m/s, mean hourly wind speed has been selected as the design wind speed for the structure. Assuming the air density suggested by the NBCC, this wind speed results in a reference wind pressure above the maximum 1 in 50 year pressure provided in the climactic data of the code (NRC, 2010). The loading pattern is selected assuming a wind perpendicular to the ridge, which is the critical case for global roof uplift pressures. Internal pressures, as suggested by the NBCC, are not applied to the structure.

4.4.2 Design Variables

Five design variables are considered: the diameter of the external cable, the diameter of the bearing cables, the initial prestressing force, the cross-sectional properties of the rigid bar and the spacing of the bearing cables. The values considered for each design variable, which have been selected at discrete points within a feasible range, are presented in Table 4.1. Each of the possible 216 retrofit system configurations are assessed numerically.

Table 4.1: Values considered for the design variables

Design Variable	Values Considered
Bearing Cable Diameter (mm)	4, 6, 8
External Cable Diameter (mm)	5, 7.5, 10, 12.5, 15, 17.5
Rigid Bar Dimensions (mm)	Base-50.8, Wall Thickness-6.35 Height-102, 152, 203
External Prestressing Force (kN)	1, 2
Bearing Cables Spacing (mm)	300, 600

4.4.3 Design Constraints

Strength constraints are placed on both the retrofit system and the structure to ensure the system is effective at a selected design wind loading.

4.4.3.1 Retrofit Strength Constraints

The cable elements used in the numerical model are assumed to be a solid steel cross section. The maximum axial stress is limited by the yield stress of steel, 350 MPa. Typical aircraft cable is made of strands, which reduce the cross-sectional area below that of a solid cross section. To be equivalent to the numerically modeled system, a full-scale retrofit system must match the cross-sectional stiffness of the solid cable, resulting in a larger cable diameter.

Shear and bending capacities are calculated for each rigid bar cross section assuming 6061-T6 aluminum alloy with a yield stress of 240MPa and an ultimate shear stress of 165mPa.

4.4.3.2 Structural Strength Constraints

Strength constraints are placed on three components of the structure to ensure the structure can withstand the demands caused by the retrofit system. The maximum bending moments in the sheathing are limited by the values provided by the CWDC for ½" CSP plywood. The strong axis bending moment is limited to 420Nm/m and weak axis bending moment to 140Nm/m. Moments are assessed at the peak of the structure, where the bearing forces applied to the structure by the retrofit system cause the maximum resulting moments.

The maximum combined bending and axial load acting in the truss member of the overhang is limited by the value given in the CWDC for a 38mm x 89mm SPF No.1/No.2 member. Combined bending and axial load is assessed on both the north and south side of the structure near the RTW connection, where the cantilever of the overhang begins. The

maximum shear force transferred from the fascia board to the truss is limited by the strength given by the CWDC for the connection, typically constructed using two, 16D nails driven into the end grains of the truss.

The selected constraints are based on structural failure. Bearing constraints are not analyzed as the goal of the system is to maintain the integrity of the structure. Slight non-structural damage is acceptable.

4.4.4 Results

Of the retrofit system configurations assessed in the parametric study, none are able to satisfy all selected design constraints. The fascia board to truss connection has insufficient strength to withstand the shear demand caused by the application of the retrofit system. While failure of the fascia board is undesirable, the fascia board is a non-structural element and the integrity of the structure remains after failure. The optimum solution is found neglecting this failure.

Table 4.2 presents the demand to capacity ratio for each component of the optimum solutions resulting from analysis at the design wind pressure. The optimum solution resulting from a 600mm bearing cable spacing is a 6mm bearing cable diameter, 10mm external cable diameter, a 102mm by 52mm with a 6mm hollow rectangular rigid bar, and 2kN initial external cable prestressing. A 300mm bearing cable spacing results in the optimum solution of a 4mm bearing cable diameter, 15mm external cable diameter, 102mm by 52mm with a 6mm wall hollow rectangular rigid bar, and 2kN initial external cable prestressing. The diameter of the bearing cables can be reduced with more frequent cables; however, the optimal solution becomes heavier than that of the optimal retrofit

system with a 600mm bearing cable spacing. A 15% reduction in weight is possible with the combination of larger a bearing cable diameter at a greater spacing with a smaller external cable diameter.

Table 4.2: Demand to capacity ratios for the optimum solutions of the parametric study

Element	**600mm Bearing Cable Optimum**	**300mm Bearing Cable Optimum**
External Cable	0.44	0.20
Bearing Cable	0.61	0.74
Rigid Bar Shear	0.04	0.04
Rigid Bar Moment	0.17	0.18
Sheathing Bending, Strong	0.07	0.10
Sheathing Bending, Weak	0.34	0.93
Combined Moment and Axial in Overhang	0.36	0.37
Shear Transfer by Fascia	1.62	1.63
Weight (kG)	145	166

The results of the parametric study show two trends that are of concern for the adaptation of the retrofit system to individual structures. First, configurations with a 300mm bearing cable spacing result in larger bending moments in the sheathing, with many demonstrating a weak axis bending failure at the design wind load. Failure of the sheathing did not occur for any retrofit system configuration with a 600mm bearing cable spacing. Second, a 300mm bearing cable spacing also results in larger shear forces being transferred by the fascia board to truss connection. From these trends, it can be concluded that the retrofit system has less negative effects on the structure when it is spaced at the same dimensions as the truss system, bearing on the sheathing above the trusses where possible.

The results of the parametric study also find that the forces acting on the rigid bar are well below the capacity of the member. None of the analyzed retrofit system configurations result in a demand to capacity ratio for the rigid bar above 35% for

bending and 10% for shear under the loading of the design wind pressure. The uniform parametric study completed in the earlier work found that the bending rigidity of the bar is critical to the performance of the system. To provide sufficient bending rigidity to create a near uniform distribution of force in the bearing cables, the bar becomes sufficiently large that the applied loads are well below the failure capacities.

The numerical model predicts that the components of the optimal retrofit system are a 6mm bearing cable diameter, a 10mm external cable diameter, a 102mm by 52mm with a 6mm hollow rectangular rigid bar, 2kN initial external cable prestressing at a 15° angle with the vertical wall. While no system could prevent failure of the fascia board, the optimal system passes all other selected design constraints. This system provides the minimum weight for a system that is effective at increasing the capacity of the structure above the selected design load.

4.5 Assessment of Optimized Retrofit under Non-uniform Pressure Distributions

The optimal retrofit system is assessed numerically and compared to the numerical results of the bare structure to determine the improvement on the uplift behaviour that results from application. The 1000 step realistic time history and the non-uniform code pressure distribution discussed in the previous sections are selected for the analysis.

4.5.1 Assessment Under Selected 35mps Time History

When analyzing the effect of the retrofit system along the length of the structure, the retrofit system proves to be effective, as shown in Figure 4.15, which presents the connection deflection under the maximum global roof uplift pressure applied during the

selected time history. The maximum RTW connection deflection at this time step is reduced from 3mm to 1.3mm, with less deflection occurring at each connection after application of the retrofit system. The optimal retrofit system is effective at reducing the deflection at the RTW connection but has little effect on the deflected shape.

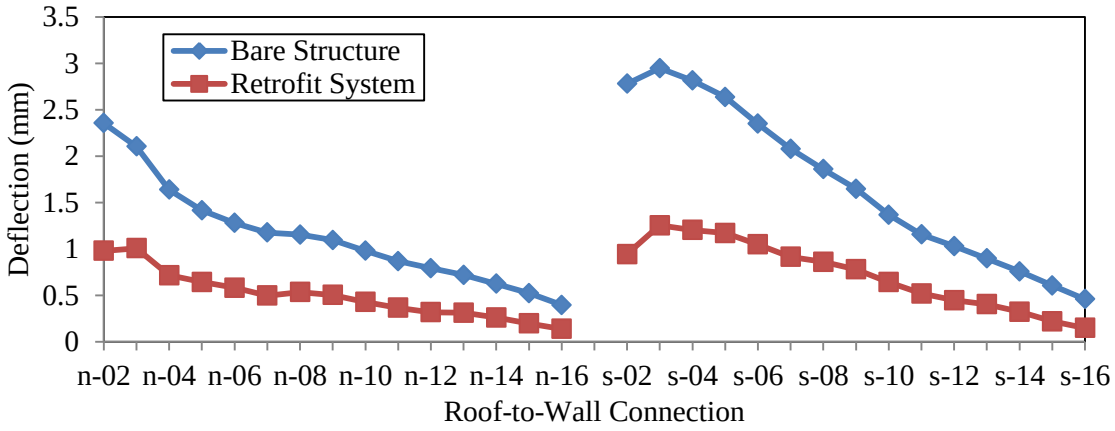

Figure 4.15: Deflected shape of the RTW connections under the maximum loading

The retrofit system is also found to be effective when analyzing the deflection of the critical connection throughout the time history, as show in Figure 4.16. The maximum deflection of this connection is reduced from 3mm to 1.1mm with application of the retrofit system. The secondary load path provided by the retrofit system results in a reduction in the maximum withdrawal force applied to the connection of 0.6kN, from 2.7kN to 2.1kN. As a result of the reduction in applied load, the connection is prevented from suffering damage during the peak pressure. The difference in deflection between the bare and retrofitted structures appears larger after the damaging peak load at step 630 as the bare structure suffers permanent connection withdrawal.

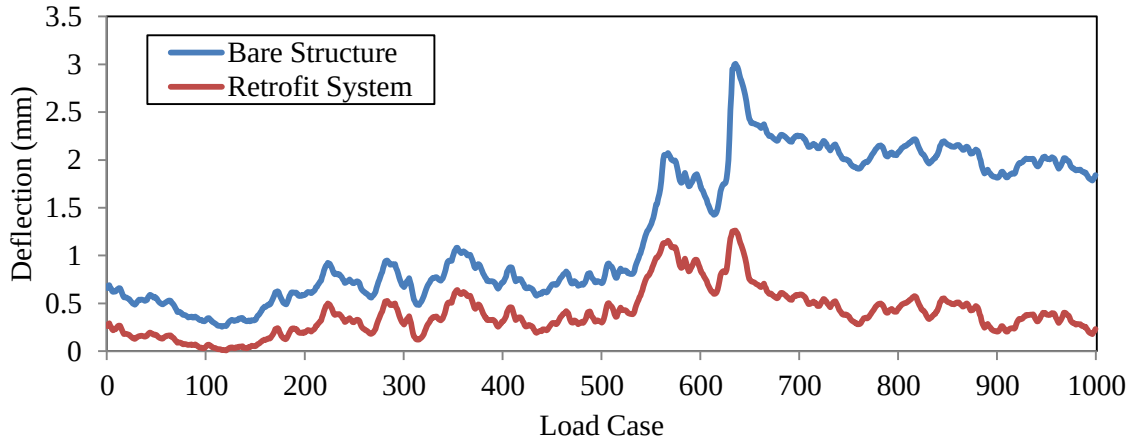

Figure 4.16: Deflection of the RTW connection S-03 through the time history

The retrofit system is also effective at reducing the deflection of the sheathing along the length of the structure, as shown in Figure 4.18, which presents the deflection of the sheathing under the maximum global uplift pressure along the section cut shown in Figure 4.17. The largest reduction in the magnitude of deflection occurs near the east gable, truss 2, where the deflection before retrofitting is the largest. While the magnitude of the reduction in deflection resulting from the application of the retrofit system reduces as the deflection of the bare structure becomes smaller, the percentage of decrease remains similar along the length of the structure.

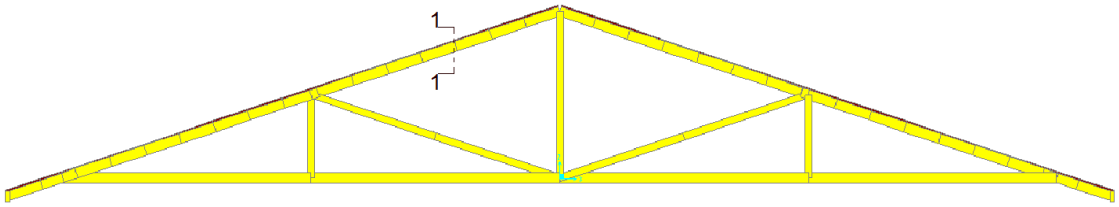

Figure 4.17: Section cut for analysis of deflected shape of the sheathing

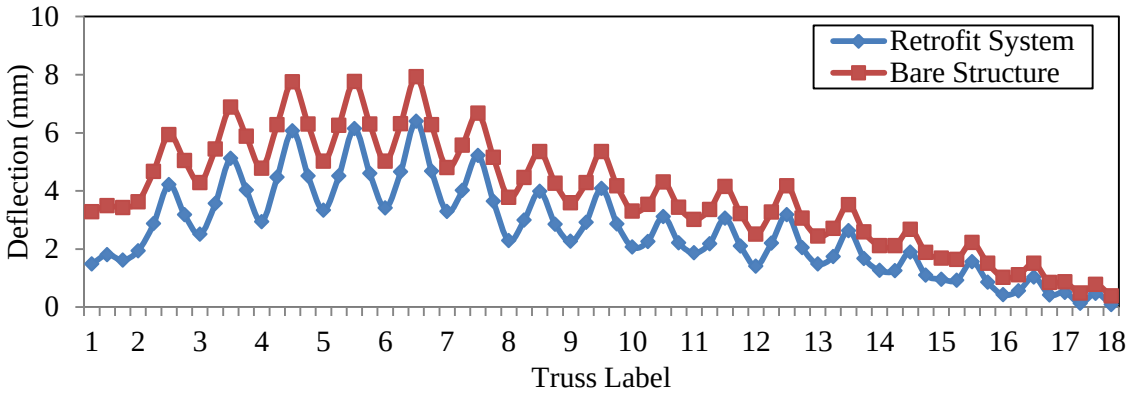

Figure 4.18: Deflected shape of the sheathing under maximum loading

It can be observed from Figure 4.18 that the deflection of the local maximum of the sheathing relative to the deflection of the nearest truss is not greatly affected by the application of the retrofit system. The average reduction in midpoint deflection relative to the nearest truss is 7%, with no value above 0.2mm. The reduction in deflection in the sheathing is caused by the reduction in the rigid body motion of the truss, suggesting that the load transferred by the STT connections is not greatly reduced with the application of the retrofit system.

The maximum force on each component resulting from the realistic 35m/s wind pressure is summarized in Table 4.3, along with the demand to capacity ratio. No component of the structure or the optimized retrofit system is near failure under this loading. The fascia board shows the highest demand to capacity ratio under this loading at 58%, confirming that this is the critical component in the structure after application of the retrofit system.

Table 4.3: Maximum force and demand to capacity ratio for each component under 35mps time history loading

Element	Maximum Force (kN, m)	Demand/Capacity Ratio
External Cable	3.079	11%
Bearing Cables	1.648	17%
Rigid Bar Moment	0.49	5%
Rigid Bar Shear	1.63	1%
Shear Transfer by Fascia	0.539	58%
Combined Axial Moment In Overhang		14%
Bending in Sheathing Strong	0.061	15%
Bending in Sheathing Weak	0.042	32%

The optimized retrofit system is shown to be effective at improving the behaviour of the structure under the 35m/s realistic wind pressure distribution. The numerical model predicts that application of the retrofit system is able to reduce the maximum withdrawal load applied to the RTW connection by 22% when compared to the unmitigated structure. The system also prevented the damage to the RTW connection under peak loading. Both the retrofit system and the structure show sufficient strength under this loading as no component of the structure or retrofit system is above a 58% demand to capacity ratio.

4.5.2 Assessment under NBCC Pressure Distribution

The design wind pressure distribution suggested by Part 4 of the NBCC, applied during the parametric study, is used to assess the improvement to the structural failure capacity with the application of the retrofit system. The wind velocity is increased until failure occurs. The reference wind pressure, q, is increased with the relationship $q = {}^{1}/_{2}\,\rho V^{2}$, as suggested by the NBCC commentary (NRC, 2010), where ρ is the air density, assumed to be 1.29kg/m^3, and V is the wind speed. Lateral loads, applied as line loads to the top plate of the shear walls, are considered in this analysis to include the effect of racking of the structure.

4.5.2.1 Comparison at Last Stable Pressure of the Bare Structure

The numerical model predicts that the highest mean hourly wind velocity that the structure can withstand before application of the retrofit system is 38 m/s. Above this wind velocity, the roof structure becomes unstable as progressive failure of the RTW connections occurs. The retrofit system reduces the average deflection of the RTW connections under this pressure distribution by a factor of three, as shown in Figure 4.19, resulting in a 45% reduction in the total uplift force transferred by the RTW connections.

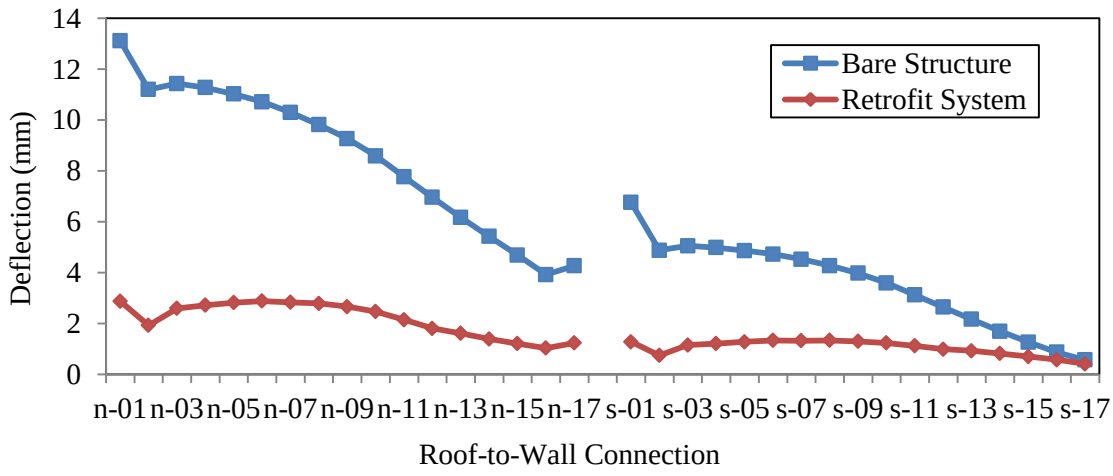

Figure 4.19: Deflection of the RTW connections under 38m/s wind loading

The retrofit system is found to have little effect on the racking deflection of the structure. The racking deflection is reduced from 13.3mm to 12.5mm with application of the optimal retrofit system, a reduction of only 9%.

4.5.2.2 Failure under Code Loading with Optimal Retrofit System

The wind velocity is increased to determine the critical velocity after application of the retrofit system. As discussed during the parametric study, the fascia board of the structure is unable to withstand the demand of the retrofit system under the pressure created by a 45 m/s mean hourly wind velocity. The numerical model predicts that failure of the fascia

board occurs under a 43m/s mean hourly wind velocity, which is an increase in the reference wind pressure of 22% above that of the bare structure. Neglecting the failure of the fascia board, the critical velocity becomes a 50m/s mean hourly wind velocity. Under the resulting uplift pressure, the bearing and external cables of the retrofit system begin to yield as RTW connection failure begins. The numerical model predicts that the optimum system is able to increase the reference pressure at failure by 75%, a 33% increase in the mean hourly wind velocity.

4.6 Feasibility Analysis of Nylon Strap

The above analysis has shown that retrofit systems constructed of steel components are effective at providing a secondary load path for the uplift forces; however, steel may not be the optimal material for the components of the retrofit system. This section focuses on the feasibility of nylon as a material for the components of the retrofit system.

4.6.1 General Discussion of Material Properties

The use of a nylon strap for the bearing cables has both advantages and disadvantages when compared to a steel cross section. A nylon strap provides a much larger bearing area for the retrofit system on the structure, consequently reducing possible negative effects caused by the high bearing forces. A 51mm wide nylon strap provides a 750% increase in the bearing area when compared to the bearing cables of the optimal system.

The ability of nylon to provide a lightweight strap with high ultimate capacity would be desirable in the design of the retrofit system. Replacing the bearing cables with 51mm wide nylon straps reduces the weight of the retrofit system by approximately 20% when compared to the optimal system, while providing greater ultimate capacity in the

components of the retrofit system. The steel cables of the optimal system are responsible for 40kg (27%) of the total mass. This is reduced to 16.1kg (11%) with the use of the nylon strap.

The use of a nylon strap for the external cables increases the ease of application, due to the ease of use of available prestressing devices. Ratcheting devices with the ability to apply strain loading are readily available for nylon straps. The external cables of the optimal system are responsible for 19kg of the total mass. Replacing the external cables with nylon straps would reduce this to 3kg. Use of a 51mm wide nylon strap for both the bearing and external cables would produce a system that weighs 105kg, a reduction of 38% over the optimal system.

The advantages of the nylon strap must be weighed against the disadvantages. The lower axial stiffness of the nylon strap when compared to the steel cable of the optimal system results in a system that is less effective at preventing RTW connection failure. As the system becomes less stiff, less force is relieved from the RTW connections by the secondary load path of the retrofit system. Increasing the resistance to elongation of the nylon strap, by including aramid fibers, could result in a very light and easy to apply system.

4.6.2 Numerical Results

The numerical model is used to assess the following two retrofit system configurations that involve the nylon strap: a system with a nylon strap used for the bearing cables and 10mm external cables, and a system with a nylon strap used for the bearing and external cables. Both assume the optimum rigid bar properties and 2kN of initial external cable

prestressing. Numerical properties of the nylon strap are approximated from the results of an experiment in which a hydraulic jack applied a deflection loading to a specimen, with load cell measuring the corresponding axial load. The specimen was tested at multiple lengths to determine an approximate stiffness for the strap.

Table 4.4, which presents the critical velocities resulting from the numerical analysis of the selected systems, shows that the use of the nylon strap reduces the effectiveness of the retrofit system when compared to the optimal system. Providing a lower axial stiffness for the components of the system reduces the ability of the retrofit system to prevent RTW connection failure.

Table 4.4: Critical mean hourly wind velocities of numerical analysis (m/s)

Case	**Failure of RTW Connection**	**Failure of Fascia Board**
Bare Structure	38	-
Optimal System	50	43
Retrofit with Nylon Bearing Cables	47	46
Retrofit with Nylon Bearing and External Cables	43	42

It can also be noticed from the results presented in Table 4.4 that the retrofit system constructed using nylon straps for the bearing cables and steel of the external cables results in the highest velocity at fascia board failure. Of the tested configurations, this system provides the largest difference between the axial stiffness of the bearing and external cables. In contrast to this, the failure of the fascia board occurs at the lowest wind velocity when the system is constructed using nylon straps for both the bearing and external cables. This system provides the minimum difference between the axial stiffness of the bearing and external cables. From this result, it can be concluded that the velocity at which the failure of the fascia board occurs is dependent on the difference between the axial stiffness of the bearing and external cables, and this property has the largest effect

on the distribution of force in the bearing cables. When the bearing cables are much less stiff than the external cables, the distribution of force in the bearing cables is nearly uniform. As this difference in stiffness becomes smaller, the rigid bar becomes less effective at creating a uniform distribution of force in the bearing cables. As the axial force in the bearing cables becomes less uniform, larger shear forces act on the fascia board to truss connection as the load is transferred through the structure to the bearing cables connected closer to the external cables. A uniform distribution of axial force in the bearing cables is necessary for preventing failure of the fascia board.

The use of nylon can be beneficial for use in an optimal system as it provides a low weight, high bearing area and high ultimate strength. However, the use of nylon straps results in a lower wind velocity at the onset of RTW connection failure than the optimal system due to the decreased axial stiffness of the retrofit components. A low elongation nylon strap should be investigated further in the design of the retrofit system, as it could provide a very efficient retrofit system design.

4.7 Conclusions

The vulnerabilities of the roof systems of residential light-framed wood structures have been exposed during past high speed wind events. Building codes and product development have worked to address the identified issues, but current solutions are difficult and expensive to apply as a retrofit. The proposed system, applied over the exterior of the structure, is intended to be an economical and easy to apply retrofit system capable of reducing the economic loss caused to these structures during high speed wind events.

A numerical model has been developed capable of modeling the plastic deformation that occurs during the damaging peak pressures of a realistic wind load. The numerical model provides a strong prediction of the results of a full-scale experiment after applying the assumption that the initial difference between the numerical and experimental results is caused by initial movement of the nailed connections within the structure. Throughout the selected time history, the average magnitude of percent difference between the experimental and numerical RTW connection deflection remains below 10% for each south side connection. A plastic RTW connection is found to be more accurate at capturing the experimental behaviour than an equivalent multi-linear elastic connection.

A parametric study has been completed to determine the retrofit system configuration with the minimum weight that satisfies the structural strength constraints when subjected to a design wind pressure as suggested by the NBCC. Results found that the bearing cable spacing should match the spacing of the truss system to reduce both the shear force transferred by the fascia board to the truss connection and the bending moment in the sheathing. The numerical model predicts that the components of the optimal retrofit system are a 6mm bearing cable, a 10mm external cable, a 52mm by 102mm with a 6mm wall hollow rectangular rigid bar, with 2kN initial external cable prestressing at a 15° angle with the vertical wall.

The optimal retrofit system has been analyzed under a 35m/s realistic wind pressure and a building code pressure distribution with increasing wind velocity. Under the 35m/s realistic wind pressure, the numerical model predicts that the retrofit system is able to prevent damage to the RTW connections, reducing the maximum withdrawal force by

22%. Under the building code pressure distribution, the model predicts that application of the retrofit system increases the critical mean hourly wind velocity from 38m/s to 50m/s.

Nylon was analyzed as a material for use in the retrofit system. While a nylon strap reduces the bearing force on the structure and the weight of the retrofit system, the decreased axial stiffness of the components results in a system that is less effective at preventing connection failure. A low elongation strap could result in a very efficient retrofit system design.

4.8 References

Baskaran, A. and Dutt, O. (1997). Performance of roof fasteners under simulated loading conditions. *Journal of Wind Engineering and Industrial Aerodynamics*, 72(0), 389-400

Canadian Wood Council (CWC), and Canadian Standards Association (CSA). (2010). *Wood design manual, 2010 :The complete reference for wood design in Canada. Ottawa*: Canadian Wood Council

Canbek, C., Mirmiran, A., Chowdhury, A., and Suksawan, N. (2011). Development of Fiber-Reinforced Polymer Roof-to-wall Connection. *J. Compos. Constr., 15*(4), 644-652.

Computers and Structures, Inc.(2009). SAP 2000 V. 14: Integrated Software for Structural Analysis and Design. Berkley, California, USA.

Datin, P. L., Prevatt, D. O., and Pang, W. (2011). Wind-uplift capacity of residential wood roof-sheathing panels retrofitted with insulating foam adhesive. *Journal of Architectural Engineering, 17*(4), 144-154

Department of Housing and Urban Development (HUD). (1993). *Assessment of Damage to Single-Family Homes Caused by Hurricanes Andrew and Iniki.* U.S., Office of Policy and Development and Research, HUD-0006262.

Federal Emergency Management Agency (FEMA). (1993). *Building Performance: Hurricane Iniki in Hawaii - Observations, Recommendations, and Technical Guidance.* Federal Emergency Management Agency.

Gurley, K., Davis, R.H., Ferrera, S.P., Burton, J., Masters, F., Reinhold, T., and Abdullah, M., (2006). Post 2004 hurricane field survey – an evaluation of the relative

performance of the Standard Building Code and the Florida Building Code. *Proc. 2006 ASCE/SEI Structures Congress*, St. Louis, MO. 8.

Kasal, B., Leichti, R. J., and Itani, R. Y. (1994). Nonlinear finite-element model of complete light-frame wood structures. *Journal of Structural Engineering,* 120(1), 100-119.

Meloy, N., Sen, R., Pai, N., and Mullins, G. (2007). Roof damage in new homes caused by hurricane charley. *Journal of Performance of Constructed Facilities, 21*(2), 97-107.

Morrison, M. J., Henderson, D. J., and Kopp, G. A. (2012). The response of a wood-frame, gable roof to fluctuating wind loads. *Engineering Structures, 41,* 498-509.

Morrison, M. J., and Kopp, G. A. (2011). Performance of toe-nail connections under realistic wind loading. *Engineering Structures, 33*(1), 69-76.

National Research Council of Canada (NRC). (2010). *National Building Code of Canada (NBCC) 2010*. Ottawa, NRCC 53301

Paevere, P., Foliente, G., and Kasal, B. (2003). Load-Sharing and Redistribution in a One-Story Woodframe Building. *J. Struct. Eng.*,*129*(9), 1275–1284.

Phillips, T., Itani, R., and McLean, D. (1993). Lateral Load Sharing by Diaphragms in Wood-Framed Buildings. *J. Struct. Eng.*, *119*(5), 1556–1571.

Stewart, M. G. (2003). Cyclone damage and temporal changes to building vulnerability and economic risks for residential construction. *Journal of Wind Engineering and Industrial Aerodynamics, 91*(5), 671-691

van de Lindt, J., Graettinger, A., Gupta, R., Skaggs, T., Pryor, S., and Fridley, K. (2007). Performance of wood-frame structures during Hurricane Katrina. *Journal of Performance of Constructed Facilities, 21*(2), 108-116.

Chapter 5

5 Experimental Testing of a Retrofit System to Increase Uplift Capacity of Light-Framed Wood Structures

5.1 Introduction

The vast majority of structures in North America are residential. Light-framed wood construction is used due to its familiar construction methods, low cost and availability of materials. Unlike other structures, national building codes do not require a structural engineer to analyze and design each structure. Instead, the construction of light-framed wood structures follows the prescriptive requirements of the governing building code, which determines member sizes and connection strengths. Damage to these structures has been a major source of economic loss during past high speed wind events. For example, the damage to light-framed wood structures represented a large portion of the US$20-25 billion of economic losses caused by Hurricane Andrew in 1992 (HUD, 1993), with approximately 95% of the losses resulting from failure of materials of the roof system (Baskaran and Dutt, 1997). A major cause of the failures that occur in the roof systems of light-framed wood structures, as identified by post-hurricane damage reports, is the lack of a continuous load path from the roof to the foundation (van de Lindt et al., 2007). Under the loading of high speed winds, the roof system is subjected to uplift pressures generated in two ways. First, as the wind flows over the roof of the structure, negative (suction) pressures are applied to the roof sheathing. Second, after a failure in the building envelope on the windward wall, positive internal pressures occur. The two generated pressures result in global uplift forces acting on the roof system. Under this loading, the sheathing-to-truss (STT) connection and the roof-to-wall (RTW) connection

have been identified as weak links in the load path (FEMA, 1993). Both types of connections rely on the withdrawal capacity of the nail to transfer the uplift forces to the foundation. Complete structural collapse can occur as a result of either failure mode, endangering the lives of the inhabitants.

To address the capacity problems of the identified critical connections, product development has occurred. An example of this is the "HurriQuake" nail developed by the International Hurricane Research Center (IHRC, 2005) to increase the capacity of the STT connection. The "HurriQuake" nail uses a harder shank when compared to a standard air nail to increase the reliability of truss penetration. The "HurriQuake" nail also has a ring shank to increase withdrawal resistance. Product development has also addressed the issue of the capacity of the RTW connection. The truss tie (hurricane clip) is a steel strap used to attach the truss to the top plate of the wall. This strap complements the toe-nail connection, removing the withdrawal demand placed on the nails. Available in many sizes, the tie can increase RTW connection uplift capacity to 7.6kN (Simpson Strong-Tie, 2008), approximately a 400% increase above that of a standard three, 16d toe-nail connection. Simpson Strong-Tie has developed steel ties for use throughout the structure to create a continuous load path from the roof to the foundation. The use of the "HurriQuake" nail and the steel straps to complement the nailed connections provides an efficient solution to the problems caused by uplift loading on new structures; however, non-structural elements limit access to both the critical connections in existing structures, making these technologies difficult to apply as a retrofit.

The issues in the capacity of the critical connections has also been addressed by increasing the requirements of the building codes, which are constantly changing as the

lessons learned from high speed wind events and research identify the vulnerabilities of the current version of the code. Major improvements were made to the South Florida Building Code following Hurricane Andrew. These changes were adopted locally in 1994 before becoming standard for the entire state of Florida in 2001 (Gurley et al., 2006). Building code changes have also occurred in Canada. For example, when compared to the previous edition, the 2010 version of the National Building Code of Canada (NBCC) (NRC, 2010) requires improved capacity of the STT connection in areas classified with a high mean hourly wind pressure. Increased connection frequency around the eaves of the structure and a longer fastener length are now required in these areas. The use of a truss tie to reinforce the RTW connection is also now required in these high wind regions.

As code improvements are made, previously constructed buildings remain with known vulnerabilities. Structures built before 1994 in the coastal regions of the United States are extremely vulnerable to uplift forces caused by wind as the majority use insufficient nails for the STT connection (Datin et al., 2011). Thus, recent changes to building codes, along with the known vulnerabilities of the structures constructed under previous editions of those codes, suggests that a retrofit system capable of improving the uplift behaviour of light-framed wood structures is needed.

As a need has been identified, research has been conducted on retrofit schemes to increase the capacity of existing structures. Datin et al. (2011) tested a sprayed polyurethane foam adhesive applied from within to the sheathing and truss members to reduce the withdrawal demand on the STT connections. The study found that the foam adhesive was effective at increasing the uplift capacity of the roof sheathing by 250-300%. In another study, Canbek et al (2011) investigated the use of a fiber reinforced

polymer (FRP) tie to create the RTW connection. Adhesives are used to bond the FRP tie to the top plate and the truss to create the RTW connection. This technology is intended to replace or improve the capacity of the current toe-nail or hurricane clip connection. The FRP tie provided a 65% increase in ultimate capacity when compared to a standard hurricane clip. While both of the presented studies are effective at increasing the uplift capacity of the critical components of the structure, access to the members is needed for application.

While the issue of large economic losses resulting from failures of light-framed wood structures in high speed wind has been addressed in many ways, little has been developed in terms of an easy-to-apply retrofit scheme. Critical connections may not be easily accessed without removing non-structural elements, requiring high labour and material costs. The identified vulnerabilities of existing structures, combined with the potential increase in intensity of extreme wind events with global warming (Emanuel 2005), suggests that an economical retrofit system must be developed.

This research aims to develop an inexpensive and easy-to-apply retrofit system for light-framed wood structures that is capable of reducing the damage and economic loss resulting from high speed winds. This chapter focuses on an experiment conducted to test the proposed system on a section of roof. The idea of the retrofit system is first introduced, with a summary of the numerical study previously completed. The results of the experiment are presented with a focus on the behaviour of the truss system after application of the retrofit system and the ability of the system to increase the uplift capacity of the structure. The experimental results are then used to validate the assumptions of the numerical model to gain confidence in its adequacy.

5.2 Proposed Retrofit System

The proposed system consists of a series of cables placed along the sheathing of the roof, identified as the bearing cables in Figure 5.1, Figure 5.2 and Figure 5.3. Along the eave of the structure, the bearing cables are attached to rigid bars. Cables containing a prestressing device, identified as the external cables, connect the rigid bars to piles that are permanently installed in the ground. When a warning of high speed winds is announced, the system can be easily applied to the roof of the building and attached to the piles. This system provides the uplift forces an alternate load path to the ground without travelling through the weak nailed connections within the structure. Figure 5.1, Figure 5.2 and Figure 5.3 show the proposed retrofit system as applied to a gable-style roof.

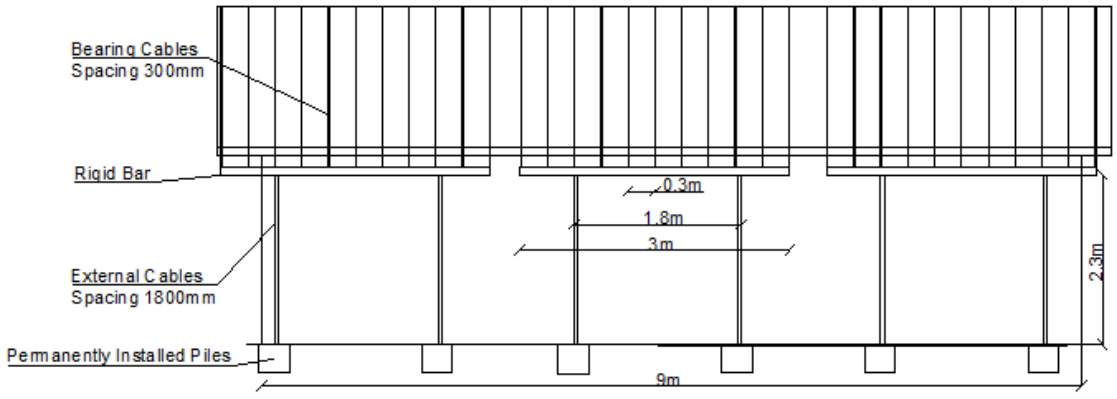

Figure 5.1: Elevation view of proposed retrofit system as applied to a gable-style roof

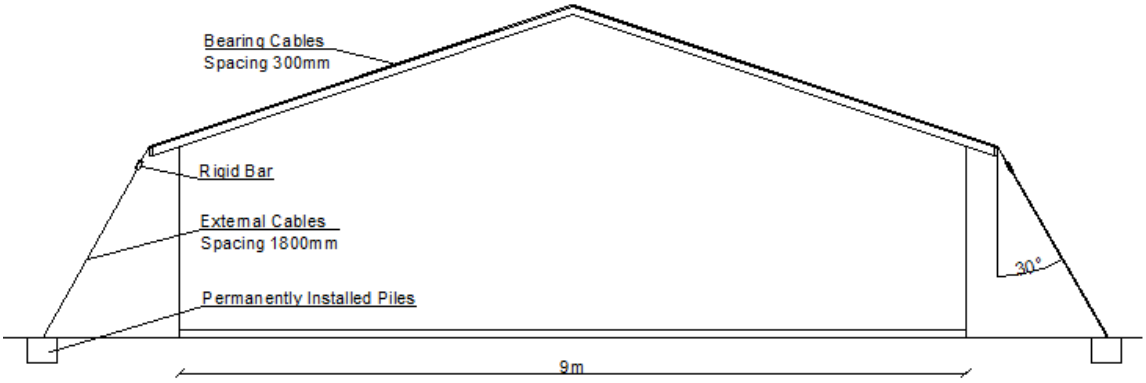

Figure 5.2: Elevation view of proposed retrofit system as applied to a gable-style roof

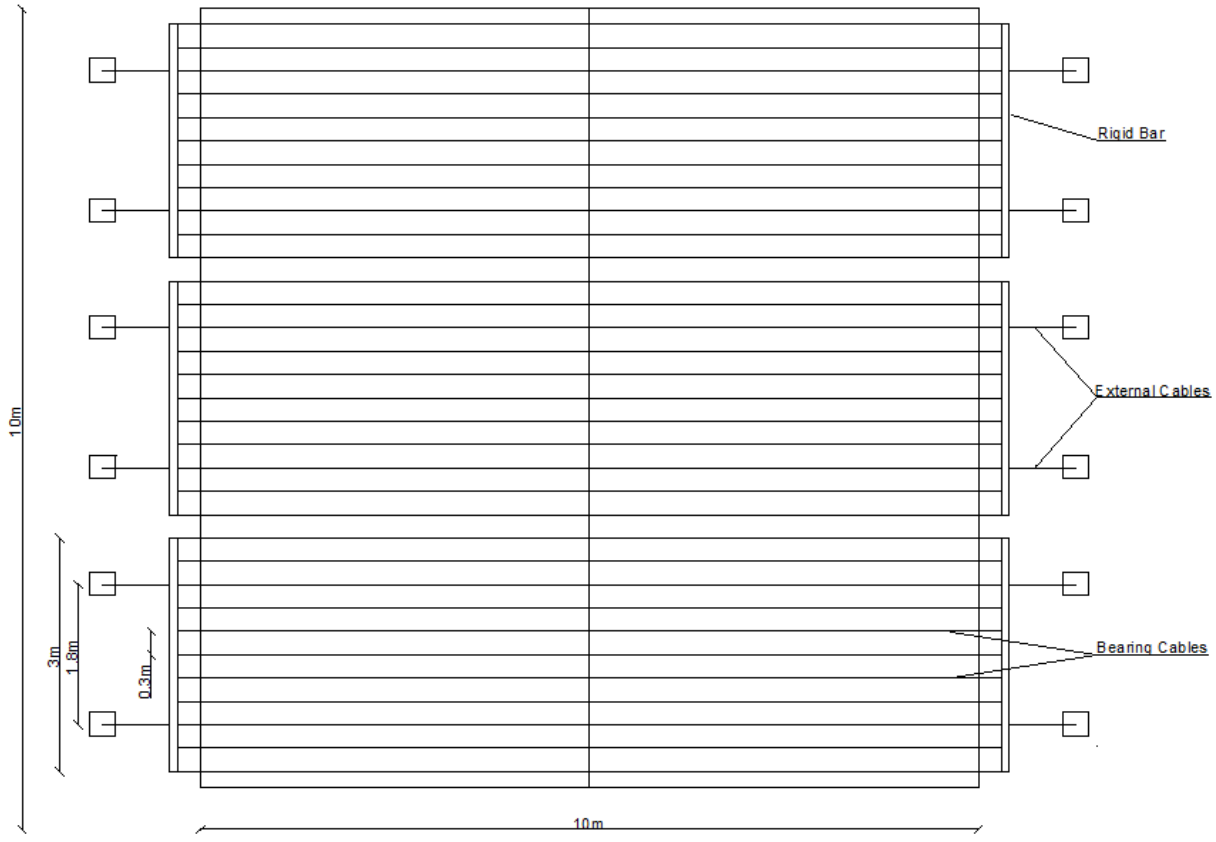

Figure 5.3: Plan view of proposed retrofit system as applied to a gable-style roof

The proposed retrofit system has been studied numerically (Dessouki, 2010) using a finite-element model developed in the commercial software, SAP2000 (Computers and Structures, Inc., 2009). A model of the roof system of a light-framed wood structure has been developed to accurately capture the behaviour under a realistic wind pressure. The

model is constructed using frame and shell elements for the structural members of the roof system. A nonlinear plastic link element is used to capture the behaviour of the RTW connection. The dimensions of the modeled house correspond to those of a full-scale experiment that was recently conducted at the Insurance Research Lab for Better Homes (Morrison et al., 2012). Built to the provisions of the Ontario Building Code, the structure matched the typical construction techniques of the area. A spatially and temporally varying realistic pressure distribution was applied to the structure while recording the corresponding deflections at the RTW connections. These experimental results were used to validate the prediction of the numerical model for the deflection of the roof structure at the RTW connections. As shown in the previous chapter, under the loading of a realistic time history load selected from the experimental data, the developed numerical model predicts a similar deflection profile along the length of the roof system to that of the test structure. The numerical model also shows the ability to capture the damage that occurred to the RTW connections experimentally during the damaging peak pressures of the realistic wind load. The strong agreement between numerical prediction and the experimental results shows that the numerical model is capable of accurately capturing the behaviour of a light-framed wood structure under a realistic wind loading.

The validated numerical model of the full-scale roof structure has been extended to include the proposed retrofit system. The rigid bars are modeled using frame elements. The bearing and external cables are modeled using nonlinear cable elements. To capture the interaction between the cables and the roof sheathing, a constraint is used to simulate bearing, neglecting the frictional forces that develop between the sheathing and the retrofit system. A small prestressing force is applied to the external cables to ensure an

initially taut retrofit system. Using this model, a rigorous assessment of the effectiveness of the retrofit system has been conducted. A parametric study has been completed to determine the component properties that result in a minimum weight while satisfying structural strength constraints at a design wind speed. As shown in the previous chapter, for a retrofit system with the dimensions presented in Table 5.1, the numerical model predicts that the retrofit system is able to reduce the maximum withdrawal force acting on the RTW connections under the selected time history load by 22%, thereby preventing the plastic damage that occurred to RTW connections of the bare structure. When assessed under the loading suggested by the NBCC, the model predicts that application of the retrofit system increases the critical mean hourly wind velocity from 38m/s to 50m/s.

Table 5.1: Initially proposed dimensions for full-scale retrofit system

Retrofit System Component	**Initial Dimension**
Bearing cables (600mm Spacing)	6mm Diameter steel cable
External cables (1800mm Spacing)	10mm Diameter steel cable
Initial prestressing force	2 kN to each external cable
Rigid Bar	Aluminum, Hollow Rectangular Section 102mm by 51mm with 6mm wall

The numerical results have shown the potential of this system to reduce the damage that occurs to light-framed wood structures during high speed wind events. The following experiment will test a section of the full-scale structure to assess the behaviour of the truss system after application of the retrofit system.

5.3 Experimental Design

An experiment is conducted and reported in this paper to determine the behaviour of a truss system under uplift loading, with and without implementation of the proposed retrofit system. The results are analyzed to validate the assumptions used in the full-scale numerical model. The apparatus and procedure are presented below, as well as the

relationship between the experimental tested retrofit system and an equivalent full-scale system.

5.3.1 Apparatus

The experiment is conducted on a section of a roof system that consists of three, Howe-style trusses, roof sheathing, and internal lateral bracing. The trusses have the same clear span (9m), slope (4/12) and spacing (600mm o/c) as those of the full-scale structure studied in numerical and experimental work described earlier. The trusses are connected to the top plate of a 600mm, 38mm by 89mm stud wall using toe-nail connections, each constructed with three, hand driven, 16d, spiral shank nails. The stud wall is attached to a wood floor system that is anchored to the laboratory floor. As the experimental truss system has the same truss span, truss spacing and RTW connection as the earlier numerical work, the initiation of RTW connection failure is expected to occur at the same applied pressure for the experimental and full-scale structures. Figure 5.4 shows an elevation view of the tested structure.

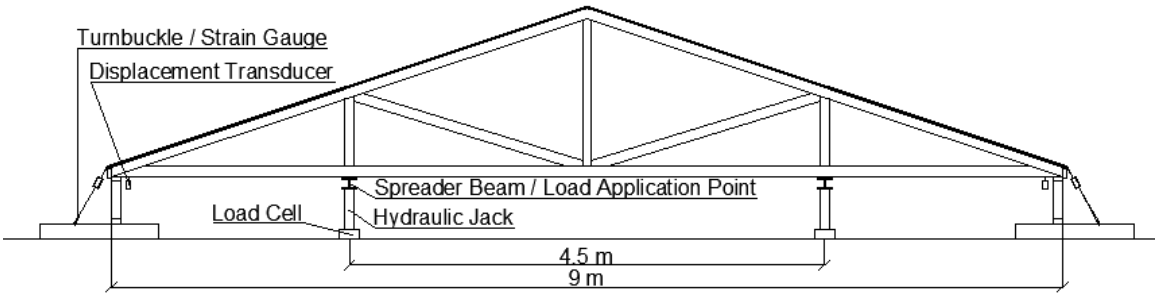

Figure 5.4: Elevation view of the experimental apparatus with retrofit system

A section of the retrofit system is constructed using 3/16”, 7x19, galvanized aircraft cable for both the bearing and external cables. The external cables are attached to the floor system using ½”, galvanized, eye and jaw turnbuckles, providing a method for

pretensioning the retrofit system. The external cables have an angle of 30° with the vertical wall.

Figure 5.5 and Figure 5.6 show the retrofit system as applied to the experimental structure and the center section of a full-scale structure. The following differences can be identified between the experimental-scale and full-scale retrofit systems: the length of the external cables, the span and structural system of the rigid bar, and the number of trusses and bearing cables supported by each section of rigid bar.

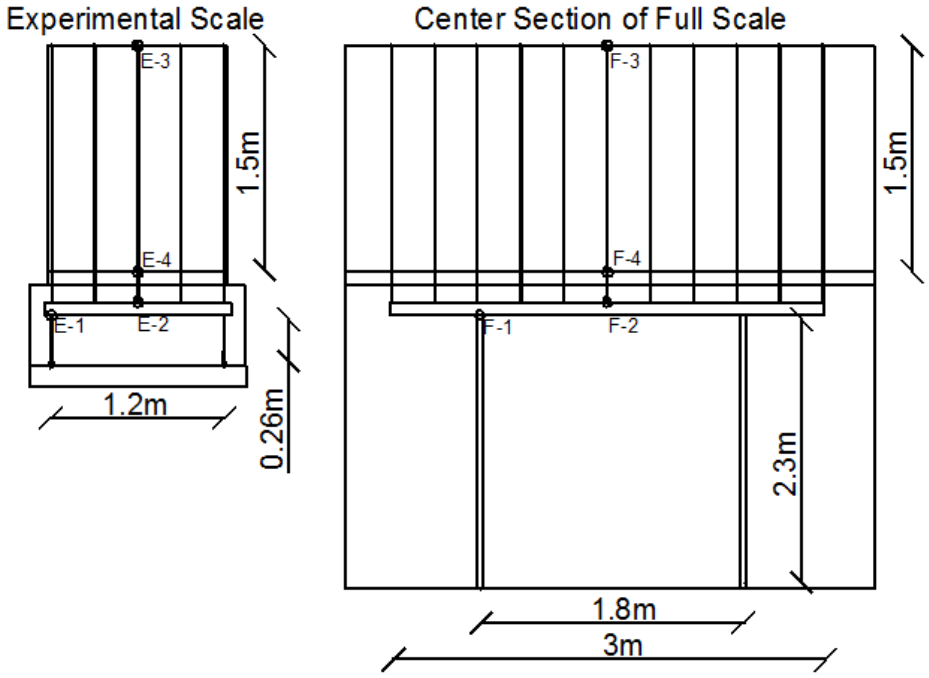

Figure 5.5: Elevation view of Experimental and Full-Scale Systems

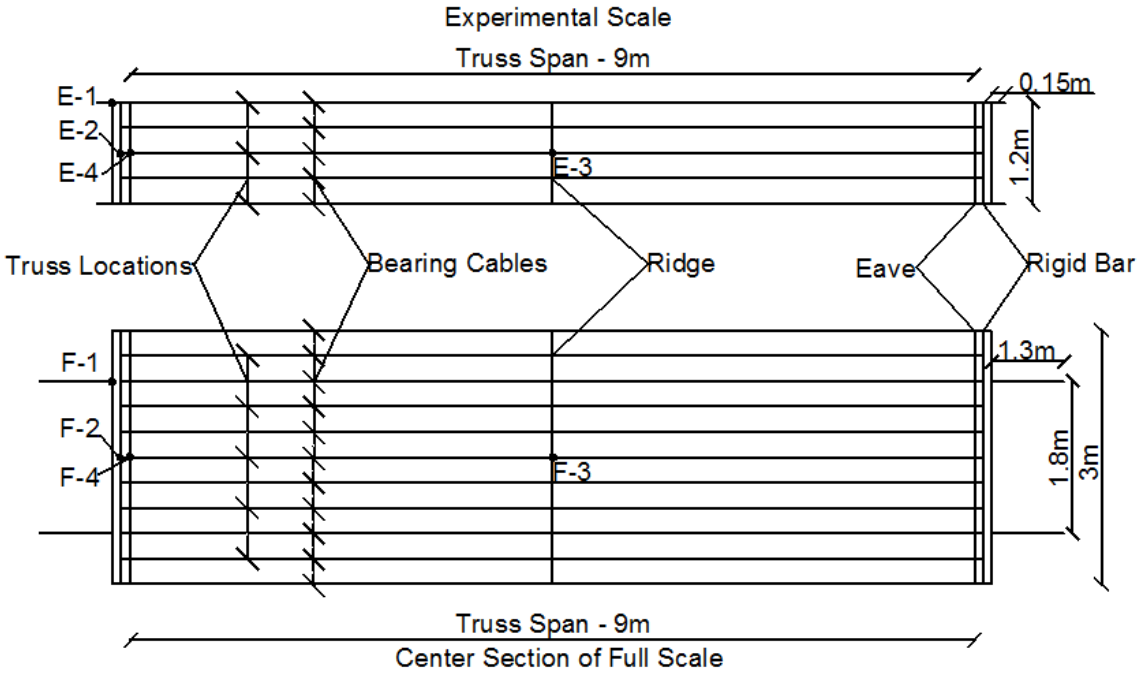

Figure 5.6: Plan view of experimental and full-scale systems

A numerical model has been developed of the experimental specimen using the same approach described above for the full-scale system. This is used to determine the geometric properties of the specimen providing equivalent stiffness to that of the full-scale retrofit system. This is accomplished by matching the following quantities between the experimental-scale and full-scale under the same level of applied pressure:

1. **Deflection of point E-1 to deflection of point F-1**: Points E/F-1 are located at the connection between the external cable and the rigid bar. Matching this deflection leads to selection of the external cable. This property is selected based on the area supported by each cable and the length of each cable.
2. **Deflection of point E-2 to deflection of point F-2**: Points E/F-2 are located at the midpoint of the rigid bar. Matching these deflection lead to the selection of the dimensions of the rigid bar. It has been determined numerically that the experimental rigid bar, with a 1.2m span and 5 points of loading, and the full-

scale rigid bar, with a 1.8m span, 0.6m cantilevers and 11 points of loading, match in deflection at the midpoint without modification of bar cross section.

3. **Deflection of point E-3 to deflection of point F-3**: Points E/F-3 are located at the peak of the structure. Matching these deflections leads to the selection of the dimensions of the bearing cables. This property is selected based on the area supported by each bearing cable and the length of bearing cable.
4. **Deflection of point E-4 to deflection of point F-4**: Points E/F-4 are located at the critical RTW connection. Matching these deflections results in the selection of the initial prestressing force. This force is selected based on the number of bearing cables supported by each rigid bar.

Table 5.2 summarizes the properties of the experimental-scale and full-scale retrofit systems resulting from the above scaling. The developed numerical models predict that the failure of both the experimental and full-scale structures will be RTW connection withdrawal. This failure is expected to occur under the same applied pressure in the experimental-scale and the full-scale.

Table 5.2: Summary of experimental and equivalent full-scale properties

Retrofit System Component	Experimental-Scale	Equivalent Full-Scale
Truss	9m span, 4/12 slope	Same
Truss Spacing	600mm	Same
RTW Connection	Three 16d, Spiral Shank Nails	Same
Bearing Cable Spacing	300mm	Same
Bearing Cables Diameter	3/16" 7*19 Galvanized Aircraft Cable	2.5mm steel cable
External Cable Diameter	½", galvanized eye and jaw, turnbuckles	8mm steel cable
External Cable Length	0.3mm	2.5m
Rigid Bar Cross Section	Aluminum, Hollow Rectangular Section, 102mm by 51mm with 6mm wall	Same
Rigid Bar Connection Details	1.2m External Cable Span	1.8m External cable span, 0.6m cantilever sections
Bearing Cable per Section of Rigid Bar	5	11
Initial Prestressing Force	1kN per Cable	2.2kN per Cable

5.3.2 Experimental Instrumentation

The location of the instrumentation is symmetric around the center web member of truss. A hydraulic jack applies an uplift load to the truss system from beneath at the two exterior, vertical, web members of the trusses, shown in Figure 5.4. The force is distributed over the three trusses using a spreader beam, resulting in the application of six point loads to the structure. As the uplift load is applied, the following three measurements are recorded during testing, with the location of each identified in Figure 5.4, Figure 5.7, and Figure 5.8:

- Load cells are installed beneath the hydraulic jacks, recording the uplift force applied to the truss system.

- Displacement transduces are installed at each RTW connection to measure the deflection relative to the laboratory floor. In total, six displacement transduces are used.

- Strain gauges are installed on each turnbuckle to quantify the tension force resulting in each external cable. The relationship between the strain and the axial force is determined for each turnbuckle before installation in the apparatus using a calibration experiment.

Figure 5.7: Experimental setup

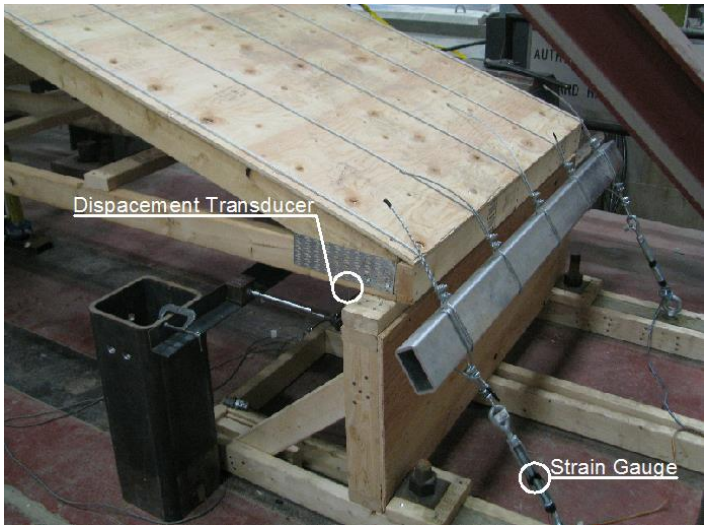

Figure 5.8: Experimental setup

The labeling convention for the experiment is presented in Figure 5.9. The apparatus contains two walls, W1 and W2, and three trusses, T1, T2 and T3. RTW connections are identified based on the wall and truss location. For example, the connection between wall 1 and truss 1 is labeled W1-L1. The 4 external cables are identified based on the closest RTW connection. The cable located closest to connection W1-L1 is labeled cable W1-T1, while the external cable near connection W1-L3 is labeled cable W1-T3.

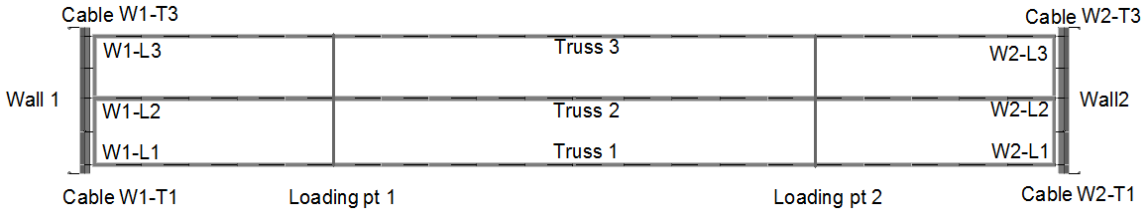

Figure 5.9: Plan view of experimental apparatus with naming convention

5.3.3 Procedure

In total, three specimens are tested. In each, uplift load is applied to the structure using a hydraulic jack, which applies an increasing displacement at the loading points (displacement controlled loading). Details of the three experiments are as follows:

Control: A truss system is loaded to failure without the retrofit system to determine the behaviour of the as-constructed truss system. Uplift load is applied until failure of the RTW connections.

'Retrofit – New': A new set of trusses is constructed to match the control experiment. The retrofit system is applied and the truss system is loaded until the axial force in an external cable reaches the load limit. This experiment acts as the primary focus of the numerical validation.

‘Retrofit – Damaged’: After failure of the control experiment, the RTW connections are replaced and this damaged truss system is tested with the retrofit system implemented. The capacity and stiffness of the damaged RTW connections will be lower than those in the ‘Retrofit – New’ experiment. This experiment is intended to investigate the behaviour of the system when applied to a structure that may have been damaged in previous high speed wind events.

5.4 Description of the Numerical Model of the Experiment

A finite-element model is created of the experimental apparatus. The model uses similar assumptions to those made in the full-scale numerical model completed in the earlier work. The following section discusses the assumptions used to develop the numerical model.

5.4.1 Truss System

In the developed numerical model, frame and shell elements are used to simulate the truss and sheathing respectively. The dimensions of the truss system match those of the experiment, presented in Figure 5.4. The system consists of three Howe-style trusses spaced roughly 600mm (2ft) on center, with a 9m clear span and a 4/12 slope. Inertia multipliers are used to reduce the bending rigidity of the sheathing in the direction perpendicular to the face grains to capture the anisotropic bending behaviour of the panel. The material properties of the truss and area elements are provided by the Canadian Wood Design Code (CWC and CSA, 2010) for SPF No.1/No.2 lumber and 13mm (½”) CSP plywood respectively.

5.4.2 RTW Connection

The load-deflection behaviour of the RTW connections is captured using a multi-linear elastic link element. The results of the control experiment are used to approximate the behaviour of the connection. The load-deflection relationship developed from the average deflection of the control experiment, Figure 5.10, has a bilinear stiffness and a failure load of 2.4kN.

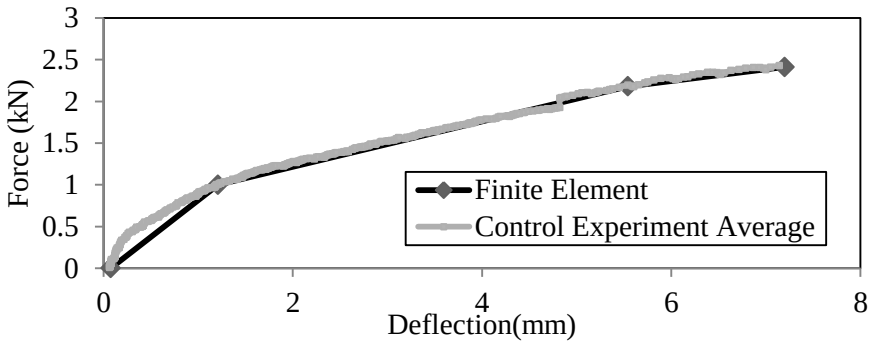

Figure 5.10: RTW connection stiffness for developed for numerical model

5.4.3 Retrofit System

The behaviour of the rigid bars is modeled using frame elements. Cable elements are used to capture the highly nonlinear behaviour of the bearing and external cables. The stiffness of the slender cables is dependent on the initial shape of the element, which is specified in the program. To simulate the interaction between the cable mesh and the roof sheathing, the nodes of the cable elements are set to have compatible displacements with the nodes of the sheathing in the axis perpendicular to the sheathing. The frictional force that develops between the retrofit system and roof is neglected, therefore, no compatibility in displacement in the in-plane direction of the sheathing is assumed. The initial pretensioning force is included in the numerical model by applying strain loads to the external cables.

5.4.4 Cable and Turnbuckle Numerical Properties

An experiment has been completed to determine an approximate stiffness for the external and bearing cables used to construct the experimental retrofit system. The turnbuckle and cable manufacturers provide working load limits for the products, but stress-strain relationships are not available. A testing apparatus is used to measure the resulting tensile force acting on the specimen as a hydraulic jack applies a deflection loading. An approximate stiffness is then determined to be used in the numerical model.

5.5 Experimental Results

5.5.1 Control Experiment

Failure of the truss system occurs at a total applied load of 16.8kN; an average withdrawal force of 2.4kN per connection. The failure mode is shown to be initiated by sudden withdrawal of the toe-nail connection, as shown in Figure 5.11. As failure of the first connection occurs, a second connection is overloaded, also failing by sudden withdrawal. After failure of these two connections, the applied uplift load is relieved from the truss system, preventing further progressive failure.

Figure 5.11: Failure of connection W1-L3 after sudden withdrawal during control experiment

The load-deflection relationship of the RTW connections, Figure 5.12, shows three phases of behaviour of the truss system before retrofitting. The first phase occurs before the dead load of the system is overcome, when no RTW connection deflection occurs. After the dead load is overcome, the RTW connection deflection varies linearly with the applied load, with an average stiffness of 340kN/m per connection. The third phase begins with failure of connections W1-L3 and W1-L2. Sudden deflection occurs and the applied load is relieved from the truss system. The RTW connections are progressively overloaded and the truss system becomes unstable, unable to resist further uplift loading.

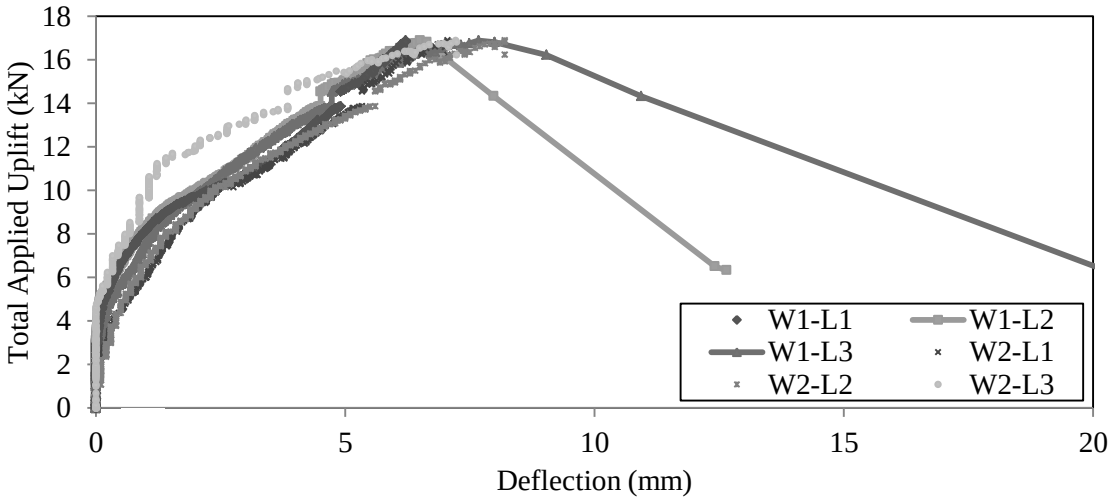

Figure 5.12: Load-deflection relationship for each RTW connections during control experiment

5.5.2 'Retrofit – New' Experimental Results

Application of the retrofit system during the experiment is found to greatly increase the uplift capacity of the truss system. RTW connection withdrawal begins at a load of 23.5kN after application of the retrofit system, a 40% increase above that of the control experiment. The maximum uplift load applied to the truss system experimentally is 36kN; more than double the load applied at failure before retrofitting. The load limit of the external cables governs the maximum applied load.

The failure mode of the truss system after application of the retrofit system remains similar to the failure of the control experiment. RTW connection withdrawal occurs as shown in Figure 5.13. The retrofit system provides a load path after failure of the RTW connections, allowing for loading after connection failure. Progressive overloading is again demonstrated; however, the failure is not sudden. The load path provided by the retrofit system changes the failure mode from sudden connection withdrawal to a ductile failure.

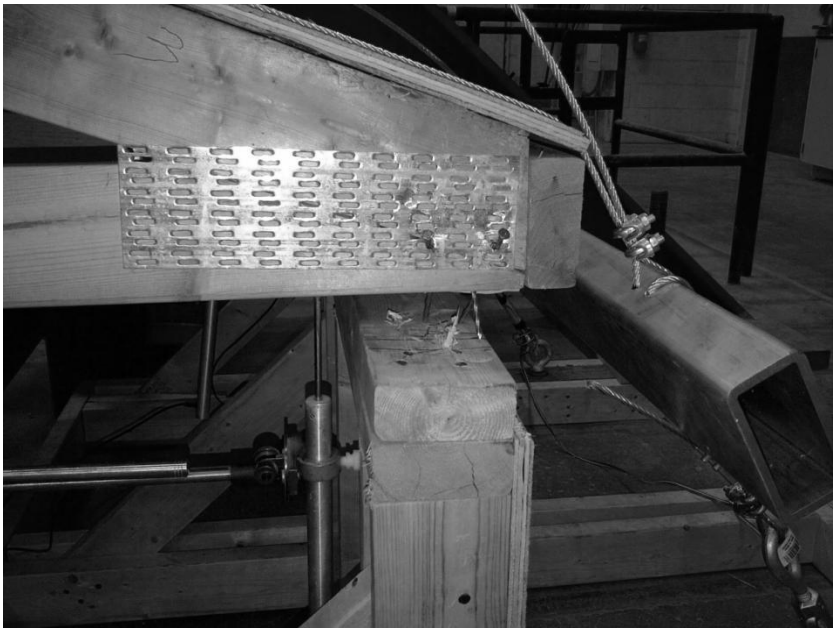

Figure 5.13: RTW connection failure after application of retrofit system

Figure 5.14 presents the load-deflection relationship for the critical RTW connection during the ‘Retrofit – New’ and ‘Control’ experiments. As discussed above, the failure mode of the connection in the Control experiment is sudden withdrawal followed by instability, shown by the decrease in applied load with deflection. After retrofitting, the load-deflection relationship of the connection during failure has a nearly horizontal slope, demonstrating the ductile response of the structure after application. The increase in applied load with deflection represents the ability of the system to resist uplift loading after connection failure.

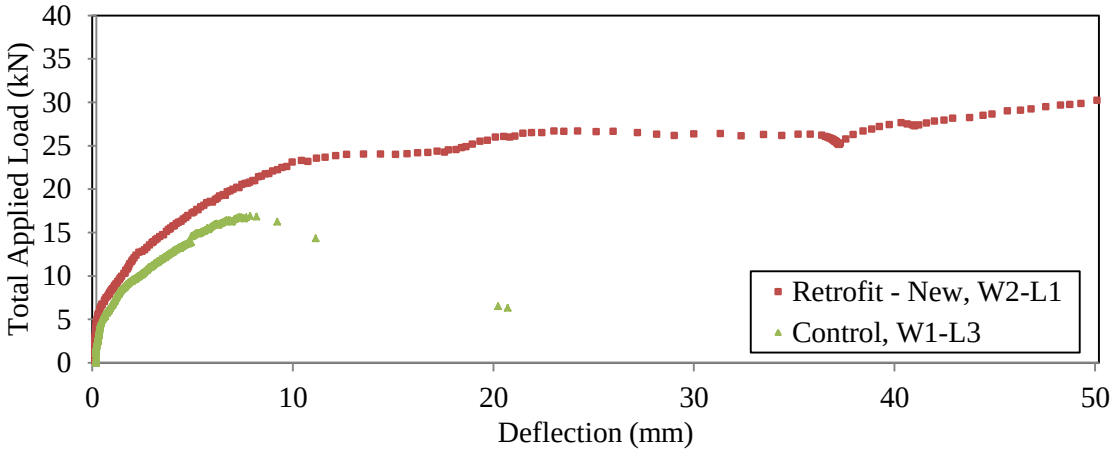

Figure 5.14: Load-defection relationship for first connection failures during 'Retrofit-New' and Control experiments

5.5.2.1 Load-Deflection Behaviour of RTW Connections After Retrofitting

The load-deflection relationship at each RTW connection of the 'retrofit-new' experiment is presented in Figure 5.15. After retrofitting, the load-deflection relationship of the truss system demonstrates four distinct phases of behaviour.

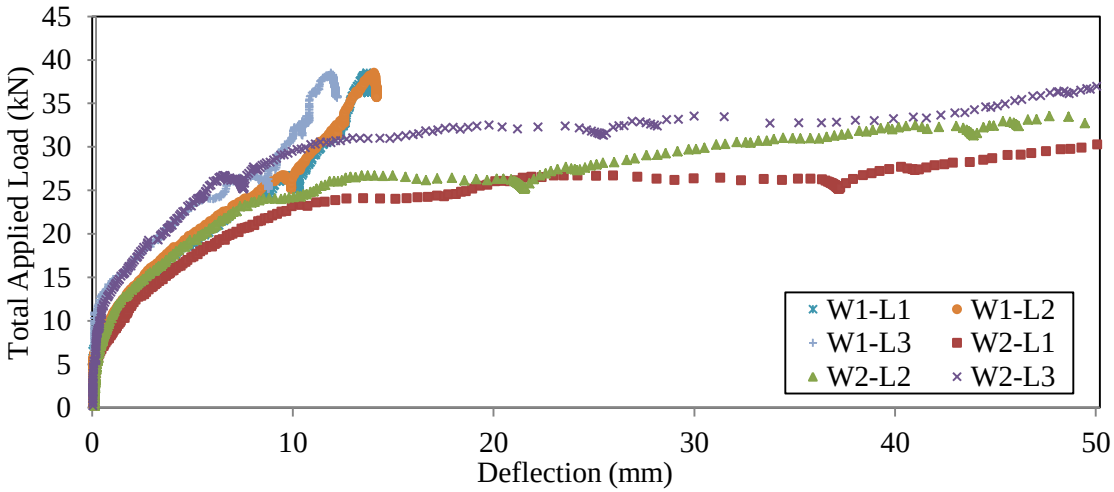

Figure 5.15: Load-deflection relationship of RTW connections of the 'Retrofit-New' experiment

The first two phases of the load-deflection behaviour are similar to those demonstrated by the truss system before retrofitting. Negligible deflection of the truss system occurs until the dead load and initial prestressing are overcome. Due to the initial vertical load applied

by prestressing, application of the retrofit system results in an average 120% increase in the uplift force required to initiate RTW connection deflection above that of the control experiment.

The second phase begins with RTW connection deflection, as the prestressing force and dead load are overcome. As with the unmitigated structure, the RTW connections demonstrate a linear applied load to deflection relationship in this phase. This stiffness is increased by an average of 140% with application of the retrofit system during testing.

The third phase begins with the initiation of RTW connection withdrawal, an applied uplift load of 23.5kN during testing. As the first RTW connection is overloaded, the truss system experiences a large increase in deflection with little increase in the applied load. A redistribution of the applied load occurs from the overloaded RTW connections to the retrofit system, shown by the nearly horizontal slope of the load-deflection relationship during failure of the connections in Figure 5.15. It can be noticed in Figure 5.15 that during connection failure, the truss system rotates about the connections that have not failed, identified as W1-L1, W1-L2 and W1-L3.

The fourth phase, as demonstrated experimentally, begins at approximately 40mm of deflection of the withdrawn connections. The stiffness at the connections that have failed increases and the truss system begins to withstand higher loads. All additionally applied uplift is transferred to the ground by the retrofit system and the stiffness is dependent on the properties of the retrofit system.

5.5.2.2 Distribution of Force between the Retrofit System and the RTW Connections

Figure 5.16 presents the distribution of the applied uplift force between the RTW connections and retrofit system during the experiment. The following three trends are shown in this figure:

- Initially, the force transferred through the wall is larger than that transferred through the retrofit system. For applied loads below the failure of the first RTW connection, 79% of the additionally applied uplift load is transferred to the ground through the wall, with the remaining 21% transferred through the load path provided by the retrofit system.

- Upon reaching the maximum uplift force transferred by the wall, at an applied uplift load of 24.2kN, a redistribution of the applied load occurs. At this critical load, Figure 5.16 shows a vertical increase in the axial force in the external cables and a vertical decrease in the force in the walls. This redistribution corresponds to the third phase of behaviour discussed above where the force withheld by the overloaded connection is transferred to the retrofit system by deflection of the truss system.

- Above the redistribution of applied uplift force, the vertical force in the cables increases at approximately the same rate as the applied vertical force. This represents the fourth phase of behaviour where all additional load is transferred to the ground by the retrofit system. This behaviour is confirmed by the horizontal slope of the force transferred though the RTW connection load path.

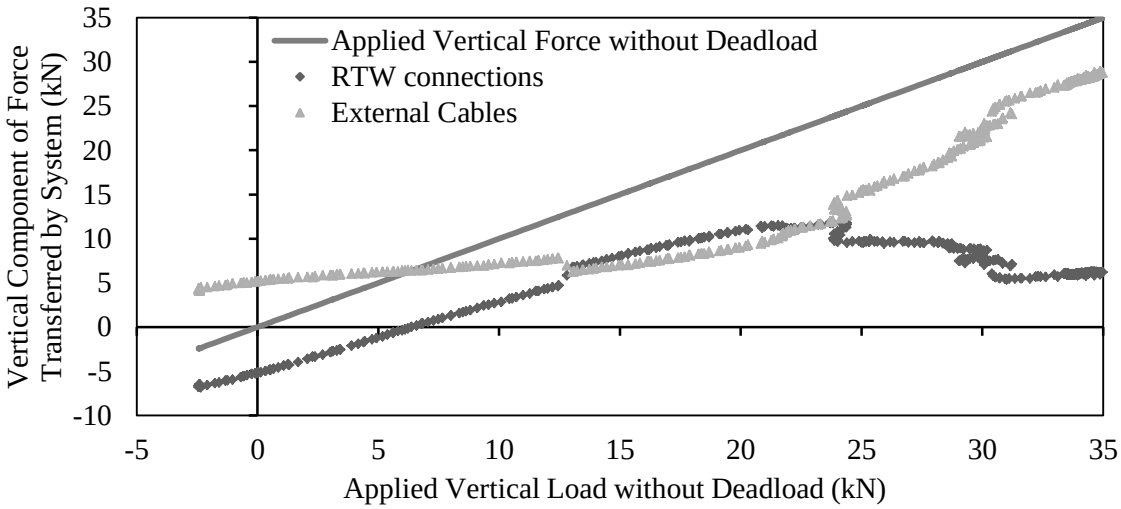

Figure 5.16: Vertical component of force in each load path

Figure 5.17 shows the tension force resulting in each turnbuckle as the uplift load is applied to the truss system. The following trends are shown in this data:

- The force transferred to the retrofit system is approximately linear with applied load until connection failure begins.

- The cable axial force increases with no increase in applied uplift to the system at 24kN, 26kN and 32kN of applied uplift, representing the redistribution of force with connection withdrawal.

- The external cable located closest to the connection that is withdrawing experiences the largest increase in force. For example, connection W2-L1 deflects 25mm between 24kN and 26kN of applied load. This large deflection results in an increase in the axial force in external cable W2-T1 of 2.6kN.

- After complete removal of the wall 2 connections, as the truss system rotates about the connections that have not failed, the external cables closest to the

withdrawn connections experience much higher axial load than those on the side without connection failure.

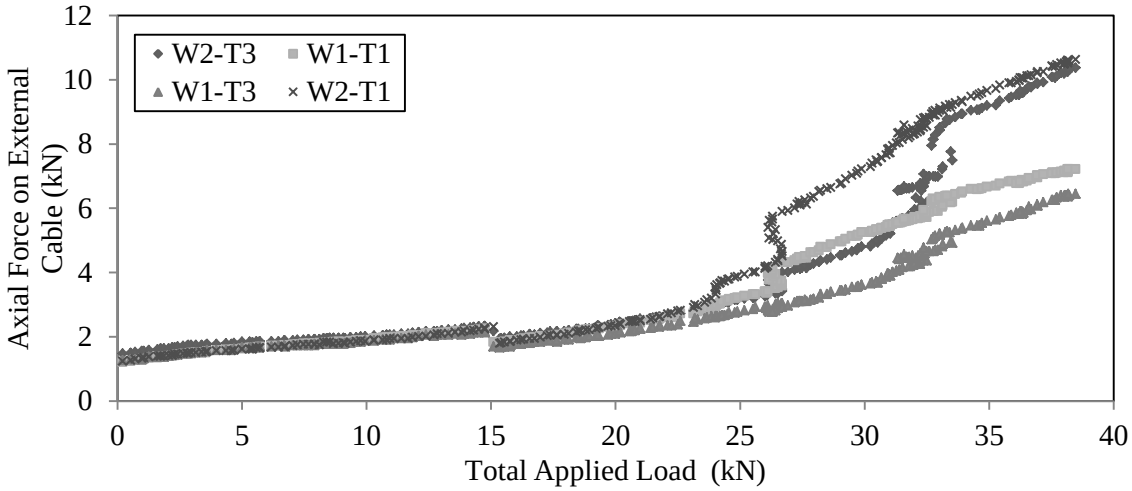

Figure 5.17: Axial force on cables of retrofit system vs. applied load

In general, the results of the 'Retrofit-New' experiment demonstrate that the retrofit system is effective at increasing the uplift capacity of the truss system. The failure mode of the truss system changes from a sudden withdrawal of the RTW connections to a ductile withdrawal with ultimate capacity dependent on the components of the retrofit system. Initially, 79% of additionally applied uplift loads are transferred through the RTW connection load path, with much of the transfer to the retrofit system occurring during the connection withdrawal.

5.5.3 'Retrofit – Damaged' Experimental Results

The results of this experiment show that the retrofit system is effective at increasing the capacity of structures that have been previously damaged. RTW connection failure begins at an applied uplift load of 26.3kN, 80% higher than that of the control experiment. The maximum load applied to the system is 29kN, governed by the maximum allowable load in the external cables.

Table 5.3 presents a summary of the critical loads for the conducted experiments. As expected, the maximum load transferred by the RTW connections is found to be 21% lower for the experiment containing damaged connections than the experiment containing undamaged connections. Despite this decrease, the applied load at which this maximum occurs is found to be 9% higher. This unexpected increase in the applied load at RTW connection failure is the result of the decreased stiffness of the RTW connections. Under the applied uplift load of 20kN, the damaged RTW connections experience approximately three times more deflection than the non-damaged connections. As the truss system becomes less stiff, the retrofit system becomes more effective at preventing failure of the RTW connections. The larger deflections that occur in a more flexible structure increase the percentage of the applied force transferred by the retrofit system. Figure 5.18 shows that the applied force transferred by the retrofit system increases more quickly for the truss system with damaged connections than the undamaged connections. This reduces the demand on the RTW connections and increases the necessary applied load to cause failure.

Table 5.3: Experimental critical applied load summary

	Maximum RTW Connections Withdrawal Force (kN)	Applied Uplift at Maximum RTW Connection Force (kN)	Maximum Total Uplift Load Applied(kN)
Control	14.6	-	-
Retrofit – New	11.8	24.2	36.2
Retrofit – Damaged	9.3	26.3	29.0

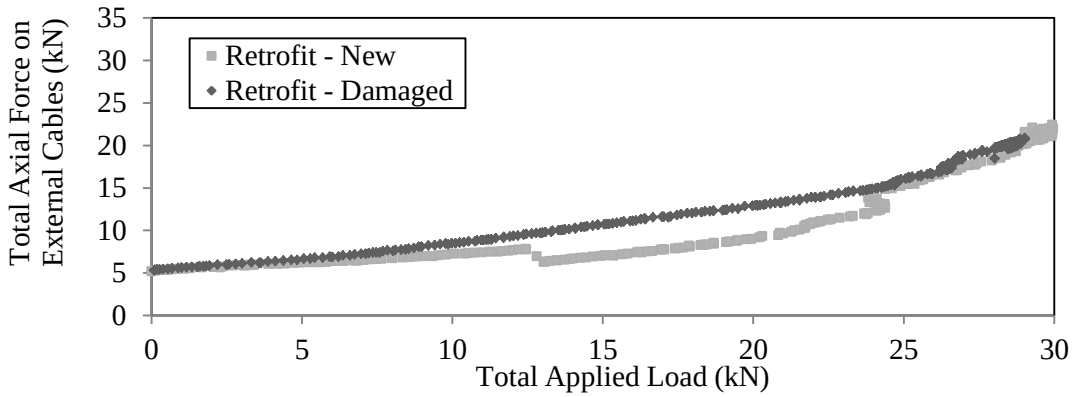

Figure 5.18: Axial force on external cables as external load applied

5.6 Numerical Response and Behaviour

The predictions of the numerical model are compared to the results from the 'Retrofit – New' experiment to determine if the model accurately captures the behaviour of the structure after application of the retrofit system. The focus of the comparison presented below is the behaviour of the load-deflection relationship of the RTW connections and the distribution of force between the connections and retrofit system.

5.6.1 Load-Deflection Behaviour of Truss System

The numerical model predicts that connection withdrawal begins at 30kN of applied uplift, 27% higher than the experimental result. The load path of the RTW connections transfers 2.5kN less uplift load during the experiment than predicted by the numerical model, an average of .42kN per connection. It is reasonable to assume this difference is a result of the variability in the capacity of the toe-nail connection failure capacity.

Figure 5.19 shows the applied load to deflection relationship for selected RTW connections from the experiment and the typical prediction of the numerical model. While the failure load and stiffness of the critical connection are larger in the numerical prediction, the model shows strong agreement in terms of behaviour of the truss system

after application of the retrofit system. The following similarities are shown between the numerical prediction and the experimental behaviour:

- The RTW connections show negligible deflection with applied load before the initial prestressing force and the dead load are overcome at the applied load of 6kN.

- The applied load to deflection relationship for each RTW connection has a linear trend until failure begins.

- Deflection of the truss system occurs to redistribute the applied uplift force from the overloaded connections to the retrofit system, shown by the horizontal slope of the applied load to deflection relationship

- The system regains strength and continues to deflect based on the properties of the retrofit system

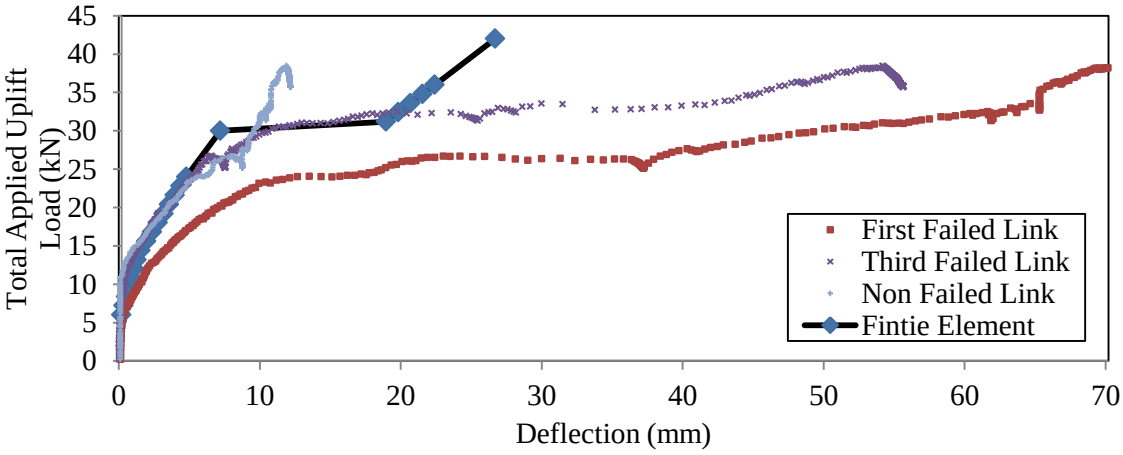

Figure 5.19: Load-deflection relationship for selected RTW connections, experimental results and numerical prediction

The numerical results presented in Figure 5.19, in which symmetry causes each RTW connection to fail simultaneously, predicts that the post failure behaviour of the

connection begins at approximately 20mm of deflection. This prediction is approximately half that of the experimental results. When the numerical model is modified to include a distribution of RTW connection failure capacities, the behaviour of the truss system becomes more similar to the experimental results, as the model captures the rotation of the truss system about the connections that have not failed that is demonstrated experimentally during the third phase of behaviour. The modified numerical model predicts an initiation of post failure behaviour at a deflection of 32mm; 20% below the experimental result of approximately 40mm.

5.6.2 Force Distribution between Load Paths

Figure 5.20 presents the force transferred to the ground through the external prestressing cables as uplift is applied to the truss system. The four phases of behaviour of the truss system are again recognized. The following observations can be made about the numerical prediction of each phase of behaviour:

- The first phase is not as clearly defined experimentally as predicted by the numerical model. The experimental data shows a small increase in the axial force in the external cables before the dead load and prestressing force are overcome, an increase that is not confirmed by the numerical prediction.

- The experimental results match the numerical prediction in the second phase, as the slopes of the linear relationship presented in Figure 5.20 differ by only 5%.

- Even though the uplift load corresponding to the onset of connection failure differs due to the difference in failure load, both the numerical prediction and the

experimental results confirm the vertical increase in external cable axial force as redistribution of the applied load occurs.

- After complete connection withdrawal, which occurs above 30kN of applied uplift, the numerical prediction and experimental results match in terms of the relationship between the applied uplift load and the tensile force acting on the external cables.

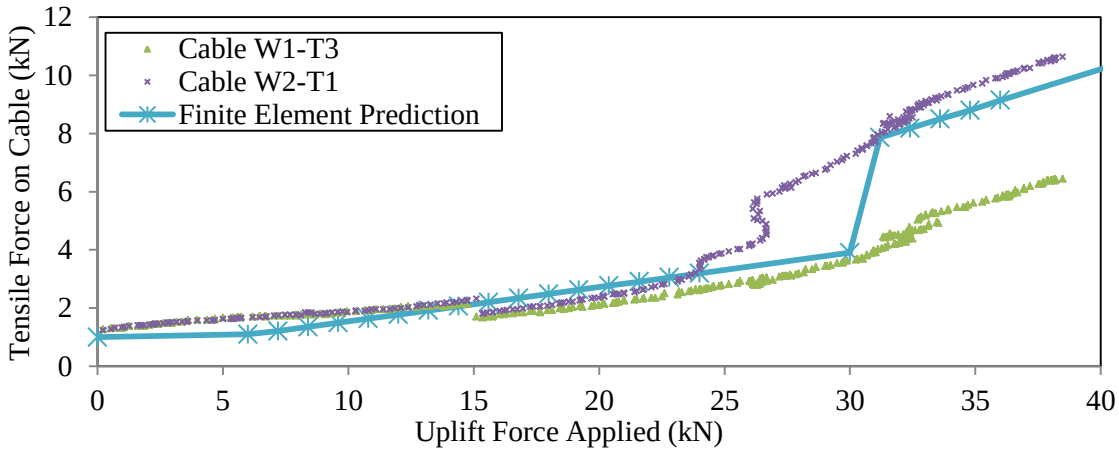

Figure 5.20: Tensile force on external cables vs. load applied

The accurate prediction of the numerical model in terms of the distribution of force between the two load paths is also shown in Figure 5.21, which presents the force transferred by the RTW connection load path. Although there is an initial difference in the value of load transferred through the RTW connections below the sudden increase that occurs at 13kN, the relationship with applied load is nearly exact, differing by less than 1%. After the sudden increase occurs, the numerical model accurately predicts the force transferred through the RTW connection load path.

While the slopes show strong agreement, the numerical and experimental results differ during failure of the RTW connections. Figure 5.21 shows that the maximum force

transferred by the RTW connections is lower during testing than that of the numerical prediction, resulting from the difference in the failure load discussed above. As each connection does not fail simultaneously during the experiment, force continues to be transferred by the RTW connection load path after initial withdrawal. This force is not present in the symmetric failure of the numerical model. Despite the difference in value, the post failure behaviour is similar, as both experimental and numerical results demonstrate a horizontal relationship between the applied force and the force transferred by the walls. This represents all additional applied uplift force being transferred through the retrofit system load path.

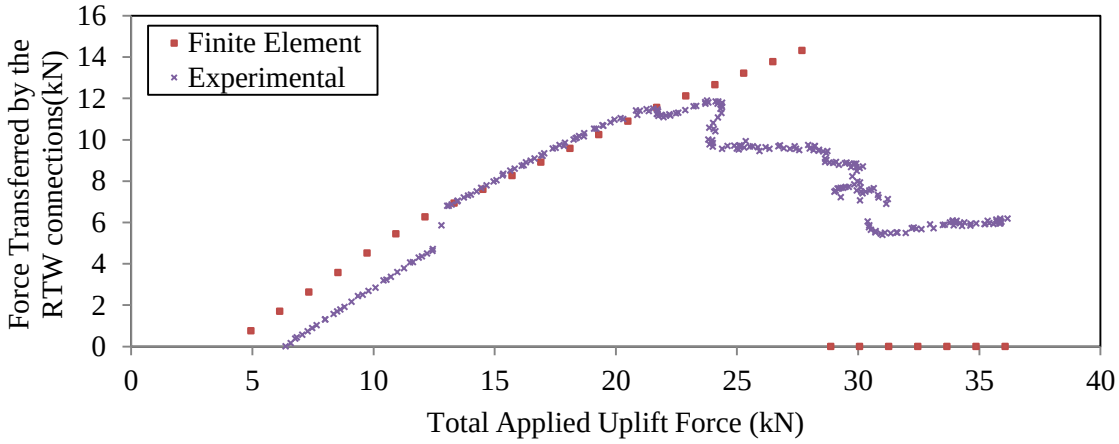

Figure 5.21: Experimental result and numerical prediction for force in RTW connections as load is applied

The numerical model predicts that the uplift load applied to the structure is transferred to the retrofit system at the eaves and peak of the structure, the locations where the bearing cables bend. High bearing loads occur at the eaves during the experiment, resulting in the damage to the sheathing shown in Figure 5.22. This damage confirms the numerical prediction that this location is responsible for a significant amount of the force transfer from the truss system to retrofit system. While the retrofit system has provided a positive

effect on the capacity of the RTW connections, the high bearing loads that are demonstrated experimentally must be addressed.

Figure 5.22: Close-up of sheathing damage at eve after completion of the experiment

In general, the numerical model is found to accurately capture the behaviour of the retrofitted truss system, confirming the four phases of the load deflection relationship of the RTW connections demonstrated experimentally. The numerical model is also very accurate in the prediction of the distribution of force between the load paths. While variability in the capacity and the stiffness of the experimental RTW connections results in differing failure loads, both the numerical prediction and experimental results show large deflections occur during connection failure to redistribute the applied uplift load from the overloaded connections to the retrofit system. The strong prediction of the numerical model in terms of behaviour and load distribution suggest this model

adequately captures the interaction between the truss and retrofit systems and will provide a reasonable approximation in further full-scale analysis.

5.7 Conclusions

The vulnerabilities in the roof system of light-framed wood homes have been exposed during past high speed wind events. Building codes and product development have worked to address the issue, but current solutions are difficult and expensive to apply as a retrofit. The system proposed in this experiment, which is applied over the exterior of the structure, is intended to be an economical, easy-to-apply retrofit system capable of reducing the economic loss caused to these structures during high speed wind events.

The following results have been found in the experimental testing of the proposed system:

- Application of the retrofit system increases the applied load at the initiation of RTW connection failure by 40%.

- The system increases the load that RTW connection deflection becomes pronounced by 120% and the stiffness of the truss system before failure by 140%.

- The retrofit system improves the failure mode of the connection from a sudden withdrawal to a ductile failure with maximum capacity dependent on the properties of the retrofit system.

- The overall capacity of the tested retrofitted truss system is governed by the capacity of the external cables. At this level, the system is able to resist more than double the applied load that the failure load of the control structure.

A developed numerical model has been validated using a comparison to the experimental results. The following similarities are shown between the numerical prediction and the experimental results:

- While connection variability resulted in a difference in the predicted failure load of the connections, both experimental and numerical results demonstrated four distinct phases of behaviour of the load-deflection relationship of the RTW connection after retrofitting.

- The numerical model is found to be very accurate at predicting the distribution of force between the walls and retrofit systems, capturing the linear slope of the force in the walls with applied load within 1% and the linear slope of the axial force acting on the cables with applied load within 5%.

- The numerical and experimental results agree that force redistribution occurs during connection withdrawal by deflection of the truss system.

- Large bearing forces occurred at the eve of the structure in both the experimental and numerical results.

This experiment is successful at proving the accuracy of the numerical model in predicting the behaviour of the retrofit system, as well as confirming that the proposed retrofit system is effective at increasing the uplift capacity of a light-framed wood truss system.

5.8 References

Baskaran, A. and Dutt, O. (1997). Performance of roof fasteners under simulated loading conditions. *Journal of Wind Engineering and Industrial Aerodynamics*, 72(0), 389-400

Canadian Wood Council (CWC), and Canadian Standards Association (CSA). (2010). *Wood design manual, 2010 :The complete reference for wood design in canada*. Ottawa: Canadian Wood Council

Canbek, C., Mirmiran, A., Chowdhury, A., and Suksawan, N. (2011). Development of Fiber-Reinforced Polymer Roof-to-wall Connection. *J. Compos. Constr., 15*(4), 644-652.

Computers and Structures, Inc. (2009). SAP 2000 V. 14: Integrated Software for Structural Anlaysis and Design. Berkley, California, USA.

Datin, P. L., Prevatt, D. O., and Pang, W. (2011). Wind-uplift capacity of residential wood roof-sheathing panels retrofitted with insulating foam adhesive. *Journal of Architectural Engineering, 17*(4), 144-154.

Department of Housing and Urban Development (HUD). (1993). *Assessment of Damage to Single-Family Homes Caused by Hurricanes Andrew and Iniki.* U.S., Office of Policy and Development and Research, HUD-0006262.

Dessouki, A. (2010). *Analysis and retrofitting of low rise houses under wind loading.* (M.E.Sc. thesis), London, Ont: Department of Engineering, The University of Western Ontario.

Emanuel, K., (2005). Increasing destructiveness of tropical cyclones over the past 30 years. *Nature, 436*, 686-686.

Federal Emergency Management Agency (FEMA). (1993). *Building Performance: Hurricane Iniki in Hawaii - Observations, Recommendations, and Technical Guidance.* Federal Emergency Management Agency.

Gurley, K., Davis, R.H., Ferrera, S.P., Burton, J., Masters, F., Reinhold, T., Abdullah, M., (2006). Post 2004 hurricane field survey – an evaluation of the relative performance of the Standard Building Code and the Florida Building Code. *Proc. 2006 ASCE/SEI Structures Congress*, St. Louis, MO. 8.

International Hurricane Research Center (IHRC). (2012). *Hurricane loss reduction for housing in Florida: Roof Sheathing Fastener Stud*y. Florida International University, Miami, USA.

Morrison, M. J., Henderson, D. J., and Kopp, G. A. (2012). The response of a wood-frame, gable roof to fluctuating wind loads. *Engineering Structures, 41*, 498-509.

National Research Council of Canada (NRC). (2010). *National Building Code of Canada (NBCC) 2010*. Ottawa, NRCC 53301

Simpson Strong-Tie Company Inc. (2011). *Technical Bulletin, Uplift Connectors, Truss-to-Wall Tiedowns (Spruce-Pine-Fir*). Pleasanton, California.

van de Lindt, J., Graettinger, A., Gupta, R., Skaggs, T., Pryor, S., and Fridley, K. (2007). Performance of wood-frame structures during Hurricane Katrina. *Journal of Performance of Constructed Facilities, 21*(2), 108-116.

Chapter 6

6 Conclusions and Future Research

6.1 Summary

The focus of this research is on developing a retrofit system to reduce the economic loss that results from damage to light-framed wood structures during extreme wind events. The proposed system provides a secondary load path for the structure when subjected to uplift loading, reducing the withdrawal demand on the sheathing to truss (STT) and roof to wall (RTW) connections. The proposed retrofit system has been developed using experimental and numerical techniques. A numerical model has been developed that, in comparison with full-scale experimental results, shows good ability to predict the deflected shape of a light-framed wood structure under a realistic wind pressure distribution. The developed numerical model is then extended to include the proposed retrofit system, allowing for the study of the behaviour of the structure after implementation of the retrofit system.

An experiment has also been conducted to investigate the behaviour of the structure before and after application of the retrofit system. The experimental results show that the retrofit system is effective at increasing the uplift capacity of the structure. The results of the experiment have been used to validate the assumptions of the numerical model.

6.2 Key Findings of the Current Work

The numerical model has shown the ability to predict the deflected shape of the structure when compared to the full experimental results. Analysing the behaviour of the structure under realistic pressure distributions resulted in the following conclusions:

- Significant load sharing occurs to the gable ends of the structure. The numerical model predicts that the force on the gable wall is 49-94% higher than anticipated by the tributary area method for pressure distributions selected from the 25m/s wind speed experimental data. This load sharing also results in the tributary area method providing a very conservative approximation of the withdrawal load on the critical connection, overestimating this force by a factor of two when compared to the prediction of the numerical model.
- Including plastic deformation at the RTW connections resulted in a more accurate approximation of the experimental results during a time history loading than an equivalent linear elastic model. During the applied time history, the numerical model predicts that the critical connection suffered approximately 2mm of permanent withdrawal.

A rigorous numerical analysis of the behaviour of the structure after application of the retrofit system is completed with the following key findings:

- Studying the effect of modification of each retrofit system component on the behaviour of the structure identified the possibility of an optimal solution. While in general, increasing the size of each design variable increases the failure load of the structure, a balance must be found between the bending rigidity of the rigid bars, the diameter of the bearing cables and the diameter of the external cables to limit local stresses in the structure.
- A parametric study has been completed to find the retrofit system configuration with the minimum weight that satisfies selected structural strength constraints when subjected to a design wind pressure. Results suggest that the bearing cable

spacing should match the spacing of the truss system to reduce both the shear force transferred by the fascia board to the truss connection and the bending moment in the sheathing. The numerical model predicts that the components of the optimal retrofit system are a 6mm bearing cable, a 10mm external cable, a 52mm by 102mm with a 6mm wall hollow rectangular rigid bar, with 2kN initial external cable prestressing at a 15° angle with the vertical wall.

- Under the 35m/s realistic wind pressure, the numerical model predicts that the retrofit system is able to prevent damage to the RTW connections, reducing the maximum withdrawal force applied to the connection by 22%.
- Under the building code pressure distribution, the model predicts that application of the retrofit system can increase the critical mean hourly wind velocity from 38m/s to 50m/s.

During the experimental testing, application of the retrofit system has shown to greatly improves the behaviour of the structure. The following results have been found in the experimental testing of the proposed system:

- Application of the retrofit system increases the applied load at the initiation of RTW connection failure by 40%.

- The system increases the load that RTW connection deflection becomes pronounced by 120% and the stiffness of the truss system before failure by 140%.

- The retrofit system improves the failure mode of the connection from a sudden withdrawal to a ductile failure with maximum capacity dependent on the properties of the retrofit system.

- The overall capacity of the experimental retrofitted truss system is governed by the capacity of the external cables. At this level, the system is able to resist more than double the applied load than the failure load of the control structure.

A developed numerical model has been validated using a comparison to the experimental results. The following similarities are shown between the numerical prediction and the experimental results:

- While connection variability resulted in a difference in the predicted failure load of the connections, both experimental and numerical results demonstrated four distinct phases of behaviour of the load-deflection relationship of the RTW connection after retrofitting.

- The numerical model is found to be very accurate at predicting the distribution of force between the walls and retrofit systems, capturing the linear slope of the force in the walls with applied load within 1% and the linear slope of the axial force acting on the cables with applied load within 5%.

6.3 Recommendations for Future Work

Further research should focus on developing the idea of the retrofit system using both numerical and experimental techniques, as well as furthering the understanding of the complex behaviour of a light-framed wood structure under uplift loading. The following topics are suggested:

- Test the idea of the retrofit system on a full-scale structure under a realistic wind pressure. The results of this experiment should be used to further validate the

numerical model, while proving that the proposed system is effective at increasing the uplift capacity of structures in extreme wind events.

- Develop a design procedure to quickly determine the optimal component sizes for the retrofit system for individual structures.
- A low elongation strap has been identified as a potential optimal material for the bearing cables of the retrofit system. A further investigation should be completed on the availability, cost and reliability of low elongation straps.
- The numerical model has identified that the additional RTW connections on the gable end wall are important in the load path of the applied uplift forces. A further investigation should be completed on the effect of the increased stiffness of the gable end wall on the probability of failure of the STT connections. This can be completed by extending the numerical model to include a link element to model the stiffness of the STT connections.
- Extend the three-dimension numerical model to a dynamic model. This will include the energy dissipation resulting from the plastic damage at the RTW connections and a dynamic wind pressure applied to both the structure and retrofit system.

Curriculum Vitae

Name: Ryan B Jacklin

Post-secondary Education and Degrees:
The University of Western Ontario
London, Ontario, Canada
2004-2010 BSc.

The University of Western Ontario
London, Ontario, Canada
2007-2010 BESc

The University of Western Ontario
London, Ontario, Canada
2010-2013 MESc

Honours and Awards:
Natural Sciences and Engineering Research Council of Canada
Industrial Postgraduate Scholarship
2011-2012

Related Work Experience
Teaching Assistant
The University of Western Ontario
2010-2012

Publications:

Jacklin, R., and El Damatty, A. A. (2012). Numerical and experimental study of retrofit system to increase uplift capacity of light-framed wood roofs. *Annual Conference of the Canadian Society for Civil Engineering 2012, June 6-9,* 3. pp. 2440-2449